INTERFACIAL ASPECTS OF GLYCOTHERMALLY SYNTHESIZED ALPHA ALUMINA

By

NELSON S. BELL

A DISSERTATION PRESENTED TO THE GRADUATE SCHOOL
OF THE UNIVERSITY OF FLORIDA IN PARTIAL FULFILLMENT
OF THE REQUIREMENTS FOR THE DEGREE OF
DOCTOR OF PHILOSOPHY

UNIVERSITY OF FLORIDA

1997

ACKNOWLEDGMENTS

I would like to thank my advisor Dr. James H. Adair for his tutelage and encouragement of my development as a colloid and surface chemist. I would also like to thank Dr. Robert DeHoff, Dr. Michael Sacks, and Dr. David Clark from the Department of Materials Science and Engineering and Dr. Daniel Talham from the Department of Chemistry for serving on my committee. I am very grateful to Dr. Ellis Verink for his support and encouragement during my studies at the University of Florida.

I am indebted to my fellow group members at the University of Florida, with special thanks to Dr. Robert Chodelka, Dr. Seung-Boem Cho, Craig Habeger, Jeff Kerchner, Paul Demkowicz, Dave Mitchell, Henrik Krarup, Robert Simpson and Dr. Melanie Carraso. I appreciate the help of my fellow graduate students during my education, specifically Mike Zamora, Jesse Arnold, Drew Amery and James Merotta. I would like to thank the staff of the Major Analytical Instrumentation Center, and Dr. Stanley Bates, Dr. Augusto Morrone, and Wayne Acree who all proved to be of exceptional assistance in sample analysis. Thanks are due to David Powell and staff for performing and analyzing gas chromotography data in the Spectroscopic Services Laboratory in the UF Department of Chemistry.

My heartfelt thanks go to my extended family for their pride and support of my career path, and most strongly to my parents Joseph H. Bell and Eunice S. Bell for their unwavering faith, encouragement and belief in my ability.

TABLE OF CONTENTS

LIST OF TABLES

LIST OF FIGURES

Abstract of Dissertation Presented to the Graduate School
of the University of Florida in Partial Fulfillment of the
Requirements for the Degree of Doctor of Philosophy

INTERFACIAL ASPECTS OF GLYCOTHERMALLY SYNTHESIZED
ALPHA ALUMINA

By

Nelson S. Bell

December 1997

Chairman: Dr. James H. Adair
Major Department: Materials Science and Engineering

A thermodynamic derivation for the equilibrium shape of a crystal precipitated in liquid solution has been developed. The conditions for equilibrium incorporate the effect of a reactive interface between the solvated components and the crystal components. Surface charge variation with solution pH has been related to surface energy, and the variation of equilibrium shape with solution pH has been demonstrated as an illustrative example.

The control of particle shape has been investigated in the 1,4-butanediol-alpha alumina system. Morphological effects of the solvent and the use of specific adsorbates have been investigated. Specific adsorbates investigated for their effect on morphology were tetrahydrofuran (THF), methanol, 2-butanol, acetic acid, nitric acid, pyridine, ammonium hydroxide, and tetraethylammonium hydroxide (TEAOH). Both ammonium hydroxide and TEAOH promote a platelet morphology, which is believed to relate to

surface charging effects. Pyridine promotes a platelet morphology but was found to inhibit growth of uniform particles. The use of Al tri(sec)butoxide as a precursor introduces 2-butanol to the solution, and the resultant morphology is plate-like and dominated by $\{11\bar{2}12\}$ facets. Tetrahydrofuran, methanol, and nitric acid had no effect on the growth morphology. Acetic acid promoted the formation of new habit planes and reproducibly forms a roughly acicular shape.

The development of surface potential for glycothermally synthesized alpha-alumina has been investigated as a function of particle habit and aging effects. The adsorption of 1,4-butanediol on the surface of the particles creates aging effects on the isoelectric point. The final isoelectric point correlates with the number of metal cation sites on the dominant habit plane through the configuration of ligand anions. It is believed that differences in surface charge and isoelectric point result from the speciation of Al^{3+} sites with OH^- ions from solution.

Sintering studies were performed on glycothermally synthesized α-Al_2O_3 hexagonal platelets to determine the effects of anisotropy upon the evolution of both an equilibrium particle morphology and particle consolidation. Evidence of sintering and densification are apparent in the morphology of the particles, but densification on the macroscopic level was inhibited by porosity. Transformation to an equiaxed morphology occurs with bulk densification.

CHAPTER 1

INTRODUCTION

The mineral alumina (Al_2O_3) is a major component of many products produced by the ceramic industry (Mad97). The manufacture of alumina in 1995 was approximately 5 million metric tons, and projections for growth are nearly 4% per year. New alumina products are requiring higher performance to satisfy needs in such applications as refractories, abrasives, and ceramics. Refractory applications for alumina involve several industries including ferrous material production, nonferrous ceramics, glass and cement manufacture, and chemical production. High performance refractories are especially demanded in steel production. Abrasives are an application that consumes approximately 80% of fused alumina production and desired properties in abrasive production are purity and durability. High purity, durable abrasives are currently being produced using sol gel technology. Alumina particles are also being applied to the next generation of aluminum and magnesium metal matrix composites as automotive components. Applications as drive shafts, brake systems, piston heads and cylinder liners are being considered. Alumina has been applied as exhaust port liners in Porsche engines. Electronic applications like circuit board substrates and catalytic converter supports also require greater material performance. Advanced ceramic applications have created a need for fine, high purity alumina with controlled and reproducible properties.

Solution synthesis techniques have the potential to satisfy many of the industrial needs for alumina products. The key advantages of solution synthesis are the production of high purity, monodisperse, unagglomerated powders of controlled shape (Daw89, Hir87, Mat87, Mat92). Additionally, cost reductions result from elimination of the need for milling to reduce particle size. Hydrothermal synthesis has successfully developed wide application in the production of metal oxides (Kat87, Som87, Som89). The use of water as a solvent under elevated heat and pressure is to reduce the melting point of the material being synthesized (Lau73). This allows growth at lower temperatures than the alternative calcination process. The use of a solvent does have disadvantages in that the growth of the material cannot be directly observed, and high pressure equipment is required.

The hydrothermal synthesis of alumina was investigated in the mid-twentieth century by several investigators (Erv51, Ken59, Kuz64, Kuz65, Kuz71, Lau43, Mat67). Hydrothermal techniques are widely used to produce gibbsite through the Bayer process, and boehmite is a popular phase used in the production of catalyst supports (Git70). The stability of the alpha phase, desired as the most thermodynamically stable phase, was found to require temperatures in excess of 400°C and reaction times ranging from days to weeks. Growth rates were measured by Kuznetsov at 600°C and highly basic conditions (Kuz64). These extreme conditions limit application of hydrothermal synthesis to the production of α-alumina, because the synthesis temperatures are above the critical point of water, and the synthesis pressures are extreme.

The utilization of non-aqueous solvents has recently demonstrated that the prohibitive high pressures of hydrothermal synthesis need not forestall low temperature

synthesis of α-alumina (Bel97, Cho95, Cho96, Ino89). Glycols have been applied as an alternative solvent, and have demonstrated the capability to form both desired crystal phases and novel phases that have not been produced in aqueous synthesis (Bib85, Fan86, Ino89, Ino91, Ino95, Ino97, Kai94, Kai95). Cho and Adair have developed the glycothermal synthesis technology of α-alumina for the control of particle shape (Cho95). The use of 1,4-butanediol has been applied to synthesize α-alumina at 270°C, and reaction times have been found to occur as quickly as 12 hours. Control of stirring rate was reported as the dominant variable in control of the morphological form of the precipitate (Cho96). High shear rates develop a platelet morphology, and low shear rates produced a polyhedral morphology. The local growth environment during growth will dictate the final particle morphology.

The capability to control the shape of a particle creates the opportunity for custom developed α-alumina powders to be fabricated for a desired application. Highly anisotropic particles can be applied to composite reinforcement as platelets or needles, and platelets can be used as nuclei to orient layers of alumina film. The effect of particle shape on a powder's effectiveness as an abrasive has not previously been investigated. Thermal barriers for refractive applications can benefit from the construction of controlled pore structures.

The synthesis and application of particles of controlled shape requires an understanding of the effect of interfacial properties. The free energy of each facet in the synthesis of particles is a function of the solvent environment, whereas growth rates are dictated by the fluid dynamics during precipitation. Particle shape is thus affected by the properties of the fluid interacting with the crystal during growth. Organic solvents add

concern for the stability of the solvent. Solvent degradation will provide new chemicals to interact with the surface and affect growth rates or the thermodynamic stability of facets. Chemical interactions between the solvent and crystal which alter surface energy are factors in the development of morphology, and the interactions of an additive which changes morphology must supersede the effect of solvent.

Particles with habit planes will exhibit differing surface electrical properties based on the prevalence of the habit planes. Colloidal dispersion is a key element in most forming technologies, and the stability of a suspension is critical to processes like tape casting or slip casting. Abrasive applications also require unagglomerated dispersions, and the electrical charging properties of a powder are critical for the design and application of successful dispersions. Faceted, anisometric particles provide an opportunity for developing an understanding of the effect of each habit plane on surface potential.

Sintering of faceted particles is based on the reduction of surface free energy. The final particle shape is determined by the equilibrium shape. The presence of defined habit planes during sintering will affect the development of fully dense products, and affects the driving force for sintering through the reduction of surface energy. Knowledge of the equilibrium shape allows the determination of the driving force for sintering a particle morphology.

The objective of this work is to examine the interfacial characteristics of faceted particles formed in glycothermal synthesis, and relate these characteristics to interfacial properties during synthesis. The effect of each habit plane on interfacial properties generates an opportunity for both a fundamental and practical understanding of the

influence of surface energy on interfacial phenomena. This dissertation is divided into six major sections. Chapter 2 presents a background on the properties of alumina, colloidal stability, surface charge, and the effect of the interface on particle morphology. Chapter 3 gives a theoretical treatment of the conditions for equilibrium of a particle that grows from the solution phase, and illustrates the effect of surface charging on surface free energy and the resultant equilibrium shape. Chapter 4 surveys the use of specific adsorbates to control particle shape in the precipitation of alpha alumina in 1,4-butanediol. Chapter 5 describes the effect of morphology on aqueous surface charging properties, and the consideration of particle history on surface potential. Chapter 6 gives observations on the sintering of platelets and their morphological development. Finally, Chapter 7 describes conclusions and future work in this system that will be beneficial to the community.

CHAPTER 2

SURFACE ENERGETICS AND INTERFACIAL PROPERTIES AFFECTING THE MORPHOLOGY OF α-ALUMINA DURING LIQUID PHASE PRECIPITATION

Introduction

α-Alumina is one of the most important technological ceramics used in industry. Its hardness, high temperature resistance and electrical properties place alumina as a key structural ceramic, refractory material, and insulator (Dor84, Mun97). Suspensions of fine particles of α-Al_2O_3 are used both as an abrasive and as a forming technique for making bulk products. When considering powder properties such as packing and rheology, the morphology of the individual particles becomes an influencing factor (Suy91). Equiaxed and anisotropic particles fulfill different roles. Structural ceramics require equiaxed particles to gain high packing densities and composites can benefit from either plate-like or needle-like morphologies. Particle morphology and the colloidal properties of varying morphologies are therefore an area of research that can affect the suitability of a powder for a particular application.

Liquid phase precipitation methods often produce powders of controlled morphology (Cho96, Mat92). The advantages of this class of methods lie in the production of unagglomerated, uniform particles, which are often faceted. Liquid

precipitation requires an understanding of thermodynamic, interfacial, and colloidal properties to the control synthesis. This chapter reviews the thermodynamics and interfacial factors necessary to understand the control of particles morphology.

Properties of Alumina

Phase Stability

In order to utilize liquid solution precipitation, the thermodynamic conditions must favor the production of the desired phase. Alumina forms several hydrated phases, as well as doped phases useful for their electronic properties. The various structures of hydrated and anhydrous aluminas are succinctly summarized by Gitzen (Git70) and Table 2-1 provides an overview. Of all the forms, α-alumina (corundum) is the most thermodynamically stable, and all other phases (excluding impure aluminas) will transform to alpha above ~1200°C in air, as shown by Figure 2-1. Hydrated phases of aluminum oxides begin with the nominal formula $Al(OH)_3$, and transition through the alumina monohydrate formula AlOOH to anhydrous Al_2O_3. Many of the variations in crystal structure of the anhydrous crystals are the result of chemical inhomogeneity. β-Alumina results from the presence of alkali or alkaline earth atoms, and the foreign cation is commonly incorporated as part of the name.

The focus of this work is the anhydrous α-Al_2O_3 phase. The crystallographic information for this phase can be found in the JCPDS files of x-ray diffraction data (Alu96). α-Alumina is often described as face-centered array of oxygen ions with two thirds of the octahedral sites occupied by aluminum ions. The crystal structure of α-Al_2O_3 is rhombohedral (hex) in space group Rb3C with Wyckoff positions "c" for the

Table 2-1. Mineralogical overview of the phases of alumina (Git70).

Phase	Density	Hardness	Crystal System	Space Group	Angle	Unit Cell Parameters		
Gibbsite	2.42	2.5-3.5	monoclinic	C_2^5h	85°26'	8.641	5.07	9.72
Bayerite	2.53		monoclinic	C_2^5h	90°07'	4.716	8.679	5.06
Boehmite	3.01	3.5-4.0	orthorhombic	$D_2^{17}h$	92°00'	2.868	12.227	3.70
Diaspore	3.44	6.5-7.0	orthorhombic	$D_2^{16}h$		4.396	9.426	2.844
Chi	3.0		Cubic			7.95		
Eta	2.5-3.6		cubic (spinel)	O_h^7		7.9		
Gamma	3.2		tetragonal			7.95	7.95	7.79
Delta	3.2		tetragonal			7.967	7.967	23.47
Iota	3.71		orthorhombic			7.73	7.78	2.92
Theta	3.56		monoclinic	C_2^3h	103°42'	5.63	2.95	11.86
Kappa	3.3		orthorhombic			8.49	12.73	13.39
α-Al_2O_3	3.98	9.0	rhombohedral	D_2^6d		4.758		12.991
			hexagonal	$R\bar{3}c$		4.758		12.991
$AlO{\bullet}Al_2O_3$	3.84		cubic (spinel)	O_h^7		7.915		

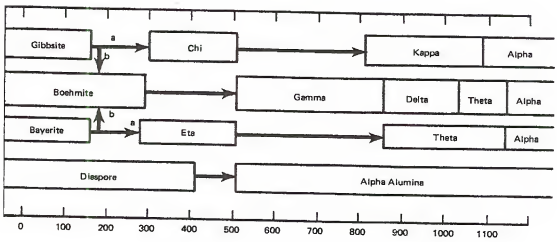

Figure 2-1. Thermal transformation characteristics of Alumina (Git70).

Al^{3+} ions and "e" for the O^{2-} ions. The Wyckoff letter indicates the coordinate transformations needed to represent the atomic positions for the symmetry of the structure. For the Al^{3+} on the "c" coordinate, the variable z has a value of 0.3523 Å and the "e" coordinate for the O^{2-} has an x variable of 0.3064 Å. The ionic radius of Al^{3+} is 0.39 Å, and the ionic radius of O^{2-} is 1.40 Å.

Solubility of Alumina

Precipitation of a desired phase from solution requires an understanding of the equilibrium solubility of the crystal components in solution. The solubility of a crystalline phase in aqueous solution can be calculated from thermodynamic properties and knowledge of the aqueous species. The solution of metal oxides proceed by the formation of aqueous metal ions or ion hydroxide complexes. For alumina, the aqueous species are $[Al^{3+}]$, $[AlOH^{2+}]$, $[Al(OH)_2^{+}]$, $[Al(OH)_3]$, and $[Al(OH)_4^{-}]$. Each ionic species is predominant in select pH regimes. Baes and Mesmer provide formation constants for the hydroxlation of each species by the following reaction (Bae86).

$$Al^{3+} + xOH^{-} \rightleftharpoons Al(OH)_x^{3-x} \qquad (2\text{-}1)$$

Formation constants are given in Table 2-2. Polynuclear ions are excluded from the determination. Polynuclear ions are only appreciable at pH values less than 3 (Bae86).

The free energy of a reaction can be determined from the formation constant using the following equation (DeH93).

$$\Delta G = -RT\ln K_{eq} \qquad (2\text{-}2)$$

Table 2-2. Formation constants for the hydroxylation of Al^{3+} aqueous species (Bae86).

Hydroxylated Species	Formation Constant (Log Q)
$AlOH^{2+}$	-4.97 ± 0.02
$Al(OH)_2^+$	-9.9 (0.1 M $NaClO_4$)
$Al(OH)_3$	-15.6 (0.1 M $NaClO_4$)
$Al(OH)_4^-$	-23.0 ± 0.3

ΔG is the Gibbs free energy of formation, T is absolute temperature, and K_{eq} is the equilibrium constant for the reaction. The free energy values can be determined for the solvation reactions described in equation 2-1 from the speciation constants. By inputting the Gibbs free energy of formation of the oxide and the ionic species, the OPAL© program generates speciation equations which can be used to generate the concentration of each ion in solution (Ada97). The sum of these ionic concentrations gives the solubility of the oxide as a function of pH. The solubility of alpha aluminum oxide is given by this method in Figure 2-2.

Hydrothermal Synthesis of α-Alumina

Hydrothermal synthesis is a material fabrication technique referring to the processing of materials in heated aqueous solution at autogeneous pressures. The high solvent power of the aqueous environment serves to synthesize low temperature

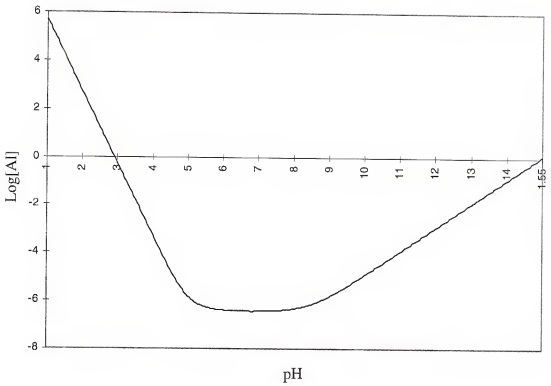

Figure 2-2. Solubility of α-Al_2O_3 in water at 25°C as calculated from speciation constants (OPAL©97).

polymorphs of refractory materials (Lau73). Additionally, seed materials can be used to increase yield or control nucleation, and scaling to industrial use is not problematic (Hir87, Klu93, Lau73, Mat92,).

The stability field of the alumina-water system was investigated in the mid twentieth century by several investigators (Erv51, Ken59, Kuz64, Kuz65, Kuz71, Lau43, Mat67). The reaction equation for the formation of α-alumina from a hydrated precursor is as follows.

$$2Al(OH)_3 \rightleftharpoons Al_2O_3 + 3H_2O \qquad (2\text{-}3)$$

The pressure temperature diagram for the formation of alumina phases is given in Figure 2-3 (Git70). This diagram presents the thermodynamically stable phases of diaspore and α-alumina, but several metastable phases such as boehmite and gibbsite are produced in practice. Gibbsite is formed at all pressures below ~135°C, and boehmite between 135°C and 375°C, with diaspore formed at higher pressures and temperature greater than 300°C. α-Alumina (corundum) is formed at temperatures greater than 400°C. Hydrothermal synthesis of corundum has not been developed for commercial application, as the reaction temperature is greater than the critical point of water (374.1°C), and the autogeneous pressure is approximately 40 MPa.

The dehydration of a precursor like gibbsite or diaspore is inhibited by the presence of water, due to the development of water as a reaction product. The use of an aqueous solvent inhibits the formation of the anhydrous phase. Investigation into nonaqueous solvents for the liquid phase synthesis of alumina has been more promising.

Glycothermal Synthesis

The principles of hydrothermal synthesis are not restricted to aqueous solutions. Several solvents with satisfactory properties can be used in a synthesis reaction. The choice of an effective solvent for the formation of a desired phase must satisfy the following requirements (Dem73).

1. Congruence of the dissolution of the test compounds.
2. A satisfactorily sharp change in the solubility of the compounds with changing temperature or pressure.
3. A specific quantitative value of the absolute solubility of the compound being crystallized.

4. The formation of readily-soluble mobile complexes in the solution.

5. A specific redox potential of the medium, ensuring the existence of ions of the required valence.

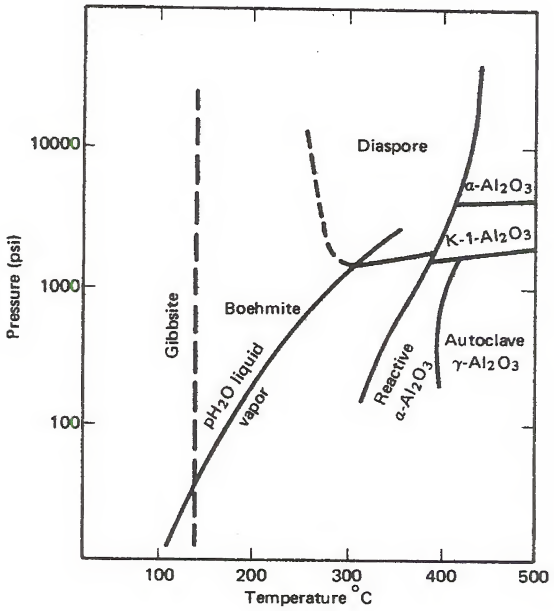

Figure 2-3. Hydrothermal stability diagram for the Alumina-Water system (Git70).

Use of a nonaqueous solvent changes the thermodynamic environment of synthesis. The stability of phases can be changed to produce novel compounds (Bib85, Ino97). Alcohols are commonly used, as well as carbon tetrachloride (Dem73). Inoue's group has performed much of the pioneering work in glycothermal synthesis. Use of glycols as solvent has been successful for producing a pseudo-boehmite alumina (Ino89), α-alumina (Bel97, Cho95, Cho96, Ino89, Kai94), yttrium aluminum garnet (Ino91), $BaTiO_3$ and TiO_2 (Kai95), gadolinium aluminum garnet (Ino95), and rare earth ferrites (Ino97). The hydroxyl groups complex with ionic species to provide transport, and in a non-oxidizing environment the glycols exhibit adequate thermal stability.

Inoue determined that pseudo-boehmite like phases of alumina could be formed in 1,6 hexandiol and that α-alumina was formed by the 1,4-butanediol solvent (Ino89). Cho investigated the use of the solvent 1,4 butanediol for the synthesis of α-alumina, and found that the dehydration reaction temperature has a lower limit of 270°C, and that synthesis could be performed in reaction times as low as 12 hours (Cho95, Cho96).

Cho determined that particle morphology could be controlled by choice of reaction conditions (Cho95). Variables influencing morphology include stirring rate, solids loading of precursor, and reaction time. Through control of process conditions, morphologies ranging from hexagonal platelets to fourteen-sided polyhedra could be formed. Figure 2-4 presents a morphodrome of reaction conditions in the 1,4 butanediol system.

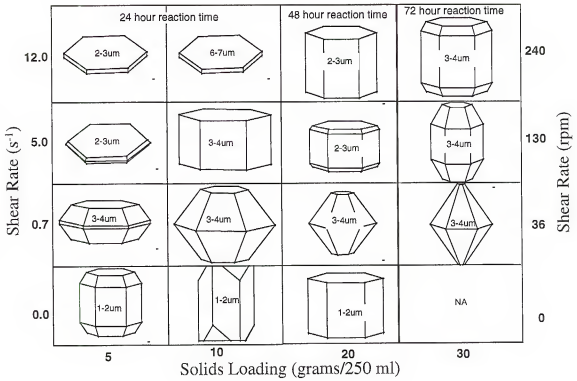

Figure 2-4. Morphodrome of particle morphologies formed in the 1,4-butanediol alumina system as a function of solids loading, shear rate, and reaction time (Cho96).

Glycol Chemistry

The use of a non-aqueous solvent requires that the solvent is understood both for solvent properties as well as chemical stability. Glycols coordinate with ionic species through the hydroxl groups. Inoue investigated the performance of glycol as a solvent as a function of the number of carbon atoms in the backbone. 1,4-butanediol performed best compared to two, three, and six carbon chain glycols due to the intramolecular participation of the hydroxyl group in cleavage of the $HO(CH_2)_n$-O-Al< bond formed by the alkoxyl exchange reaction (Ino91).

However, glycols are susceptible to oxidation by strong acids or high oxidation state transition metals. Secondary glycols oxidize to become ketones and primary alcohols form carboxylates (Atk90). Glycols specifically react to form esters, ethers, and acetals. Dehydration of 1,4-butanediol produces either butadiene or tetrahydrofuran. In the temperature range 250°C to 350°C and with a suitable catalyst, tetrahydrofuran is the principle product. Nitric acid is used with 1,4-butanediol to form succinic acid. Butadiene is produced in the presence of cuprous oxide or sodium dihydrogen phosphate. In the presence of alumina, 1,4-butanediol and ammonia at 400°C produces pyrrolidine. With hydrogen sulfide in place of ammonia at the same conditions, tetrahydrothiophene is produced (Cur52). The stability of the glycol solvent in the presence of additives will certainly affect the success of the glycothermal synthesis, and consideration of the catalytic properties of reaction components should be factored into their use in glycothermal synthesis.

Surface Chemistry of Alumina

Alumina is an amphoteric oxide. Crystallographic alpha alumina is known to be unstable in an aqueous environment compared to the hydrated phases. Alumina tends to react with the water present in the atmosphere to develop a surface terminated by hydroxyl groups (Git70, Isr92). It can have either negative or positive surface charge as a result of the surface dissociation of these hydroxyl groups. Potential determining ions are assumed to be H^+ and OH^-. Heat treatments are known to dehydrate the surface of alpha alumina, and render the surface hydrophobic. Exposure to water either as liquid or vapor causes the surface to age and redevelop hydroxyl groups.

Gitzen provides a review of colloidal behavior of aluminum oxide phases (Git70). The point of zero charge (pzc) of the phases of alumina are given in Table 2-3. Corundum and the aluminum hydroxides have a particularly wide range of pzc values. Possible reasons include different measurement techniques (electroosmosis, microelectrophoresis, pH of lowest solubility), variations in surface hydration, or the presence of impurities. The point of zero charge of alpha alumina is particularly dependent on the calcination history. It is believed that the surface structure of the hydroxide groups have a significant effect on the charging behavior. Disordered surfaces (perhaps induced by grinding) may form $Al(OH)_3$ surface groups, and more ordered surfaces may exhibit AlO•OH surface groups. Finally, surface curvature will affect surface structure.

Surface charge can also be developed in non-aqueous solvents. The colloidal properties in ethanol were investigated by Wernet and Wernet (Wer94) who found by titration experiments that the point of zero charge in ethanol is pH 9.5.

Surface Energy of Alumina

Material surface energy values are applied in precipitation, contact angle measurements, and sintering to understand processing phenomena. The surface energy of α-alumina is anisotropic as a result of the hexagonal crystal structure. Surface energy measurements are environmentally specific, and techniques for measurement differ accordingly. Solid-vapor energies are usually measured near the melting point of the material where some degree of fluid flow is present. Surface energy between the solid-vapor interface for α-Alumina has been measured at 1850°C (DeH93) to give a value of 905 mJ/m^2. This value is an average and is not specific to a crystallographic direction.

Table 2-3. Point of Zero Charge of Aluminum Oxide Phases (Git70).

Phase	Point of Zero Charge (pH)
Gamma Alumina	9.0
Amorphous $Al(OH)_3$	9.4
Gibbsite	9.20
Boehmite	9.40-9.45
Corundum	6.7 - 9.4
Aluminum Hydroxides	5.1 - 9.4

At room temperature, the solid-liquid interface surface energy of the basal plane of alumina in deionized water has been measured by Ducker using the atomic force microscope (Duc94). Through force of adhesion measurements, a value of 75 mJ/m^2 was determined. If solvent adsorption does not relate to the crystal structure, this value can be used to relate surface energies of various habit planes via the Gibbs-Wulff construction.

Colloidal Properties

The stability of particle suspensions is a function of the attractive and repulsive forces between particles. Central to the stability of the particle dispersion is the development of surface charge which forms an energy barrier to particle agglomeration. Electrical forces are approximately one thousand times stronger than Brownian motion (Rin96). The surface charge is measured by the zeta potential of the colloid, which in turn is a function of the electrical properties of the interface. An explanation of fundamental surface charge and electrical double layer structure is needed for

interpretation of experimental results. The governing equations for colloidal interface structure are covered in a variety of sources (Ada90, Isr92, Ros88) and detailed information is available in Hunter (Hun87).

Development of Surface Charge

Colloids in suspension develop surface electrical charges by reaction with the surroundings. The four mechanisms that cause the surface of a colloid to develop charge are the presence of defect structures or polarization of surface ions in the lattice, dominant ion surface composition, ion adsorption or ionic exchange and, dissociation of surface groups (Hun87). The presence of defect structures cause charge imbalance in an ionic crystal, and lead to electrical fields. Such defects can occur by ion exchange between material ions and an aqueous species, where the replacement is of different charge. Space charge can also be generated by vacancies within the crystal, which manifest as surface charge (Kli65a, Kli65b). The crystal structure of a salt can favor the presence of one ion over the other on the surface to give a surface charge dependent on the concentration of the ions in solution. A colloid can be composed of surface molecules which exhibit acid-base behavior. Last, ions or ionic molecules can be adsorbed on the surface to such an extent that charge is generated. Those ions which adsorb on the surface to control the surface charge are termed the potential determining ions.

Metal oxides are believed to form surfaces of hydroxide groups which dissociate amphoterically by the following equations (Git70, Hun87).

$$AH_2^+ \rightleftharpoons AH + H^+ \qquad (2\text{-}4)$$

$$AH \rightleftharpoons A^- + H^+ \qquad (2\text{-}5)$$

The electric charge at the surface attracts ions of opposite charge and repels like-charged ions. The metal oxide layer is made more complex because the activity of the potential determining ions on the surface is related to the potential of the surface. Oxides are known to generate much higher charge magnitudes as a function of pH than sparingly soluble salts (Hun87).

The modeling of the acid-base character of amphoteric oxides was developed by Healy and White (Hea78, Hea80) to represent the development of surface charge as a function of pH. The ratio of the concentration of surface species are controlled by the following surface dissociation constants.

$$K_{+} = \frac{[AH][H^{+}]_{s}}{[AH_{2}^{+}]} \tag{2-6}$$

$$K_{-} = \frac{[A^{-}][H^{+}]_{s}}{[AH]} \tag{2-7}$$

The net surface charge density of the interface, σ, is related to the number of surface groups per unit area, N_s, by the following relationship.

$$\sigma = eN_{s}\frac{[AH_{2}^{+}]-[A^{-}]}{[AH]+[AH_{2}^{+}]+[A^{-}]} \equiv eN_{s}\alpha \tag{2-8}$$

The fraction α has a range of plus to minus one, and the quantity relates the net number of charge sites to the total number of dissociation sites. The surface concentration of potential determining ions $[H^+]_s$ is related to the bulk concentration $[H^+]$ by the Boltzmann factor.

$$[H^{+}]_{s} = [H^{+}]\exp\left(-e\Psi_{0}/kT\right) \tag{2-9}$$

In a combined expression, the surface charge and the surface potential Ψ_0, are related by the dissociation constants K_+ and K_-.

$$\sigma = eN_s \frac{(H^+ / K_+)\exp(-e\Psi_s / kT) - (K_- / H^+)\exp(e\Psi_s / kT)}{1 + (H^+ / K_+)\exp(-e\Psi_s / kT) + (K_- / H^+)\exp(e\Psi_s / kT)} \qquad (2\text{-}10)$$

The Double Layer Model

The presence of electric charge on a particle in aqueous solution causes oppositely charged ions to be attracted to the charged surface. The counter charge may be either a diffuse layer, or an adsorbed layer and a diffuse layer. This model is called the double layer to reflect the two layers: the adsorbed surface layer or Stern layer and the diffuse layer of counter ions near the surface. The diffuse or Gouy-Chapman layer can extend a appreciable distance from the surface of a particle (Hun87).

The structure of the double layer describes the distribution of ions near the particle surface, as shown in Figure 2-5 (Ada90). The surface exhibits a surface potential Ψ_0. The surface potential arises through various mechanisms dependent upon the colloid and environment. The Stern or Helmholtz layer is composed of adsorbed ions which may be transient. The adsorbed ions can only approach as closely as their hydrated radius for cations, or ion radius for anions. As no species exist between the surface and the adsorbed ions, the potential difference between the surface and the Stern layer Ψ_s, is linear. The adsorption of ions in the Stern layer is related by an adsorption function similar to the Langmuir expression (Ada90).

$$\frac{\Theta}{1-\Theta} = C\exp\frac{ze\Psi + \Phi}{kT} \qquad (2\text{-}11)$$

Θ is the fraction of the surface covered by adsorbed ions, C is a constant and Φ refers to

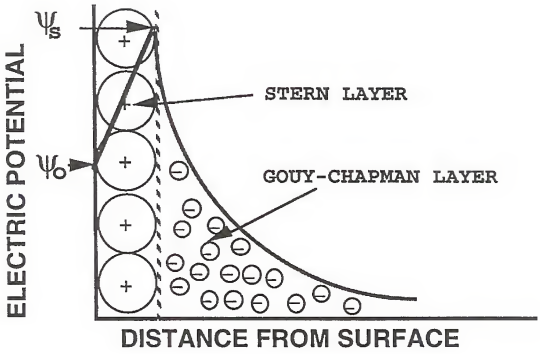

Figure 2-5. Electrical double layer interface indicating strong cation adsorption at the interface and diffuse anion cloud decreasing with distance from the surface (Hun87).

the chemical contribution to the adsorption energy of the ions in the Stern layer to the surface.

In the Gouy-Chapman layer, counter ions are attracted to the surface charge, and like ions are repelled. Thermal motion keeps the ions in the diffuse layer from becoming attached to the surface. The electrical potential in the diffuse layer decays by the Boltzman equation from the Stern potential to zero.

$$n_k = n_{k0} \exp\left(\frac{-z_i e\Psi(x)}{kT}\right) \qquad (2\text{-}12)$$

n_{k0} is the concentration in the bulk of the solution of ion k, k is the Boltzmann constant, and T is the absolute temperature. The charge density of the solution, ρ, is the sum of the ionic charges per unit volume.

$$\rho = \sum z_k e n_k = \sum z_k e n_{k0} \exp\left(\frac{-z_k e\Phi}{kT}\right) \tag{2-13}$$

The relation of the charge density to the electrical potential Φ is given by the Poisson equation.

$$\nabla^2\Phi = -\rho / \varepsilon\varepsilon_0 \tag{2-14}$$

ε is the dielectric constant of the liquid phase, ε_0 is the permittivity of free space, and ∇^2 is the LaPlacian operator. The negative sign is used in the equation because as the surface is assumed positively charged, and thus the potential in the solution is negatively charged. By incorporating the Boltzmann charge density expression into the Poisson equation, the Poisson-Boltzmann equation is derived, to relate the potential as a function of distance from the interface.

$$\nabla^2\Phi = -\frac{1}{\varepsilon\varepsilon_0}\sum z_i e n_{i0} \exp\left(-\frac{z_i e\Phi}{kT}\right) \tag{2-15}$$

A universal, exact analytical solution for this equation does not exist, and several simplifying assumptions have been used for special cases (Hun87).

Surface charge density is determined by integrating the net charge of the double layer from the surface to infinity, and reversing the sign of the charge. Therefore it has the same sign as the potential.

$$\sigma = -\int_a^\infty \rho dr = \int_a^\infty \varepsilon\varepsilon_0 \nabla^2\Phi dr \tag{2-16}$$

Although the Poisson-Boltzman equation must be solved for specific boundary conditions, analytical solutions for simplified cases allow predictions for the probability of agglomeration to be derived. A common simplification used in colloid science is the Debye-Huckel approximation, in which the surface potential is assumed to be relatively small (~25 mV). Under these conditions, the expression for the Poisson-Boltzman equation for a flat plate is as follows.

$$\nabla^2\Psi = \frac{8\pi n_0 z^2 e^2 \Psi}{\varepsilon\varepsilon_0 kT} = \kappa^2\Psi \tag{2-17}$$

where κ is the Debye length and $1/\kappa$ is considered to be the ion atmosphere radius. κ^2 can be calculated from the expression:

$$\kappa^2 = \frac{4\pi e^2}{\varepsilon\varepsilon_0 kT}\sum_i n_i z_i^2 \tag{2-18}$$

The summation term divided by two is the ionic strength of the solution, and n_i and z_i are the concentration and valence of the ions in solution. Highly concentrated ionic solutions, or the presence of highly charged ions can cause the ion atmosphere radius to collapse. This allows particles to approach very closely and aggregation can occur due to van der Waals forces. The distribution of ions as a result of the surface potential in the Gouy-Chapman layer is determined from the solution by the simplified Poisson-Boltzmann equation (Ada90).

$$\Psi_j(r) = \frac{z_j e}{\varepsilon\ \varepsilon_o}\exp(-\kappa r) \tag{2-19}$$

Zeta Potential

Zeta potential is the potential at the "slipping plane" between the moving and stationary phases, where the potential in the bulk of the liquid phase is considered to be zero. It cannot correspond to the potential nearer to the solid phase than the plane of closest approach of fully hydrated counter ions.

Zeta potential measurements determine the potential away from the surface beyond which the ordered solvent layers are no longer bound to the surface. This is affected by ionic strength of the solvent (i.e. the concentration of ions in the solvent). The Stern assumption is that the zeta potential is measured at the inner Helmholtz plane where the centers of the adsorbed ions lie on the surface. Alternatively, the zeta potential can be assumed to lie at the outer Helmholtz plane; the distance of closest approach of fully hydrated ions in solution. Specifically adsorbed ions will likely be dehydrated and thus closer to the surface as opposed to the distance of approach of fully hydrated ions.

Morphological Control of Precipitates

The morphology of a precipitate dictates processing behavior of a material, and is of fundamental interest in synthesis. Shape is influenced by internal crystal structure, environment and temperature. An amorphous precipitate will generally be spherical as the surface energy is isotropic, but a crystalline product will develop facets corresponding to low energy habit planes. External conditions that affect morphology include pH, temperature, reactant concentration and proportion, the presence of additives, solvent interactions and agitation.

The crystal morphology relates to either the equilibrium shape determined by the surface energy of the interface, or to growth shapes dependent on the formation mechanism. Surface energy is a function of both the solvent or additive adsorption on the interface and the material crystal structure. Growth rates of crystal habit planes depend on the mechanism of addition of solute to the precipitate and the supersaturation. The effect of adsorbates is to either reduce habit plane surface energy or slow their growth so that they are not eliminated. By considering the effects of the variables involved in crystal growth, control of the desired particle shape can be realized.

Equilibrium Shape

The derivation of the equilibrium shape of a crystal was first developed by Wulff (Wul01). Assuming that a crystal will minimize the sum of the products of surface energy and area, a crystal with anisotropic surface energy will develop facets to reduce the surface energy component of the system (Cur85). The surface energy properties of a crystal are modeled by the Wulff plot, which is a three dimensional vector representation of the surface energy of the crystal. Each crystal orientation is represented by a vector centered at the origin of magnitude equal to the surface energy. Faceted crystals exhibit pointed minima or cusps corresponding to facets with lower values of surface energy.

By considering the condition of mechanical equilibrium for such a crystal (DeH93), the surface energy of a plane {hkl} divided by its perpendicular distance from the center of mass of the particle to the facet, λ_{hkl} is equal to a constant.

$$\frac{\gamma_{hkl}}{\lambda_{hkl}} = \frac{kT}{2V_m} \ln \frac{p}{p_0} = \text{constant} \qquad (2\text{-}20)$$

V_m is molecular volume and p and p_0 are the actual and equilibrium vapor pressure of components. Liquid phase growth assumes concentration terms in place of pressure. This constant is equal for all facets, {hkl}. The central distance λ_{hkl} is, therefore, proportional to the surface energy of the face. An equilibrium shaped crystal will be dominated by those facets which have the lowest free energy according to the condition that $\sum_{hkl} \gamma_{hkl} A_{hkl}$ is minimized, where A_{hkl} is the area of facet {hkl}.

This derivation was performed for the solid-vapor interface, and does not consider the complications present in growth from solution. Surface energy is highly dependent upon the environment in which the crystal exists. The presence of solvent molecules can significantly reduce surface energy by interacting with the surface, and the presence of ions can modify pH or surface structure via adsorption. An explanation of the variation of surface energy with environmental effects is needed to understand the effect of solution conditions on the equilibrium shape.

Compositional Variation of Surface Energy

Surface energy is an interfacial property of thermodynamics, and texts on the subject should be consulted for in depth discussions (Def66, DeH93, Lup83, Sut95). It utilizes surface excess properties, which describe the difference between the energy in the real system and the energy computed from the hypothetical Gibbs model interface (DeH93). All excess properties like surface energy are defined per area of interface. Adsorption for example is a surface excess of one of the components in the system.

The thermodynamic property of surface energy has been defined in several ways by different authors. DeHoff describes the surface energy as the change in internal energy

of a two phase system with a change in internal area (DeH93). Adamson defines surface energy as the reversible work needed to increase the surface area of a phase (Ada90). In terms of specific surface excess properties, the definition of surface energy, γ, is given by DeHoff (DeH93).

$$\gamma \equiv U^s - TS^s - \sum_k \mu_k \Gamma_k \tag{2-21}$$

In this definition, U^s and S^s are the internal energy and entropy, μ_k is the chemical potential of each component k and Γ_k is the specific adsorption of each component. Surface energy is usually reported in terms of mJ/m^2, and is dependent upon the environment of measurement and crystallographic orientation.

Surface energy variation with composition is given by the Gibbs adsorption equation. The change in surface energy for uncharged components at constant temperature and pressure is given by the Gibbs adsorption isotherm over all components, k (Ros88).

$$d\gamma + S^s dT = -\sum \frac{n_k^\sigma}{A} d\mu_i = -\sum \Gamma_k d\mu_k \tag{2-22}$$

$$\Gamma_k = n_k^\sigma / A \quad \{\text{moles/m}^{-2}\} \tag{2-23}$$

Electrical Variation of Surface Energy

Ionic materials like most ceramics require additional terms to represent their electrochemical behavior. The surface of ceramics develop charge and exhibit polarization. The presence of an external field causes the potential of charged components to vary with position within that field. The saturated components in the liquid phase are affected as a result, and the effect of the field necessitates the use of

electrochemical potential. The electrochemical potential, η_k^α, is defined by the following relation (Ada90, Gra47, Haa69, DeH93).

$$\eta_k^\alpha = \mu_k^\alpha + z_k e\Psi \tag{2-24}$$

where z_k is the valence of the ion including sign, e is the electron charge and Ψ is the electrical potential. The condition for equilibrium in an electrostatic field requires that the electrochemical potential gradient is zero (DeH93, Haa69). The gradient in chemical potential and thus composition depends on the sign of the ion, z_k.

The presence of surface charge at the interface affects the particle's equilibrium shape through the effect of electrical charge on surface energy (Gra42). A direct substitution of electrochemical potential for chemical potential in the Gibbs adsorption equation is not strictly accurate as charge components are related through the condition of electroneutrality. One component must be dependent to maintain charge balance (Gra42).

Electrocapillarity theory requires a model of the behavior of the electrode or surface in order to relate electrical properties to observable phenomena. The ideal polarized electrode (IPE) is applicable to the ceramic interface. The IPE has the property that no continuous current is allowed to flow as the potential difference is altered slightly from the ideal state. In the case of a ceramic surface, the ideal electrode can be assumed as long as there is no dissolution of the surface. For intermediate pH's, this assumption is sufficient. The variation of surface energy with the potential at the interface is given by Grahame and Whitney (Ada90).

$$d\gamma + S^s dT = -\sum^{c} \Gamma_i d\mu_i - F\sum^{\beta} \Gamma_i z_i d\left(\Phi^\beta - \Phi^\alpha\right) - \sum^{c} \Gamma_i z_i d\mu_{dep} \tag{2-25}$$

F is the Faraday which is equal to Avagadro's number of electrons (96,490 Coulombs), and Γ_k is the specific adsorption of components of valence z_k. As the condition of electroneutrality requires that charge cannot be varied independently, one component of the system must be made dependent. The Gibbs adsorption equation uses a substitution for chemical potential of the components that reflects the dependent component.

$$\mu_k = \eta_k + z_k \eta_{dep} \tag{2-26}$$

This substitution gives the relationship between components. If we assume that $[H^+]$ is the dependent component, the electrochemical potential of $[H^+]$ becomes related to the potential of all other components. As a result, the expression for the change in free energy of the electrochemical interface is written as follows.

$$d\sigma + S^s dT = -\varepsilon^\beta d\left(\Phi^\beta - \Phi^\alpha\right) - \sum_k^{c'} \Gamma_k d\left(\eta_k + z_k \eta_{dep}\right) \tag{2-27}$$

Here the number of components, c′ is equal to c-1.

The quantity ε_β is a thermodynamic quantity proposed to be equivalent to the surface charge density.

$$\varepsilon^\beta = F \sum^{\beta} \Gamma_k z_k = \delta \tag{2-28}$$

However, this term for excess surface charge is only strictly valid for a completely polarized surface (Ada90). The presence of ions on either side of the surface makes the choice of the dividing surface a variable for the determination of the value of the specific surface adsorption of the surface components.

For a constant composition, the electrocapillarity equation reduces to the Lippmann equation (Ada90).

$$\left(\partial\gamma/\partial E\right)_{\mu} = -\delta \qquad (2\text{-}29)$$

Crystal Structure Theory

Early theories of morphology were based on aspects of crystal structure. Donnay and Harker proposed a theory that linear growth velocity of a habit plane is inversely proportional to interplanar spacing (Don37). Observed crystal faces are those with the highest "reticular densities", and the degree of density determines the prominence of the form. Reticular density is related to the packing arrangement of the surface ions or molecules.

Surface energy was incorporated by Hartman and Perdok (Har55) by consideration of periodic bond chains (PBC). A PBC is an uninterrupted chain of strong bonds within the crystal lattice (Har55, Har73). Crystal faces are described by the number of periodic bond chains parallel to the facet. A flat face (F) has at least two PBC's parallel to the surface, stepped faces (S) have one PBC parallel to the surface, and kinked faces (K) have no PBC's. Kink sites can form the most bonds with growing components. Linear growth is assumed to be fastest in those directions in which attachment energy is greatest. That is, kinked faces have the greatest linear growth rate, G, and therefore are eliminated quickly. The flat faces are the slowest growing and therefore dominate at low supersaturations. Figure 2-6 shows the formation of F, S, and K faces for a cubic structure.

Hartman and Bennema (Har80) describe the attachment energy, E_{att}, as a habit controlling factor. An expression is derived for the specific surface energy of a face {hkl} based on the interaction energy per mole of a slice d_{hkl} with the i^{th} underlying site.

$$\gamma = \left(fZd_{hkl} \sum iE_i \right) / 2V_{UC} \qquad (2\text{-}30)$$

In this equation, f is a conversion factor, Z is the number of molecules in the primitive unit cell, d_{hkl} is the interplanar distance of face {hkl}, and V_{UC} is the volume of the primitive unit cell. The attachment energy is defined as the bond energy released when one building unit is attached to the surface of a crystal face. Increasing attachment energy increases relative growth velocity. The attachment energy model only considers bond energies, which is incorrect for cases other than vapor phase synthesis.

Growth Morphology

The shape of a precipitate grown from a supersaturated liquor depends less on surface energies than the growth rates of the characteristic facets (Soh92, Wal79, Klu93, Mat92). The growth mechanisms of crystals are understandably necessary to understand the rate of habit movement. The BCF theory describe the stability of a face with respect to the crystal structure, but the mechanism of nucleation and growth cannot be dismissed in a discussion of morphology.

Nucleation

The driving force for nucleation lies in the degree of supersaturation of the solute expressed as the difference in chemical potential. All materials have some degree of solubility within a solvent. If the level of concentration of the material components are in excess of equilibrium, then precipitation will occur in order to restore equilibrium chemical potential. The difference in chemical potential, $\Delta\mu$, of a component is related to the equilibrium concentration c_0 and the actual supersaturation, c.

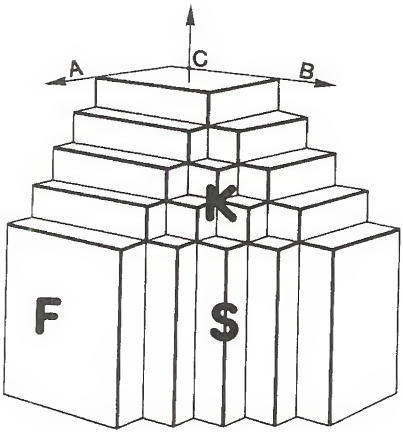

Figure 2-6. Flat, stepped and kinked faces in the periodic bond chain model for a cubic crystal structure (Rin96).

$$\Delta\mu = kT\ln\left(\frac{c}{c_0}\right) \tag{2-31}$$

The supersaturation can be represented by several expressions such as $S = c/c_0$, $\sigma = (c-c_0)/c_0$ or $c - c_0$ (Boi88). Relative supersaturation is given by $\sigma = (c-c_0)/c_0 = S - 1$.

The formation of a crystal from homogeneous solution requires the development of a stable nuclei. Nuclei formation is broadly classified as either homogeneous or heterogeneous. Homogeneous nucleation occurs without the interaction of an interface with another phase and requires high supersaturation levels. A more common occurrence

is heterogeneous nucleation in which an impurity phase assists in the formation of a nuclei (Soh92).

Homogeneous Nucleation

Classical approaches determine the critical size for a homogeneous nucleus as a balance between the decrease in Gibbs free energy from the formation of the bulk phase and the increase in energy through the formation of the interface. For a spherical cluster of radius r, the formation energy is expressed as

$$\Delta G_f = \frac{4}{3}\pi r^3 \Delta G_v + 4\pi r^2 \gamma \tag{2-32}$$

ΔG_v is the bulk free energy of the bulk volume. The balance of the volume energy decrease and the increase in energy due to the surface creates a critical size for a stable nucleus. Nuclei that exceed this size are thermodynamically stable for increasing growth. The Gibbs-Thomson equation can be used to relate the volume free energy to supersaturation.

$$\Delta G_v = \frac{\Delta \mu}{V_m} = \frac{\rho}{M} RT \ln S \tag{2-33}$$

ρ is the density of the solid phase, M is the molecular weight, and V_m is the molecular volume. The critical size for a stable nuclei, r^*, is found from the derivative of the free energy of formation as follows.

$$r^* = -\frac{2\gamma}{\Delta G_v} = -\frac{2\gamma V_m}{kT \ln S} \tag{2-34}$$

The free energy of formation is thus:

$$\Delta G^* = \frac{16\pi\gamma^3 V_m^2}{3(kT\ln S)^2} \tag{2-35}$$

The rate of nucleation is generally assumed to follow an Arrhenius form like that of chemical reaction kinetics. The rate of nucleation, J, is given by the expression:

$$J = K\exp\left(-\frac{\Delta G^*_f}{kT}\right) = K\exp\left(-\frac{16\pi\gamma^3 V_m^2}{3k^3T^3(\ln S)^2}\right) \tag{2-36}$$

The constant K relates the diffusional energy barrier to the jump frequency. Above a critical supersaturation, an exponential burst of precipitation occurs. Increases in supersaturation increase nucleation rate, as does a decrease in surface energy.

The kinetic equations for determining the activation energy for nuclei formation do not consider the formation of a surface energy, but rather the interaction of a molecule and a cluster (Ruc90). The formation of a nucleus is modeled as the aggregation of components resulting from collisions or aggregation. The collisions of multiple clusters is not considered as the probability of this event will be rare compared to that of individual collisions. A stable cluster exists at some number of components N. Dynamic equilibrium in the system gives expressions for the nucleation and growth of a nucleus.

Nucleation $\quad A_N + A_1 \rightleftharpoons A_{N+1}$

Growth $\quad A_{N+1} + A_1 \rightleftharpoons A_{N+2}$

The expression for the critical radius of a nuclei, R_*, is complicated and requires a numerical solution. Comparison with the classical theory shows greatest difference at high supersaturation, but general trends and phenomena agree with classical results (Ruc90). The nucleation model states that nucleation rate is proportional to the ion

concentration as a power law expression, with an exponential, p, between 2 and 6 (Wal79).

$$J = k_1 c^p \tag{2-48}$$

The specific differences due to the nucleation of ionic species were addressed by Chiang et al. (Chi88a) and Chiang and Donohue (Chi88b, Chi88c). According to this theory, addition of material to a cluster of ions requires the formation of neutral ions on the surface before integration into the lattice can occur. Nucleation rate is related to growth rate by a power law with an exponential which depends on the particular mechanism of material addition.

Heterogeneous Nucleation

Heterogeneous nucleation involves the use of another solid phase as a template to reduce the activation energy needed for the formation of a stable nucleus. The lattice mismatch between dissimilar materials will create dislocations and/or surface stress (Wal79). Nucleation is distorted by this mismatch, and the solid-solid interface modifies the surface energy requirements. Liquid phase precipitation models have been applied to solid-solid interface precipitation (Soh92).

$$\Delta G^*_{het} = \frac{\beta_g \gamma^2 \nu^2 f(\Theta)}{\Phi^2} = \Delta G^*_{\text{hom}} f(\Theta) \tag{2-38}$$

β_g is a geometric factor relating volume to surface area, ν is the number of ions in a neutral molecule, Φ is the affinity defined by the change in chemical potential due to precipitation, and $f(\Theta)$ depends on the wetting angle of the solid phase by the liquid.

$$f(\Theta) = \left(2 - 3\cos\Theta + \cos^3\Theta\right)/4 \tag{2-39}$$

The function $f(\Theta)$ in the case of solid-solid interface relates the nucleation effect of the substrate without carrying a physical meaning, and may have a different expression. When the free energy of the precipitate-solution interface is greater than the difference between the precipitate-substrate interface and the substrate-solution interface, the activation energy for heterogeneous nucleation is less than that of homogeneous nucleation.

Growth Rates

Solvents affect growth rates by the transport of supersaturated solute through a quiescent layer of solvent and absorbed solute at the solid-solution interface. The steps of integration of material at the solid solution interface involve diffusion from the bulk to the surface, surface adsorption, surface diffusion to a high energy site, desolvation, and integration into the lattice. The released solvent must then counter diffuse from the surface into the bulk (Nan87). The slowest of these processes becomes rate limiting. Based on diffusion, the rate of mass transport, *dm/dt*, relates to the supersaturation by the following equation.

$$dm/dt = \frac{D}{\delta} A(c - c_0) \tag{2-40}$$

A is the interfacial area, c is the supersaturated concentration and δ is the thickness of the laminar film of adsorbed solvent. By increasing shear rate in the solution (agitation), the film thickness is reduced and the growth rate increased.

Modifications to the diffusion transport theory were made by considering the incorporation of components into the crystal as a rate limiting mechanism. Reaction for the diffusion and the surface reaction are represented by separate equations (Nyv85).

$$dm/dt = k_d A(c - c_0) \tag{2-41}$$

$$dm/dt = k_r A(c - c_0) \tag{2-42}$$

where k_d and k_r are the mass transfer coefficients for the diffusion and the surface reaction. These equations can be combined through an overall coefficient K defined as follows.

$$\frac{1}{K} = \frac{1}{k_d} + \frac{1}{k_r} \tag{2-43}$$

The diffusion mass transfer coefficient is related to the laminar thickness of the solvent layer and the diffusion coefficient by $k_d = D/\delta$. If the surface reaction is fast, the coefficient due to diffusion is rate limiting. By increasing the agitation, the growth rate increases due to compression of the solvent layer until a maximum rate is achieved at which point the growth of a crystal layer is controlled by surface integration mechanisms (Nyv85, Soh92, Wal79).

The overall growth rate in terms of characteristic dimension G is given by the following expression.

$$G = \frac{dL}{dt} = K_1(c - c_o) = K_1 S \tag{2-44}$$

K_1 is a constant, and S is the supersaturation. Each habit plane will have a different rate constant. The final morphology will depend on the relative growth rates of each habit plane (Boi88).

Surface Integration Models

The mechanism through which new material joins the crystal depends on the nature of the interface. For a perfectly smooth interface with no defects, growth of a new

surface layer is modeled via the adsorption of solute components and their coalescence to form a stable nucleus. The rate at which the nucleus spreads to cover the entire surface determines the type of growth. Mononuclear growth occurs when the spread of the nucleus is fast, such as in the case of a small crystal where there is not much area needed for growth. At the opposite extreme is polynuclear growth in which nuclei form on growing nuclei before an entire surface layer is covered. In the birth and spread model, nuclei are considered to spread at a constant rate independent of size. The overall growth rate is given as follows.

$$G = \frac{dL}{dt} = K_2 (S-1)^{2/3} [\ln S]^{1/6} \exp\left[-\frac{K_3}{T^2 \ln S}\right] \qquad (2\text{-}45)$$

K_2 and K_3 are constants. The formation of two dimensional nuclei is the rate limiting step of this mechanism. In this case, bulk diffusion and the surface reaction are ignored. However, this model fails to explain growth at low supersaturation.

Screw Dislocation Growth

Burton, Cabrerra and Frank (Bur51) proposed that the activation energy for growth of a plane surface would be reduced by the presence of a screw dislocation. The dislocation would provide edge sites for the addition of components which would eliminate the need for the formation of two dimensional nuclei.

The growth rate is expressed differently for cases of low supersaturation and high supersaturation. For the limiting cases, the growth rate is expressed as follows.

Low supersaturation $$G = K_4 \left(S^2 / S_c \right) \qquad (2\text{-}46)$$

High supersaturation $$G = K_5 S \qquad (2\text{-}47)$$

Here K_4, K_5, and S_c are constants. At low supersaturation, the growth rate is parabolic but growth becomes linear at high supersaturation. According to this theory, growth is controlled by surface diffusion and the distance between kinks or surface steps which is itself a function of supersaturation and crystal size. This derivation assumes vapor phase growth.

Chernov modified the BCF theory by considering the bulk mass transfer limitations between vapor and liquid phase growth (Mye93). Vapor growth is not limited by mass transfer due to its rapid speed. The presence of solvent limits the rate of material transfer to the crystal surface, creating bulk diffusion control of growth. The parabolic dependence at low supersaturation is also predicted. The importance of hydrodynamic conditions in crystal formation is therefore satisfied.

Surface Reaction Theory

Nielson (Nie83) and Estrin (Est93) describe the kinetics and mechanisms for ionic crystal growth from solution involving less soluble solutes. Models assume that the rate limiting step for the growth rate is the surface reaction.

$$G = K_6(S-1)^q \tag{2-48}$$

K_6 is a constant, and q is the order of the reaction. Parabolic growth has a reaction order of two, and is dominant for sparingly soluble salts such as $BaSO_4$, $CaCO_3$, and $CaC_2O_4{\cdot}H_2O$.

A chemical consideration of growth has been developed by Chiang and Donohue which considers the electrical double layer interface of colloids (Chi88b, Chi88c). In ionic crystals, surface lattice sites are treated as reactant species, and growth is considered to proceed via chemical reaction with adsorbed ions. By consideration of the linear

adsorption isotherm from the electrical double layer, second order dependence of growth rate on supersaturation is derived. Ionic crystals are represented by either the surface reaction/molecular integration model (Mechanism 1) or sequential ionic integration (Mechanism 2). In Mechanism 1, component ions A and B adsorb separately to the surface, and must diffuse until they react to form an adsorbed surface species AB. This surface species AB then migrates until it can be integrated at a lattice site. In Mechanism 2, component ions adsorb and integrate into the crystal separately.

Those methods controlled by bulk diffusion have growth rate expression similar to equation 2-45, with separate rate constants for each ion, and equilibrium concentration equal to the cation or anion concentration at the interface. The growth rates of cation and anion are equal in order to satisfy electroneutrality (Soh92).

Morphological Forms Resulting from Growth Rates

As can be seen, facet growth rates are limited either by component diffusion to the interface or by the integration mechanism into the lattice. Lattice integration has been modeled for rate limiting mechanisms of integration. Addition may be direct for kink or step facets, but flat faces require the birth of two dimensional nuclei. Growth of the surface nuclei can become the rate limiting step of facet growth. The mechanism of component addition can require the formation of neutral surface species before integration with the lattice. Surfaces which support direct integration will have faster growth rates.

Habit plane growth rates are considered as functions of supersaturation levels. Near equilibrium, growth rates are proportional to surface energy. Low supersaturation levels promote compact shapes with habit planes corresponding to faces in the BCF

theory. The surface is largely composed of flat facets as these surfaces have the lowest surface energy. Side and kink facets provide more sites for component addition, and therefore have higher surface energy. Integration of components will be swift, and thus these facets will have growth rates that are diffusion controlled. Lower diffusion rates will increase the amount of surface area of S and K faces on the crystal. As supersaturation increases, the particle morphology deviates from equilibrium. Diffusion of components is increased, and component adsorption on the surface and integration with the lattice likewise increase. The particle surface will become dominated by facets which are interface controlled. Increases in stirring rate or temperature increase diffusion rates.

Dendrites are formed under conditions in which there are concentration gradients in the adsorbed layer of solvent. This is a function of fast growth rates (Wal79). Hydrodynamic forces reduce the thickness of the diffuse solvent layer near sharp edges faster than in the center of planes (Soh92). The higher concentration near the edge either creates a higher driving force for precipitation or permits faster rates of mass transport, and this creates protrusions. If the supersaturation is high enough, growth will continue and form elongated structures. Whisker formation is generally associated with the screw dislocation model of Burton Cabrerra, and Frank (Bur51). Impurity adsorption on a specific family of habit planes can also promote this type of growth.

The Effect Of Solvent

Solvents affect the morphology of precipitates both by influencing surface energy and by modifying growth rates via transport properties. The interaction of the solvent

with the crystal structure establishes a solvent specific Wulff plot for the system. The supersaturation and growth rate of the crystal dictate the growth form.

The nature of the solvent will influence the stability of a growing interface by the types of intermolecular bonding mechanisms that the solvent supports. The role of the periodic bond model with respect to solvent properties states that the solvent will adsorb to the interface structure of the habit plane. Faces with more PBC's are expected to adsorb more strongly, and therefore reduce surface energy to a greater degree. It is likely that solvent will order at the interface, and the order may create PBC's that are not related to the crystal structure (Boi88). The solvent characteristics can affect the type of interfaces stabilized in the crystal. The interaction of a polar solvent like water with oxygen ions in a crystal can lead to the promotion of specific habit planes (San97). Compounds containing polar molecules like -OH or $-NH_2$ have habit planes that are stabilized by solvents which can exhibit hydrogen bonding (Wal79).

Growth of an interface is specifically affected by the solvent's transport properties. The viscosity, density, mass transport, heat transport and diffusivity of the solvent at temperature will affect growth rates (Klu93). Viscous forces arise from solute-solvent and solvent-solvent interactions. Solvation forces will dictate the structure of the solvent near the solid-solution interface, and prediction of solvation effects on viscosity remain under investigation (Isr92, Man96).

Electrolyte solutions have been modeled by Myerson et al. for the effect of electrolyte concentration on viscosity and diffusivity (Mye97). Ions in electrolyte solutions affect the thermodynamics of the solvent as a result of the electrostatic forces between them. In supersaturated solution, the solvent diffusivity is strongly decreased as

supersaturation increases. Solvent viscosity is less dependent upon solute concentration. The difference in behavior reflects the formation of ion pairs which diffuse at slower rates than individual ions, and supersaturated solutions will have higher concentrations of ion pairs or aggregates (i.e. unstable nuclei).

Solvation of the surface will affect crystal growth. Growth requires the addition of growth units, whether individual ions or surface ion pairs. These units are generally solvated, and after integration into the solid, the liberated solvent must diffuse to the bulk. The diffusivity of the solvent can contribute to the growth rate of a facet. Complexes can form in solution that "capture" components. The additional bonds must be broken before integration can occur, and this increases the activation energy for growth. A lower rate results. Higher adsorption energy of solvent stabilizes surface energy and lowers growth rate (Klu93).

The effect of hydrogen bonding on surface energy is hard to quantify, as the structure of hydrogen bonds is not well characterized. It is known that the interaction energy is proportional to the inverse second power of distance (Isr92), and that highly polar molecules like water can form discrete layers of polarized molecules (Hor90). The arrangement of these molecules produces an oscillatory force close to the surface as measured by atomic force microscopy (Duc94). Hydrogen bonding should be highly dependent on the arrangement of surface ions and the surface charge.

Surface Energy Reduction via Solvent Interactions

The solute-solvent interface controls the energetic stability of a habit plane during precipitation. Solvent molecules interact with the surface through intermolecular potentials. Table 2-4 gives the intermolecular potentials typical of ionic solids (Isr92).

Table 2-4. Intermolecular and surface forces in vacuum. (Adapted from Isr92).

Type of Interaction	Interaction Energy w(r)
Charge-Charge (Coulomb energy)	$\frac{Q_1 Q_2}{4\pi\varepsilon_0 r}$
Charge-Dipole (fixed) Charge-Dipole (freely rotating)	$\frac{-Qu\cos\Theta}{4\pi\varepsilon_0 r^2}$ $\frac{-Q^2u^2}{6(4\pi\varepsilon_0)^2 kTr^4}$
Dipole-Dipole (fixed) Dipole-Dipole (freely rotating)	$\frac{-u_1u_2[2\cos\Theta_1\cos\Theta_2-\sin\Theta_1\sin\Theta_2\cos\Phi]}{4\pi\varepsilon_0 r^3}$ $\frac{-u_1^2u_2^2}{3(4\pi\varepsilon_0)^2 kTr^6}$ [Kessom energy]
Charge-nonopolar	$-Q^2\alpha \Big/ 2(4\pi\varepsilon_0)^2 r^4$
Dipole-non-dipolar (fixed) (freely rotating)	$\frac{-u^2\alpha(1+3\cos^2\Theta)}{2(4\pi\varepsilon_0)^2 r^6}$ $\frac{-u^2\alpha}{(4\pi\varepsilon_0)^2 r^6}$ [Debye energy]
Hydrogen Bonding	proportional to $-1/r^2$ complicated, short range

Interaction energies can be divided according to the type of interaction, of which dispersive, polarization, and hydrogen bonding are usually considered for ionic solids. The interaction energy, or pair potential between atoms or molecules $w(r)$, must accommodate both the effects of the solvent as well as the solute.

In practical terms, a solvent that has an appreciable dipole moment will become ordered at an electrically charged interface. The degree of ordering will scale with the magnitude of the dipole moment. The change of entropy due to solvent polarization can be measured through the heat of immersion, ΔH_{imm}. The heat of immersion relates the change in surface energy between the solid-vapor and solid-liquid interface, but cannot provide information on the absolute values of the interfacial energy in either state. The heat of immersion will depend on the various components of intermolecular interaction: dispersive forces, polarization, hydrogen bonding, and habit plane effects. The total heat of immersion can thus be considered to be the sum of these interactions.

$$\Delta H_{Imm} = \Delta H^{d}_{imm} + \Delta H^{p}_{imm} + \Delta H^{H-bond}_{imm} + \Delta H^{habit}_{imm} \qquad (2\text{-}61)$$

Predictions of the components due to dispersive interactions have been investigated by Fowkes (Fow63), but qualitative predictions of the components of free energy related to molecular forces have not been well developed. Attempts to understand the role of solvent on surface energy employ models relying of predicting interactions between individual components of the solid and liquid.

The Jackson α Factor

An expression to relate the effect of the solvent molecules near the solid-solution interface was derived by Jackson in 1958 (Klu93). By a consideration of the number of

extra molecules on the surface, the change in free energy of a planar surface can be related to the fractional coverage of the surface, Θ.

$$\frac{\gamma_{tension}}{nkT} = \alpha = (1-\Theta)\Theta + \Theta\ln\Theta + (1-\Theta)\ln(1-\Theta) \qquad (2\text{-}49)$$

$$\alpha = (\Delta H_{solvent}^{dissolution} / RT)\Xi \qquad (2\text{-}50)$$

$\Delta H_{solvent}^{dissolution}$ is the heat of dissolution. α is a "surface entropy factor" and it measures the degree of smoothness of the crystal face at the atomic level. Ξ is the fraction of the total binding energy that binds a molecule to other molecules at the solid-liquid interface. Ξ is equal to n_s/n_b, where n_s and n_b are the number of nearest neighbors on the surface and in the bulk. Low index plane have Ψ values between 0.5 and 1.

The regular solution model has been applied to the α factor for solvents that do not significantly interact with the surface. Such solvents avoid hydrogen bonding, solvation or complex ion formation. Qualitatively satisfactory results were found by assuming the heat of dissolution to be equal to the heat of vaporization plus the heat of mixing. Using an ideal expression for the entropy of mixing, the α factor is expressed as

$$\alpha = \Psi\left[\frac{\Delta H^{fus}}{RT_m} - \ln X_{H,liq}^{sat} + \frac{1}{R}\int_T^{T_m}\frac{\Delta C_p}{T}dT\right] \qquad (2\text{-}52)$$

X is the solubility of the material at temperature T. ΔH^{fus} is the heat of fusion at the melting point. Solvent interaction increases the solubility of the solute and gives a negative heat of mixing. A lower α factor increases the growth rate indicating that higher solubilities promote rapid crystallization (Klu93).

The α factor qualitatively expresses the various growth mechanisms. If α is lower than 3, fast growth occurs with linear relationship to supersaturation. For an α factor

between 3 and 5, step limited growth occurs, and the growth rate is typical of the birth and spread type. For α above 5, growth is dislocation controlled, and a parabolic dependence of supersaturation like that of the BCF model prevails.

Interfacial Cell Model

Liu has developed a model for the interface structure that has shown promise in the prediction of crystal morphologies (Liu97). The model employs an inhomogeneous cell model in which solute composition and concentration, solvent, and impurities are explicitly incorporated. Thermodynamic differences are described by the surface scaling factor, $C^*_{I(hkl)}$.

$$C^*_{I(hkl)} = \frac{\Delta H^{diss}_{A(hkl)}}{\Delta H^{diss}_{A}} = \ln \frac{X_{A(hkl)}}{\ln X_A} \approx \frac{\phi_j}{\Phi_j} \tag{2-53}$$

$\Delta H^{diss}_{A(hkl)}$ is the enthalpy of dissolution at the crystal surface (face specific), and ΔH^{diss}_{A} is the enthalpy of dissolution in the bulk. $X_{A(hkl)}$ and X_A are the mole fraction of solute at the crystal faces {hkl} and in the bulk. ϕ_j is the change in bond energy per structural unit in direction j at the surface and Φ_j is the corresponding energy in the bulk. Calculations of $X_{A(hkl)}$ can be performed using computer analysis, and the effect of solvent at the interface is largely characterized by $C^*_{I(hkl)}$ (Liu97).

The process to characterize morphology with this model requires use of an interfacial structure analysis using computer models. Calculation techniques include Monte Carlo or molecular dynamics techniques, the application of density-functional theory calculation or self-consistent field lattice theory.

The scaling factor is employed in the determination of relative growth rate of a face by the following relationship.

$$G_{hkl}^{rel} \propto \frac{n_{hkl} d_{hkl} X_A^{C^*_{1(hkl)}}}{C^*_{1(hkl)} \xi_{hkl}} \exp\left[- C^*_{1(hkl)} \xi_{hkl} \Delta H_A^{diss} / n_{hkl} kT \right] \quad (2\text{-}54)$$

In this expression, d_{hkl} is the interplanar distance for orientation {hkl}, n_{hkl} is the number of non-coplanar PBC's in crystal slice {hkl}, ξ_{hkl} is the orientation factor equal to E_{hkl}^{slice} / E^{cr} where E_{hkl}^{slice} is the 2D latttice energy. X_A, ΔH_A^{diss} and T are all experimentally measurable. The calculation of the scaling factor is the most elusive parameter. In this model, development of an accurate computational model is needed in order to have successful prediction of morphology.

The Effect of Adsorbates

Adsorbates in crystal growth are used in order to control various characteristics of the growth process. Adsorbates have four primary effects: crystal habit modification, growth rate modification, crystallographic modification, and phase transformation control. Crystal habit modification obviously affects the morphology by specific adsorption of an adsorbate on a specific habit plane or planes. The growth of the adsorbed surfaces is retarded to give that habit plane more dominance over the crystal shape. Examples include the modification of NaCl crystals by urea (Wal79), $CaSO_4$ habit modification by organic derivatives of phosphoric acid (Soh92), and modification of protein crystals by chemically similar proteins (Hir97). The effect of adsorption has been found to increase with increased concentration, but optimum levels of coverage exist. Part of the effect of adsorbates can be attributed to solvent extrusion. By exclusion of

solvent from the interface, the transport of growth units is inhibited. The desolvation of the surface creates an additional activation energy barrier to the integration process.

The behavior of adsorbates can be considered from two extremes. An adsorbate can exist as a strongly bound molecule that is effectively immobile. Adsorbates will preferentially fill kink sites as these sites provide the highest attachment energy. Low concentrations of additive can saturate kink sites quickly. Step sites and face adsorption follow. These three types of adsorption sites were observed experimentally by Boistelle in 1974 (Klu93). Immobile adsorbates can become incorporated into the crystal, and are expected to have greater effects on crystal growth rate. The adsorbate can also interact with the surface structure to generate a "surface phase" that interacts laterally to create a new surface tension.

The reduction in growth rate of a moving step has been related to the presence of strong, immobile adsorbates. The adsorbates pin the growth front, and passage of the growth front creates curvature. The movement of a growth step is postulated to cease when the distance between impurities is less than twice the radius of curvature of the growing interface, ρ_c.

$$v_A = v_P\sqrt{1-2\rho_c d^{1/2}} \tag{2-55}$$

$d^{1/2}$ is the average density of impurities ahead of the step, v_A and v_P are the velocities of the adsorbed and pure surfaces. When impurity concentration pins the growth front, growth will cease. A critical two dimensional nuclei size can be related to impurity adsorption on the surface by the following expression.

$$2\rho_c = \frac{2A\gamma}{kTS} \tag{2-56}$$

A is the lattice constant, and S is supersaturation. A critical nucleus depends inversely with the supersaturation. Low concentrations of adsorbate do not affect growth significantly so that classical derivations hold, but higher adsorbate concentrations require greater supersaturations for growth.

The adsorbate can otherwise be considered to be mobile and diffuse two dimensionally through the surface. Mobile adsorbates are expected to be "swept away" by a growth front, and incorporation into the lattice is less common. Retardation of growth rates is also less severe (Klu93).

Habit modification results from the specific adsorption of an additive on only one type of habit plane. Such adsorption relates to the arrangement of components on that face, as well as the solution chemistry during the reaction. By its presence on the habit plane, growth rates are slowed, and the adsorbed face becomes more dominant on the surface structure (Hir97).

Summary

At the crystal interface, bulk properties of interaction energy are interrupted, and surface ions must compensate either via the transfer of electrons (valence transfer) or by rearrangement of ions to create polarization. Both mechanisms generate surface charge. The presence of the liquid interface provides a reduction of surface energy via the interaction of the solvent molecules. The solvent can interact with the surface by chemical bonding, hydrogen or hydrophobic bonding, dispersive forces, and polarization due to surface potential (Wal79, Par83). The degree of interaction is highly dependent on

the arrangement of ions on each surface, and obviously will differ between habit planes. The composition of the surface in turn will depend on the crystallographic habit plane, potential determining ions in solution, presence of defects in the lattice structure, and the presence of specific adsorbates.

The solvent and method of precipitation affect the resulting morphology of the precipitate. The solvent affects the equilibrium shape by preferentially interacting with crystal facets to reduce surface energy and by influencing the transfer of solvated components to the surface. The stable morphology is a result of a combination of reaction conditions including stirring rate and supersaturation. Growth shapes are transitional shapes in the achievement of the equilibrium shape and are dependent on kinetic and environmental factors (Boi88). Supersaturation and the rate of supersaturation generation are important factors for supply of components for crystal growth, and the incorporation of components into the precipitate can be limited by several mechanisms. These mechanisms include the diffusion of components from the bulk, desolvation of the surface, adsorption of growth units (ions), surface transport of growth units to low energy sites, and the incorporation of components into the lattice, as well as the reverse process of dissolution (Nan87). The stirring rate can affect the rate limiting mechanism for particle growth by influencing the hydration layer of the particle surface, or increasing diffusional transport rates between the bulk solution and the particle surface. Stirring rate and solids loading will control the growth shape of a precipitate as it develops the equilibrium morphology, but the equilibrium shape is not necessarily realized under conditions of growth. Equilibrium morphology will be attained after

annealing at constant solubility product, where material on high energy facets is dissolved and precipitated on low energy facets.

CHAPTER 3

DERIVATION OF THE EQUILIBRIUM SHAPE OF AN ALUMINA PARTICLE WITHIN A SOLVENT

Introduction

Curie first proposed the concept that at equilibrium, a faceted particle will have minimum surface energy by achieving the lowest summation of the products of facet area and surface energy (Cur85). The thermodynamic derivation of the equilibrium shape of a particle has been performed by Wulff (Wul01) and contributions using this derivation have arisen from many authors (Bra75, Cah74, Def66, Her50, Her51, Hof72, Sea94, Sto92). The results of this work indicate that there exists a simple relationship between the pressure in each phase and the distance from the center of mass of the particle. The condition for mechanical equilibrium is as follows.

$$P^c = P^v + 2\gamma_j / \lambda_j \qquad (j = 1, 2, \ldots, F) \qquad (3\text{-}1)$$

P^c and P^v are the pressure within the crystal and vapor respectively, γ_j is the surface energy, and λ_j is the central distance for each facet j. F is the total number of facets for the crystal. The central distance is the perpendicular distance from the center of mass to the surface of the facet. This relationship is the basis for the Gibbs-Wulff construction which states that the ratio of the surface energy to the perpendicular distance is a constant for all facets (DeH93).

$$\gamma_i / \lambda_j = \text{constant} \tag{3-2}$$

This relationship results if the pressure in the vapor (or liquid) phase is identical for all facets. The equilibrium shape is modified by several additional factors resulting from the solid-liquid interface. Surface charge is commonly developed within a solvent (Soh92). The surface charge will affect the fluid pressure near the surface according to the field strength (Ada90). Additionally, the solid-vapor interface does not consider chemical reactions in the transition from one phase to another, and common components are considered to be present in both phases. Solution growth can involve chemical transformation from solution components in the formation of crystal components. The effect of electrically charged species (ions and/or electrons) add the requirement that electroneutrality is maintained within the system. Ceramic oxides require consideration of the above factors in the derivation of equilibrium shape.

Conditions for Equilibrium

This derivation assumes Gibb's model of the interface. The system is assumed to consist of a faceted particle of α-alumina in equilibrium with a liquid solvent which supports ionic species. The components of the α phase are $Al^{3+}(\alpha)$ and $O^{2-}(\alpha)$ ions. No explicit defect structures are considered in this work. The liquid phase is considered to support $Al^{3+}(l)$, $OH^{-}(l)$, and $H^{+}(l)$. The number of species is kept to a minimum for ease of discussion, but additional components could be included in a generalized derivation.

The expression for the total entropy of the hypothetical system is as follows.

$$\partial S'_{sys} = \partial S'^{\alpha}_{hyp} + \partial S'^{l}_{hyp} + S^{s} dA \tag{3-3}$$

The superscripts α and l refer to the alpha and liquid phases, and the prime states that these are extensive thermodynamic properties. S^s is the specific superficial excess entropy of the interface. The use of charged components (ions) requires a consideration of the electrical effects in the derivation. The expression for internal energy can be separated into chemical and electrical components to give the following expression (Ada90).

$$dU'+dE_{pot} = dU'^{\alpha}+dU'^{l}+U^s dA + dE_{pot} \tag{3-4}$$

U′ is the internal energy of each phase (alpha and liquid), U^s is the specific superficial internal energy of the surface, and dE_{pot} is the electrical potential resulting from the phase transition. The change in electrical potential of a species during a phase transition is related to the change in the number of moles by the following equations (Ada90).

$$\partial E_{pot} = \sum_k z_k F(\Phi^{\alpha} - \Phi^{l}) dn_k^{\alpha} = \sum_k z_k F(\Phi^{l} - \Phi^{\alpha}) dn_k^{l} \tag{3-5}$$

Φ is the electrical potential in the bulk of each phase and z_k is the ion valence for each ion,k,. Therefore the expression for the change in internal energy can be expressed as follows (Ada90, DeH93).

$$dU'^{\alpha} = T^{\alpha} dS'^{\alpha} - P'^{\alpha} dV'^{\alpha} + \sum_{k=1}^{c} \mu_k^{\alpha} dn_k^{\alpha} + \sum_k z_k F(\Phi^{\alpha} - \Phi^{l}) dn_k^{\alpha} \tag{3-6}$$

The summation expressions can be combined into the statement recognized as the definition of electrochemical potential, η_k, where F is Faraday's constant.

$$\eta_k = \mu_k + z_k F \Delta\Phi_k \tag{3-7}$$

where μ_k is the chemical potential, and $\Delta\Phi_k$ is the change in electrical potential between phases. Grahame claims that μ_k is not the ordinary chemical potential, as it depends on temperature, local concentration of components and the local electrical field (Gra47).

The expression for the internal energy of the alpha phase is therefore given by the usual expression with the use of electrochemical potential terms instead of chemical potential (DeH93).

$$dU'^{\alpha}_{hyp} = T^{\alpha} dS'^{\alpha} - P'^{\alpha} dV'^{\alpha} + \sum_{k=1}^{c} \eta_k^{\alpha} dn_k^{\alpha} \tag{3-8}$$

This expression can be rearranged to give the differential for entropy of the α phase.

$$dS'^{\alpha}_{hyp} = \frac{1}{T^{\alpha}} dU'^{\alpha} + \frac{P^{\alpha}}{T^{\alpha}} dV'^{\alpha} - \sum_{k=1}^{c} \frac{\eta_k^{\alpha}}{T^{\alpha}} dn_k^{\alpha} \tag{3-9}$$

Corresponding expressions apply to the liquid phase. Using expression 3-3, the entropy of the system can be expressed as follows.

$$\begin{aligned} \partial S'_{sys} = {} & \frac{1}{T^{\alpha}} dU'^{\alpha} + \frac{P^{\alpha}}{T^{\alpha}} dV'^{\alpha} - \frac{1}{T^{\alpha}} \sum_{k=1}^{c} \eta_k^{\alpha} dn_k^{\alpha} + \\ & \frac{1}{T^{l}} dU'^{l} + \frac{P^{l}}{T^{l}} dV'^{l} - \frac{1}{T^{l}} \sum_{k=1}^{c} \eta_k^{l} dn_k^{l} + S^{s} dA \end{aligned} \tag{3-10}$$

The isolation constraints in the system are constant internal energy, constant volume, and conservation of atoms.

$$dU' = 0 = dU'^{\alpha} + dU'^{l} + U^{s} dA \tag{3-11a}$$

$$dV' = 0 = dV'^{\alpha} + dV'^{l} + V^{s} dA \tag{3-11b}$$

$$dm_k = 0 \tag{3-11c}$$

The following relationships result.

$$dU'^{\alpha} = -dU'^{l} - U^{s}dA \tag{3-12a}$$

$$dV'^{\alpha} = -dV'^{l} \tag{3-12b}$$

There is no specific superficial volume as it is defined to be zero. In addition, the relationship between volume and facet area for a polyhedron is given by a geometrical expression (DeH93). The volume of the crystal is thus proportional to the surface area of the facets and the central distance, λ_j.

$$dV^{c} = \frac{1}{2}\sum_{j=1}^{F} \lambda_j dA_j \tag{3-13}$$

The expression for the entropy of the system with internal energy and volume constraints now appears as follows.

$$\begin{aligned} dS'_{sys,iso} = &\left(\frac{1}{T^{\alpha}} - \frac{1}{T^{l}}\right)dU'^{\alpha} + \left(\frac{P^{\alpha}}{T^{\alpha}} - \frac{P^{l}}{T^{l}}\right)\left(\frac{1}{2}\sum_{j-1}^{F}\lambda_j dA_j\right) \\ &- \sum_{k=1}^{c}\left[\frac{\eta_k^{\alpha}}{T^{\alpha}}dn_k^{\alpha} + \frac{\eta_k^{l}}{T^{l}}dn_k^{l}\right] + \left(S^{s} + \frac{U^{s}}{T^{l}}\right)dA \end{aligned} \tag{3-14}$$

Reactions of the crystal with the solvent (i.e. dissolution and precipitation) will now be considered separately and inserted into the derivation upon completion. The conservation of atoms statements are as follows.

$$dm_{Al} = 0 = dn_{Al3+(\alpha)} + dn_{Al3+(l)} \tag{3-15a}$$

$$dm_{O} = 0 = dn_{O2-(\alpha)} + dn_{OH-(l)} + \Gamma_{OH^-}dA \tag{3-15b}$$

$$dm_{H} = 0 = dn_{H+(l)} + dn_{OH-(l)} + \Gamma_{OH-(l)}dA + \Gamma_{H^+}dA \tag{3-15c}$$

Γ is the specific superficial excess concentration of the components. The expression for the electrochemical potentials can be written:

$$-\frac{1}{T}\left(\begin{array}{l}\eta_{Al3+(\alpha)}dn_{Al3+(\alpha)}+\eta_{O2-(\alpha)}dn_{O2-(\alpha)}+\eta_{Al3+(l)}dn_{Al3+(l)}\\+\eta_{OH-(l)}dn_{OH-(l)}+\eta_{H+(l)}dn_{H+(l)}\end{array}\right) \tag{3-16}$$

Substituting for the conservation of atoms,

$$-\frac{1}{T}\left(\begin{array}{l}\left(\eta_{Al3+(\alpha)}-\eta_{Al3+(l)}\right)dn_{Al3+(\alpha)}+\left(\eta_{OH-(l)}-\eta_{O2-(\alpha)}-\eta_{H+(l)}\right)dn_{OH-(l)}\\+\left(-\eta_{O2-(\alpha)}-\eta_{H+(l)}\right)\Gamma_{OH-}dA+\left(-\eta_{H+(l)}\right)\Gamma_{H+}dA\end{array}\right) \tag{3-17}$$

The first two terms give the following reaction equations.

$$OH^{-}(l) \rightleftharpoons O^{2-}(\alpha) + H^{+}(l)$$

$$Al^{3+}(\alpha) \rightleftharpoons Al^{3+}(l)$$

Where chemical (or electrochemical) reactions can be written, the thermodynamic property of *Affinity* is applied to represent the reaction. Therefore, for a reactive interface the following relationships prove useful.

$$dn_k = \sum_r \upsilon_{kr} d\xi_r \tag{3-18}$$

where the variable r designates the different independent chemical reactions possible in the system, υ_{kr} are the stoichiometric coefficients for the components of the reactions, and $d\xi_r$ is a property called the extent of reaction. The extent of reaction is the difference between an initial amount of each component, n_0, and the component amounts at equilibrium, n_f. The extent of reaction determines the number of molecules of each kind in the phase, as well as the electrical charge on each phase. The relative positions and charge magnitude determine the electrical field in the system, thereby determining the electrical energy of the system (Def66).

The affinity of each reaction is given by A_r.

$$A_r = -\sum_k \upsilon_{kr}\mu_k \tag{3-19}$$

Thus the expression for the entropy of the isolated system is as follows.

$$\begin{aligned} dS'_{sys,iso} = &\left(\frac{1}{T^\alpha}-\frac{1}{T^l}\right)dU'^\alpha + \left(\frac{P^\alpha}{T^\alpha}-\frac{P^l}{T^l}\right)\left(\frac{1}{2}\sum_{j=1}^{F}\lambda_j dA_j\right) - A_{O2-}d\xi_{O2-} \\ &- A_{Al3+}d\xi_{Al3+} + \left(S^s - \frac{U^s}{T^l} + \left(\eta_{O2-(\alpha)} + \eta_{H+(\alpha)}\right)\Gamma_{OH-} + \left(\eta_{H+}\right)\Gamma_{H+}\right)dA \end{aligned} \tag{3-20}$$

If we define surface energy to be

$$\gamma_j = U_j^s - TS_j^s - \sum_m \eta_m \Gamma_{mj} \tag{3-21}$$

and let the total surface area, dA, be represented as

$$dA = \sum_{j=1}^{F} dA_j \tag{3-22}$$

then the expression for the entropy of the system results.

$$dS'_{sys,iso} = \left(\frac{1}{T^\alpha}-\frac{1}{T^l}\right)dU'^\alpha + \left(\sum_{j=1}^{F}\left(\frac{P^\alpha}{T^\alpha}-\frac{P^l}{T^l}\right)\frac{1}{2}\lambda_j - \frac{\gamma_j}{T^c}\right)dA_j - \sum_{m=1}^{r} A_m d\xi_m \tag{3-23}$$

The equilibrium conditions are found from setting the argument of each differential equal to zero. The equilibrium conditions become clear.

Thermal Equilibrium: $T^\alpha = T^l$

Reactive Equilibrium: $A_r = 0$

Mechanical Equilibrium: $P^\alpha = P^l - \dfrac{2\gamma_j}{\lambda_j}$

The expression for thermal equilibrium agrees with previous derivations involving multiple phases (Ada90, Def66, DeH93). The reactive condition assumes that electrochemical potentials are used in the expression. The expression for the reactive

equilibrium satisfies the requirement that the exchange of material across the interface is not independent of the species, for in the exchange of charged particles electroneutrality must be maintained (Gra47). The inclusion of a reactive surface is a solution to the generation of charge at the interface. The extent of reaction allows for equilibrium to be attained and accounts for the generation of surface charge. Grahame utilized the chemical potential of electrons in his derivation to account for the generation of charge (Gra47). Such an inclusion in an ionic material would be inappropriate.

Morphological Variation with Surface Charge

The conditions of precipitation have shown that differences in morphology can be controlled as a function of solution conditions such as stirring rate, solids loading, pH, additive concentration and reaction time (Nyv85, Soh92). The equilibrium shape also is dependent on solution conditions through changes in surface energy. Surface energy has been related to the charge on colloidal particles through the electrocapillarity studies of Grahame and Whitney (Gra42, Gra47). Reductions in surface energy occur as the electrical charge on the particle surface differs from the point of zero charge. The relationship between particle charge and surface energy is given by the Lippmann equation which states that the change in surface energy is equal to the negative of the surface charge density times the change in potential.

$$\frac{d\gamma}{d\Phi} = -\sigma \tag{3-24}$$

Surface charge generation in ceramic colloids has been described by Healy and White assuming that the surface is composed of terminating hydroxyl groups (Hea78, Hea80). These hydroxyl groups regulate surface charge through the addition or loss of a

proton, and therefore relate to the solution pH. The electrocapillarity curve for a ceramic surface can thus be generated by manipulation of the surface charging relationship for ionizable surface groups, and the effect of pH on surface energy can be estimated. If the various planes of a particle are characterized by different charge constants and point of zero charge, the pH of the solution can be related to the equilibrium morphology.

The surface potential, Ψ_0, for the Healy-White model is found from the solution to the equality

$$\frac{\sinh(e\Psi_0 / 2kT)}{\gamma_{ion}} = \frac{\delta \sinh(\frac{e\Psi_N}{kT} - \frac{e\Psi_0}{kT})}{1 + \delta \cosh(\frac{e\Psi_N}{kT} - \frac{e\Psi_0}{kT})} \tag{3-25}$$

where γ_{ion} and δ are terms concerning the solution ionic strength and surface charging characteristics respectively, and Ψ_N is the Nernst potential. The fraction of ionized groups, α_{ion}, is given by the right hand side of the equality. Surface charge is determined from the number of active sites and the fraction of ionized groups by the following relationship.

$$\sigma_0 = eN_s\alpha_{ion} \tag{3-26}$$

e is the charge on an electron and N_s is the number of surface sites per unit area. Surface energy can be related to the surface charge by graphically integrating the σ vs. pH curve (Stu92). The resulting data requires an integration constant K which is the surface energy at the point of zero charge. The relationship is written as follows.

$$\gamma = \frac{RT}{F}\int \sigma_0 dpH + K \tag{3-27}$$

For considerations of the equilibrium shape, the Gibbs-Wulff construction depends on the value of surface energy, and it is obvious that equilibrium shape will differ as surface charge is modified. For instructive purposes, the effect of pH on shape can be estimated by characterizing the surface charging behavior of a material as a function of the specific habit plane. Surface energy at the point of zero charge must be determined. As an illustration, the surface energy and surface charging characteristics of alumina will be estimated and related to morphology. Table 3-1 gives the assumed surface energy and surface charge characteristics for three habit planes of α-alumina. The site density is taken from the number of aluminum sites present on each surface, where it is assumed that the reaction of a hydroxyl ion from solution with the Al^{3+} ion provides all the sites on the surface. The basal plane has been found to have the lowest surface energy at the solid-vapor interface (Cho97) and this is reflected in the choice of lowest surface energy at the point of zero charge which was estimated from information presented by Ducker et al. (Duc94).

The surface potential for each habit plane was calculated from equality 3-25 using the assumed values for acid dissociation constants, and is presented with the fraction of dissociated surface groups in Figure 3-1. The solution to equality 3-25 was performed using Mathcad Version 7 (Mat97), and surface charge was calculated from the potential using equation 3-26. An ionic strength of 10^{-4} M background of 1:1 electrolyte was assumed for all calculations. The surface charge was related to the surface energy by determining the slope between data points, and the differences were summed from the point of zero charge to give the electrocapillarity curve for each habit plane. The surface

Table 3-1. Illustrative examples of the assumed surface energy and surface charge constants for three planes of α-alumina.

Habit Plane	Site Density (sites/nm^2)	Point of Zero Charge	pKa_1	pKa_2	γ_{PZC}
{0001}	1.25	3	-1	7	75
$\{11\bar{2}0\}$	1.1	7.5	5	9	120
$\{10\bar{1}2\}$	0.85	10	6	14	135

energy constant for each plane was added to give a curve for the surface energy for each habit plane presented in Figure 3-2. Solution pH values of 2, 7 and 12 were used to evaluate the theoretical equilibrium morphology. These theoretical morphologies are presented in Figure 3-3.

As each habit plane reaches it's point of zero charge, it's surface energy is maximized and therefore the plane becomes less prominent over the equilibrium shape. At pH 2, the basal plane is near its isoelectric point, and surface energy is relatively high. In contrast at pH 12, surface charge has lowered the surface energy and the basal plane has become more dominant. This relationship correlates with observations of growth rates of corundum under alkaline conditions (Kuz65). The basal plane grows slowly under alkaline conditions, suggesting that surface energy is low. Likewise the decahedral plane is prominent at pH 2 due to the reduction of its surface energy. The hexagonal prism plane does not experience significant reduction in surface energy and is least prominent at pH 7 near its isoelectric point.

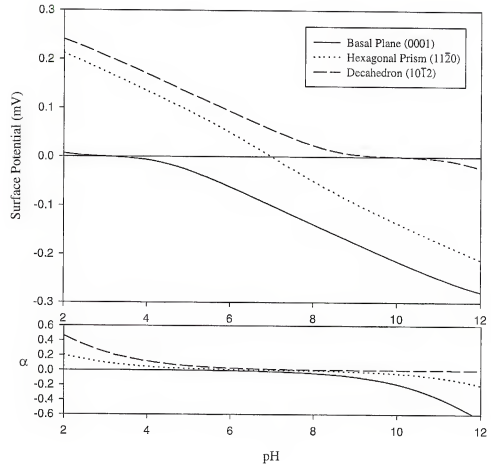

Figure 3-1. Surface potential and fraction of charge surface groups, α, for the hypothetical habit planes given in Table 3-1. Surface potential increases away from the point of zero charge as a result of the development of charge from the protonation or deprotonation of surface hydroxyl groups.

In order to employ these types of relationships, the surface energy and surface charge characteristics for a material must be determined as a function of habit plane.

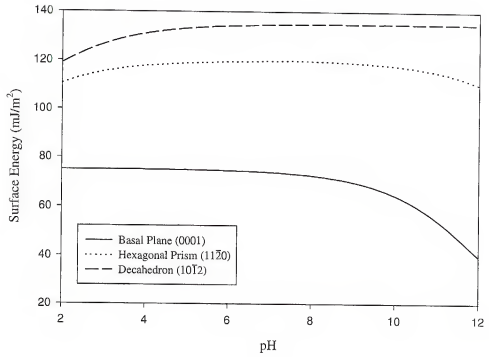

Figure 3-2. Calculated surface energy curves for each habit plane as a function of pH and surface charging from the assumed surface energy and charge constants. As each habit plane experiences the development of surface charge, surface energy is decreased.

Information of this type is becoming available for alumina through several investigations using the atomic force microscope (Duc94, Lar97).

Assumptions used in this derivation require that the solution to the equality 3-25 is performed with a monovalent background electrolyte, which will not be the case during precipitation of ceramic oxides due to the presence of higher valence cations. Additionally, the concentration of background electrolyte will vary with the solubility of the oxide in solution. Precipitation is assumed to occur near equilibrium levels in order

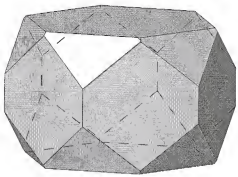

A

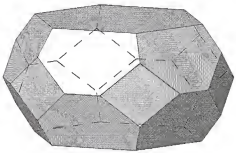

B

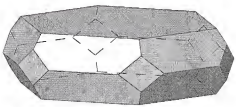

C

Figure 3-3. Particle morphologies as a function of pH. A. pH = 2. B. pH = 7. C. pH = 12.

for surface energy to influence the morphology. A complete description requires an inclusive program that involves aspects of colloidal chemistry and solubility.

CHAPTER 4

ADDITIVE EFFECTS ON PARTICLE MORPHOLOGY

Introduction

Precipitation techniques for the manufacture of ceramic powders have the primary advantage of removal of the need for milling to eliminate agglomerates. Additional benefits of using precipitation methods for material synthesis lie in reducing the cost of fabrication, control of particle size distribution, or control of particle morphology. The control of morphology creates an opportunity for designing powders with specific properties. If particle properties are tailored to the needs of an application, the final properties of objects made using those particles are superior. Control of the shape results from well defined synthesis conditions, and the degree of quality control necessary can be a factor in determining the usefulness of the technique. A robust method for control of powder properties is needed in order to apply a precipitation technique to large scale production. This chapter presents investigation into the use of adsorbates for the specific modification of the morphology of α-alumina, and characterizes the condition of the solvent during the reaction for its effect on morphology.

Background

Facets develop in liquid phase precipitation through solvent-precipitate interactions that stabilize a low energy configuration of the surface. Different solvents stabilize different facets as a result of either the conformation of the solvent molecule adsorbed on the surface or the molecular forces between the solvent and the precipitate surface. The particle morphology in liquid phase precipitation is a function of the growth rates of the habit planes formed during synthesis. Factors that influence particle morphology include the degree of supersaturation, the fluid flow dynamics, the reaction time and the effect of specific adsorbates. The interaction of the solvent and precipitates determines the lowest energy facets, and the kinetic conditions of growth affect the development of the facets to influence the shape of the crystal.

The stability of α-Alumina habit planes during hydrothermal synthesis has been investigated by Kuznetsov (Kuz64, Kuz65, Kuz71). This work utilized alkali mineralizers (NaOH, KOH, Na_2CO_3, $NaHCO_3$, etc.) and high temperatures (600°C) to measure growth rates in corundum. Under these reaction conditions, the growth rates of crystallographic faces were found to relate as $(81\bar{9}6)$ scalenohedron > $(10\bar{1}1)$ rhombohedron > $(22\bar{4}3)$ hexagonal dipyramid > $(11\bar{2}0)$ hexagonal prism >> (0001) basal. Facets that appeared on a sphere were the (0001) basal, $(10\bar{1}1)$ rhombohedron, $(11\bar{2}0)$ hexagonal prism, and $(22\bar{4}3)$ hexagonal dipyramid, which eventually reduced to the stable basal and hexagonal prism facets. The most stable habit planes are the basal plane and the hexagonal prism facets under hydrothermal conditions and basic pH. Kuznetsov proposed that rate limiting steps are connected to the surface chemical

structure, so that adsorption kinetics and the dehydration of crystal faces dominate the growth process.

The glycothermal technique for the synthesis of α-alumina has shown that several particle morphologies can be formed dependent upon reaction conditions (Cho95). These shapes range from platelets which are dominated by the (0001) basal plane and the $(11\bar{2}0)$ hexagonal prism facets, to polyhedra dominated by the $(10\bar{1}2)$ habit planes. Control of the formation of the dominant habit plane was found to be a function of stirring rate, solids loading, and reaction time (Cho95). However, the influence of specific adsorbates in glycothermal synthesis has not been investigated. In order for a chemical additive to be effective in changing the morphology, it must have an affinity for the surface of the precipitate. Additionally, the additive must not catalyze solvent degradation, or itself suffer degradation under synthesis conditions. Finally, additives must not alter the thermodynamic conditions to change the development of a desired phase.

In order to serve as a specific adsorbate, the additive used must have a chemical interaction with the surface. In adsorption on ionic solids, the presence of charged ions, dipolar molecules, or available bonding orbitals will promote adsorption. The effect of surfactants on the stability of alumina suspensions provide a broad basis for categorizing the compounds that adsorb at the interface (Big95, Esu95, Hua95, Koo95, Lee88), and alumina is often used as a substrate for infrared examination of adsorption (Kis75, Mor80).

An additional concern in the evaluation of non-aqueous synthesis techniques is the specific adsorption of the solvent itself. Alcohols are known to interact chemically

with alumina at elevated temperatures (Gre62, Kag67). Alumina is known to have a catalytic effect for the production of some organic chemicals (Pin87), and the effect of solvent degradation on morphology and glycothermal synthesis has not been investigated to date. Additives will change the solution speciation of components, and may promote the formation of new chemicals in the reaction system. Solvent degradation must be considered as a factor will influence the thermodynamic stability of the system, supersaturation levels, and flow dynamics via viscosity changes. The 1,4-butanediol used in this study is sensitive to oxidation. In order to maintain the solvent, oxidizing additives must not be employed, and sources of oxidation should be avoided as much as possible.

The influence of adsorbates on the surface energy of the various habit planes can be used to promote controlled growth and therefore control morphology. The morphology of crystals grown in solution is determined by the habit plane with the slowest growth rates. In situations where the supersaturation is low and the surface energy influences the growth of habit planes, the equilibrium form can be related to the effect of adsorbates on surface energy. When adsorbates do not interact, the stable habit planes are believed to be those with close packed ions, as these planes are believed to have lower surface energy. Adsorbates which interact to form stable film structures can stabilize non-closely packed planes. However, adsorption can be so strong that growth rates of the particle can be reduced.

Materials and Methods

Alpha alumina is synthesized in 1,4-butanediol by reaction of gibbsite powder[1] at 300°C for 36 hours under a stirring rate of 460 rpm and autogeneous pressures. A 600 ml stainless steel hydrothermal reaction vessel was used for the reaction[2]. The solvent purity was assured by vacuum distillation of the solvent prior to each synthesis run.

Gibbsite powder was ground in an alumina mortar and pestle with methanol to provide dispersion. The suspension of gibbsite in methanol was added to 150 ml of vacuum distilled 1,4-butanediol. The suspension was placed under agitation and 60°C for 12 hours to remove the methanol carrier. The suspension of gibbsite in 1,4-butanediol was loaded into the 600 ml vessel, and the container was rinsed with 50 ml of 1,4-butanediol. The solution pH was measured using a solid-state pH meter[3] both before and following the addition of the desired amount of additive. The vessel was placed under vacuum for 10 minutes to remove entrapped air in the solvent. The interior of the vessel was then purged with nitrogen gas for 10 minutes. The heating schedule used a three hour ramp from room temperature to 300°C, a hold period at temperature for 36 hours, and a one hour ramp to room temperature. The autogeneous pressure due to 1,4-butanediol remained below 29 kPa (200 psi), but vessel pressures could ascend to 100 kPa.

---

[1] Spacerite S-11, ALCOA, Pittsburgh, PA.
[2] Parr Autoclave Model , Parr Instrument Company, Moline, IL.
[3] Sentron 1001 pH System, SENTRON Inc., Federal Way, WA.

Following synthesis, the solvent was measured for pH and a sample was taken for analysis. Gas chromatography[4] and infrared spectroscopy[5] were performed on the solvent. The precipitate was collected and washed by five cycles of centrifugation and dispersion in methanol. The precipitate was characterized by scanning electron microscopy[6], x-ray diffraction[7], and diffuse reflectance infrared spectroscopy[8]. Scanning electron microscopy samples were prepared by allowing a suspension of the precipitate in methanol to dry on a sample mount, followed by 5 minutes sputter coating with Au-Pd.[9] X-ray samples were prepared by placing a drop from a suspension of the precipitate in methanol on a dry glass slide, and allowing the methanol to evaporate. Scans were run from 10 to 70 degrees 2Θ, with a 0.05 degree step size. IR samples were prepared by mixing dry precipitate with dry KBr in a 1:100 ratio by weight. The materials were ground by hand in an agate mortar and pestle and dried at 115°C for 1 hour before measurement. The heating rate for gas chromotography was an initial temperature of 30°C, a heating rate of 10°C/minute, and a five minute hold at 250°C.

One synthesis run was performed by the reaction of Al-tri(sec)butoxide with water in 1,4-butanediol. A volume of 17 ml of Al-tri(sec)butoxide were added to 200 ml of solvent in a 1000 ml vessel. The Al-tri(sec)butoxide reacted with water present due to

---

[4] Gas Chromatography, Hewlett Packard 5890A.

[5] Infrared Spectroscopy, 20SXB FT-IR spectrometer, Nicolet Analytical Instruments, Madison, WI.

[6] Scanning Electron Microscope, JSM 6400, JEOL, Boston, MA.

[7] X-ray Diffractometer, APD 3720, Cu-Ka, Fine Tube, 40 kV, 20mA, Phillips Electronics, Mahwah, NJ.

[8] Infrared Spectroscopy, 20SXB FT-IR spectrometer, Nicolet Analytical Instruments, Madison, WI.

condensation from the atmosphere to form a hydrous gel and 2-butanol. The reaction was performed at 130 rpm and 300°C for 24 hours.

Results and Discussion

An attempt to characterize the full spectrum of adsorbate effects is beyond the scope of this study. To couple the reaction variables of solids loading, stirring rate and reaction time to the effect of a specific adsorbate would be a tedious study requiring excessive material and time. This survey is designed to identify those adsorbates which will adsorb strongly to form new habit planes or inhibit growth such that morphology is modified. To that end, one experimental condition was chosen as a reference point for study of the effect of adsorbates. The synthesis conditions are 300°C for a period of 36 hours under a stirring rate of 460 rpm, which is expected from experience with this vessel to be a medium level of agitation. The expected morphology for this reaction condition is a columnar shape with height approximately equal to the dimension of the basal plane. The surface is bound by the basal plane (0001) and the hexagonal prism planes $\{11\bar{2}0\}$. These habit planes have previously been observed as the most stable facets of α-alumina in hydrothermal growth (Kuz64). Using this shape as a reference allows the effect of an adsorbate to be seen qualitatively in the promotion of new particle morphologies, or in the modification of habit growth rates to promote rod-like or plate-like morphologies. Batch nucleation in the vessel creates a near monosized particle size distribution. Deviations in the size distribution can also be attributed to adsorbate effects.

---

9 Sputter Coater, Hummer II, Technics, Inc., Alexandria, VA.

Investigation of Solvent Degradation

The importance of solvent purity in crystal growth is highly stressed in the literature (Buc51, Nan87, Nyv88, Soh92). Unlike hydrothermal techniques, the purity of the non-aqueous solvents must be evaluated to characterize the effect on morphology. Figure 4-1 shows gas chromatography (GC) results for three samples of 1,4 butanediol. Figure 4-1A is the result of a vacuum distillation of 1,4 butanediol, used to purify the solvent before use. The single, strong peak beginning at 16 minutes, 40 seconds is characteristic of 1,4 butanediol. Four small peaks are present at later times resulting from column bleed and polysiloxanes from the injection port. This data indicates that the vacuum distillation procedure (Appendix A) is satisfactory for providing pure, initial solvent. Figure 4-1B is a GC scan showing the chemical components after glycothermal synthesis at 300°C for 36 hours. The 1,4 butanediol peak dominates, but two new peaks are present. The smallest peak results from water, produced as a by-product of the synthesis reaction and as adsorbed from the atmosphere during sample preparation. The second peak at 8 minutes has been characterized as tetrahydrofuran by mass spectroscopy performed with the gas chromatography.[10]

The tetrahydrofuran (THF) is produced by dehydration of the solvent. Dehydration of 1,4-butanediol produces either butadiene or tetrahydrofuran. In the temperature range 250°C to 350°C and with a suitable catalyst, tetrahydrofuran is the principle product. The pure solvent was held at 300°C for 48 hours and found to form THF without the presence of reactant precursors. Thus, alumina does not participate in

[10] GC/Mass Spectroscopy, Model 4500, Finnigan MAT, San Jose, CA.

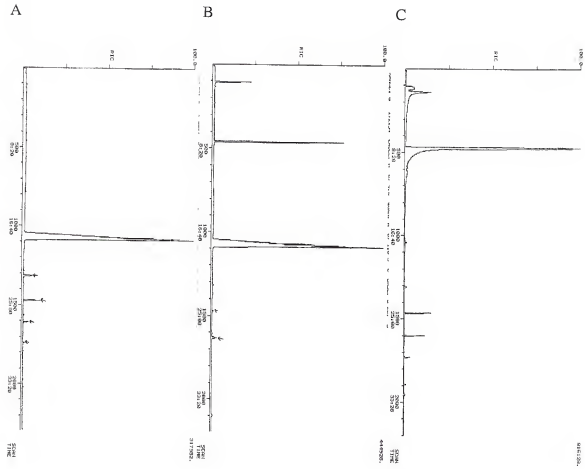

Figure 4-1. Gas Chromotrogaphy evaluation of solvent degradation during glycothermal synthesis. GC thermal schedule was 1 minute at 30°C, heating at 10°C/minute to 250°C. A. Vacuum distilled solvent. B. Post synthesis without discoloration. C. Post synthesis with discoloration.

the formation of THF at 300°C. Some proportion of the water peak is therefore the result of the solvent degradation. In the usual synthesis reaction, there is no discoloration of the solvent. Sample 4-1C is of solvent which has been greatly degraded and has changed color from a transparent liquid to an orange color. The GC data indicates that no 1,4

butanediol is present, all having been transformed to tetrahydrofuran. The characteristic peak due to water is also present.

The production of THF does not alter the color of the solvent, and the vacuum applied to the solvent prior to synthesis effectively prevents discoloration. If the vacuum is not applied or if the integrity of the vessel is compromised, the solvent can degrade and change the color to a yellow hue (or orange). Varying degrees of discoloration have been noticed. Figure 4-2 presents transmission infrared spectroscopy of the vacuum distilled solvent and three solvents that experience either no discoloration, light yellow color, or strong yellow color. The broad peak between 3400 and 3300 cm^{-1} indicates hydrogen bonding between hydroxyl groups. The pair of peaks at 2940 and 2872 cm^{-1} are characteristic of $-CH_2$ vibrations. The peaks below 1600 cm^{-1} are the "fingerprint" region of 1,4-butanediol and are indicative of various modes of $-CH_2$ and C-O-H symmetric and asymmetric vibrations (Pin87).

The clear solvent contains 1,4-butanediol, tetrahydrofuran, and water. The presence of water creates the broad low peak near 2200 cm^{-1}, and the cyclic ether bond of the THF appears at 1776 cm^{-1}. Other than the new peaks at ~2200 and 1776 cm^{-1}, there are no peaks indicating the presence of new molecular groups. That is to say, no oxidation of the solvent is occurring. Oxidation of the solvent should produce carboxylate groups from each primary alcohol. The characteristic infrared vibration of

The carboxylate group occurs between 1725 and 1695 cm^{-1}. Hydrogen bonding between carboxylate groups creates to a broad unusual peak between 3100-2200 cm^{-1}. These vibrations are not evident in the spectra of any of the solvent degradation samples. The lightly discolored solvent shows a similar profile to the clear solvent, with a slight

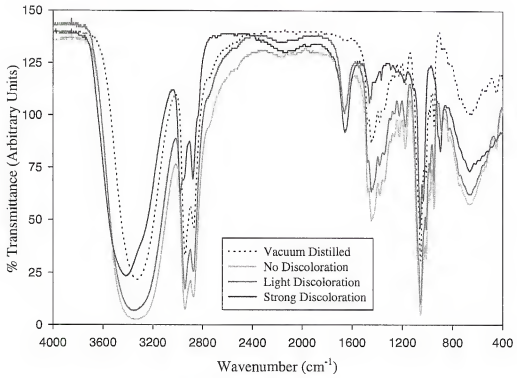

Figure 4-2. Infrared spectroscopy of solvent degradation.

shift in the hydrogen bonding peak from 3343 to 3353 cm^{-1}. No solvent oxidation to produce carboxylate is evident.

The strongly discolored solvent shows a shift in the hydrogen bonding peak from 3330 in the distilled solvent to 3413 cm^{-1}, and the peak is no longer symmetric, being skewed to the higher wavenumber. This indicates that the degree of hydrogen bonding in the material has been reduced. The peaks at 2979 and 2877 cm^{-1} are reduced in intensity with respect to the -OH hydrogen bonding peak. This reduction is also seen in the peaks

between 1550 and 1350 cm^{-1}. The C-O-C peak at 1776 cm^{-1} has increased in intensity suggesting that many more ether groups are present. No strong, broad peak between 3600 and 2500 cm^{-1} typical of carboxylate groups is evident. The absence of carboxylate groups suggests that the source of discoloration of the solvent is not oxidization but rather polymerization. The mechanism of polymerization is not known, and may be changed by the additives in the system. Use of the vacuum to remove trapped gases in the solvent prior to synthesis effectively prevents discoloration.

Phase Purity of Precipitate

The thermodynamic phase stability of the system must not be affected by the use of a specific adsorbate in order for the precipitation of the desired phase to occur. X-ray diffraction (XRD) was used to determine the phase purity of the precipitate formed in the synthesis reaction. Figure 4-3 shows the XRD results for the pure solvent condition as well as the phase purity for the use of each adsorbate. In each case, the characteristic peaks of α-alumina are sharp and well defined. Differences in peak magnitude between samples is an effect of sample preparation. Differences in peak proportion results from preferred orientation of the particles. Particles of high aspect ratio can align so that certain crystallographic planes are proportionally over-represented. This can affect the magnitude of peak height. However, in all the scans, high intensity peaks remain strong, and low intensity peaks are weak, in qualitative agreement with literature values.

Effect of Adsorption by Solvent and Alcohols

The characterization of the effect of adsorption by the various components can be related to the chemical reactive sites of the additive. Glycols and alcohols are characterized by the presence of hydroxyl groups which bond chemically through the

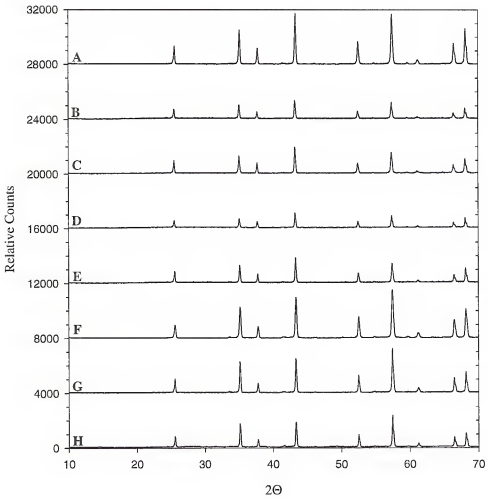

Figure 4-3. X-ray diffraction pattern of glycothermally produced α-alumina as a function of the adsorbate additions. A. As synthesized. B. Tetrahydrofuran. C. Methanol. D. Acetic acid. E. Nitric Acid. F. Ammonium hydroxide. G. Pyridine H. Tetraethylammonium hydroxide (TEAOH).

deprotonation of the alcohol in conjunction with a surface oxygen (Gre62, Kag67, Kis75). The reaction creates an alcohol group and a hydroxyl group on the surface according to equation 4-1.

$$ROH + O^{2-} \rightleftharpoons RO^{-} + -OH \qquad (4\text{-}1)$$

The presence of the surface alcohol group will affect the surface energy according to the degree of adsorption. The degree of adsorption should be affected by the size of the steric group of the molecule, and the nature of the alcohol (primary, secondary, or tertiary). Theoretically, glycols can react at two sites.

In the absence of specific adsorbates, the surface of the precipitate must be dominated by the adsorption of the solvent. The morphology resulting from the glycothermal synthesis without the use of adsorbates is shown in Figure 4-4A. The shape is as expected from the reaction conditions, and the particle is bounded by the basal plane (0001) and the $\{11\bar{2}0\}$ habit planes. The kinetic factors affecting growth promote a columnar shape in which the length perpendicular to the c-axis is approximately equal to the length parallel to the c-axis. This aspect ratio of the parallel to perpendicular length c/a can be used to characterize changes in growth morphology. The presence of tetrahydrofuran formed during the synthesis may well affect the final morphology of the particles. Examination of the effect of THF on the morphology was examined by adding it as an initial component at two levels; 5 and 12.5 volume percent. The final particle morphology for the 12.5% addition is shown in Figure 4-4B. The morphology of the 5% addition is indistinguishable from the higher level. The scanning electron micrographs show that the morphology is qualitatively unaffected by the addition of THF, as the

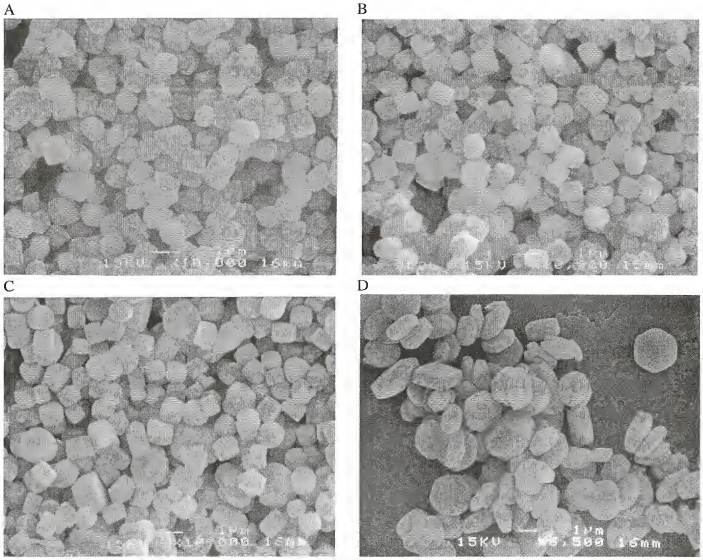

Figure 4-4. Effect of Hydroxyl groups on morphology. A. As synthesized. B. Tetrahydrofuran (12.5 Volume %). C. Methanol (13.6 volume %). D. Sec-butoxide.

aspect ratio c/a is still approximately 1. Tetrahydrofuran does not show evidence of specific adsorption.

Figure 4-4C indicates the effect of the addition of methanol. A volume of 30 ml of methanol was added to the reaction vessel (15 vol%). Methanol has been observed to specifically adsorb on the $\{11\bar{2}12\}$ habit planes to promote a platelet morphology (Cho95). The presence of the steric methoxy group on the surface is believed to stabilize the high angle facet so that its surface energy is lower than the basal plane. The development of the high angle $\{11\bar{2}12\}$ facets by adsorption of methanol were not observed in these experiments. The morphology resembles the expected morphology with no new habit planes evident in the particles. Growth rates of the facets are also unaffected as no change in aspect ratio is evident.

Figure 4-4D shows the resultant morphology when Al-tri(sec)butoxide was used as a precursor material in place of gibbsite. The resulting morphology is plate-like and exhibits the high angle $\{11\bar{2}12\}$ planes expected from prior research (Cho95). The particle size distribution is broader than the pure solvent case, with particles between 1 and 4 microns. This suggests that particle nucleation is affected.

Effect of Adsorption by Carboxylate Groups

Carboxylate groups are expected to adsorb through a dissociated hydroxyl, but the proximity of the double bonded oxygen will affect the strength of the adsorbate bond and can stabilize a new surface structure by its presence. 588 µl of glacial acetic acid was added to serve as a specific adsorbate. The pH of the suspension was changed from ~8.0 to 5.1 by this addition. The morphology produced is shown in Figure 4-5. These

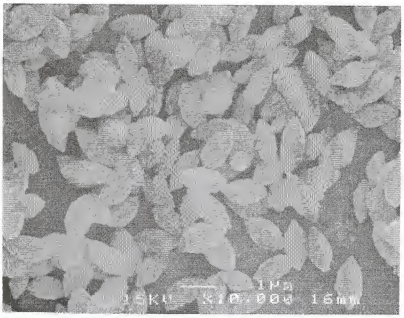

Figure 4-5. Morphological changes induced by the addition of Acetic Acid. The synthesis was performed in the 600 ml hydrothermal vessel. 588 µl of glacial acetic acid was added to 200 ml of 1,4 butanediol with 8 g of gibbsite. The solution pH was adjusted from 8 to 5.1 by the addition. The stirring rate used was 460 rpm.

particles show that the specific adsorption of acetic acid stabilizes the $(11\bar{2}2)$ habit planes in place of the basal plane. The resulting morphology is acicular and uniform with an aspect ratio of ~2.5. This indicates that the presence of acetic acid does not bond so strongly that the nucleation rates are disturbed.

Effect of Adsorption by Nitrogen Compounds

Nitrogen atoms within a molecule will adsorb via the unbonded electron orbital. The nitrogen compounds that were investigated include nitric acid, ammonium hydroxide, pyridine, and tetraethylammonium hydroxide. Use of these compounds adds additional complexity as each of these ions has acid or base properties, and various steric effects.

The effect of nitric acid is shown in Figure 4-6A. The additive synthesis was performed using 400 µl of 1.0 M HNO_3. The pH was altered from pH 8.4 to pH 4.8 by the addition of the nitric acid. The morphology is approximately equivalent to the case of no adsorbate addition. Particle surface is not as well characterized by the $\{11\bar{2}0\}$ planes, but a general short column-like morphology is dominant. In addition, some small particle aggregates can be seen of approximately 1/100th the size of the large particles. This indicates that some specific adsorption may have occurred to affect the nucleation rates of the reaction. Solution pH changes during the synthesis may have contributed to the bimodal size distribution.

The effect of ammonium hydroxide is shown in Figure 4-6B. The additive synthesis was performed using 3 ml of 1.0 M NH_4OH. This addition altered the pH from pH 8 to pH 10. The particle morphology has assumed a more plate-like configuration with an aspect ratio of 0.5. The particles are approximately monosized, indicating that the adsorption does not affect the nucleation kinetics of the synthesis. There are additional particles present that are approximately $1/100^{th}$ the size of the faceted particles that are of irregular shape.

The effect of pyridine is shown in Figure 4-6C. The additive synthesis was performed using 10 ml of pyridine. The change in pH was not measured. The change in morphology is striking for the case of the pyridine addition. Plate-like particles with well defined habit planes are obvious and the aspect ratio is ~0.2. The facets dominating the surface are the basal plane (0001), the $\{11\bar{2}0\}$ and $\{11\bar{2}2\}$ habit planes but the growth rates of the facets vary, so that a single characteristic shape is not defined. Pyridine adsorbs through the unbonded orbital of the nitrogen atom, and the predominance of the

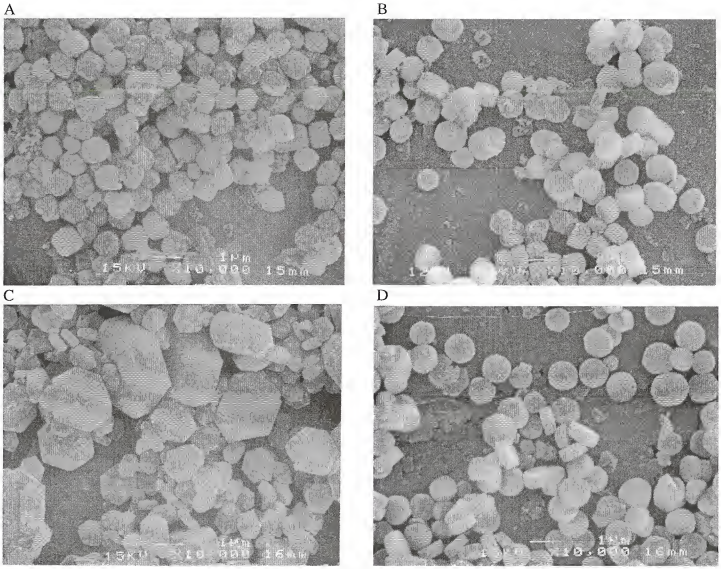

Figure 4-6. Effect of nitrogen compounds on morphology. A. Nitric acid. B. Ammonium Hydroxide. C. Pyridine. D. Tetraethylammonium Hydroxide.

basal plane indicates that pyridine adsorbs most uniformly on that plane.

In addition, the particle size distribution of the particles has been profoundly affected. In place of the approximately monosized distribution at one micron effective diameter, the particles range in size from 0.5 micron to 7 microns. This indicates that the specific adsorption of pyridine has affected nucleation kinetics. Fewer nuclei are formed initially, and as a result the initial nuclei grow very large. The nuclei formed during the latter stages of precipitation have less material available for growth, and are smaller. If the vessel were held at reaction temperature for long periods of time, the smaller particles would become dissolved to precipitate on the larger particles.

The effect of tetraethylammonium hydroxide is shown in Figure 4-6D. The additive synthesis was performed using 350 µl of 1.0 M TEAOH which altered the suspension from pH 8 to pH 12.2. The particles formed are more plate-like than expected, with an aspect ratio of ~0.5. This morphology echoes the previous effect of ammonium hydroxide. The steric groups of TEAOH have not affected adsorption and modification of growth rates. The similarity of habit modification to the effect of ammonium hydroxide suggests that the presence of base has modified the surface energy of the facets, to promote the platelet morphology.

Surface Characterization of Precipitates

Diffuse Reflectance Infrared Fourier Transform Spectroscopy (DRIFTS) was used to characterize the surface structure of each precipitate formed with the use of adsorbates. Figure 4-7 presents the % transmittance of infrared radiation. Due to a power spike in the instrument, there is an erroneous spike at 1350 cm^{-1}. The infrared spectra of corundum is described by Gadsden (Gad75). There is a broad shoulder expected at 800

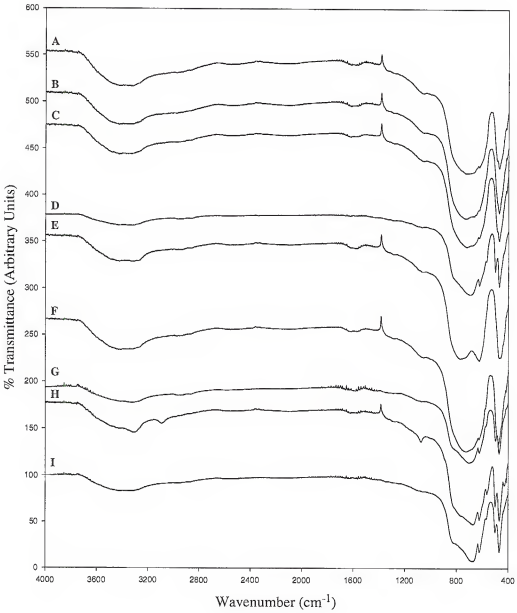

Figure 4-7. DRIFTS spectra of adsorbate particle surface structure. A. Pure Solvent B. Methanol (15 Volume %). C. Tetrahydrofuran (12.5 volume %). D. 2-Butanol. E. Acetic Acid (pH 5.1). F. Nitric Acid (pH 5.1). G. Ammonium Hydroxide (pH 10.9). H. Pyridine (5 Volume %). I. Tetraethylammonium Hydroxide (pH 12.2).

cm^{-1}, and then a series of four peaks between 790 and 560 giving a broad adsorption band. Peak assignments are 790-750, 720, 640 and 600-575 cm^{-1}. The peak at 640 is a shoulder, whereas all the other peaks are sharp. There is a second group of low wavenumber peaks characterized by a weak peak at 520, a shoulder at 490, a sharp peak at 450-432 and another shoulder at 375 cm^{-1}. Figure 4-7 gives the spectra of all precipitates. The region below 1000 cm^{-1} contains each of the expected peaks but the intensity of the peaks varies with the particle morphology. This fingerprint region is the same for cases in which the particle morphology was columnar (Figures 4-7A, 4-7B, 4-7C, and 4-7F) or plate-like (Figure 4-7G and 4-7I). The scattering factor of each particle morphology may influence the peak intensities, or the planar interfaces may emphasize or de-emphasize vibrational modes. Above the structural region, all samples exhibit a broad low peak at 3400 cm^{-1} and another low peak at 1650 cm^{-1}. These peaks indicate that water is physisorbed on the particle surface (Kis75).

The presence of water on the surface and the large particle size of the precipitates prevents detailed examination of the individual surface structures for each morphology. The data does indicate weak shoulders near 2940, 2837, and 1050 cm^{-1}. The adsorption of CH_2 groups has been characterized with peaks in these regions. Chemisorption of 1,4-butanediol is believed to be involved in the formation of these peaks. Organics are expected to adsorb on the surface through substitution on a surface hydroxyl group (Mor80). Acetic acid is expected to produce three strong peaks near 1590, 1432-1405, and 1335 cm^{-1}, but no detail can be seen in the spectra of Figure 4-7E (Kis75, All80). The only spectra which clearly shows adsorption is pyridine in Figure 4-7H, which has a single peak at 3150 cm^{-1} and a weak but sharp peak at 1050 cm^{-1}. Pyridine adsorbs

through hydrogen bonding with surface hydroxyl groups and chemisorbs via a coordinate bond with aprotic acid centers on the surface (Kis75). Characteristic adsorption bands are located at 1632 and 1459 cm^{-1}. The characteristic pair of peaks at 2940 and 2839 are absent, suggesting that pyridine has displaced the adsorption of 1,4-butanediol. The structural peaks below 1000 cm^{-1} are much more sharply defined than the pure solvent synthesis conditon.

As might be expected, those morphologies which were not affected by the addition of adsorbates have very similar spectra. The spectra for tetrahydrofuran (Figure 4-7B), methanol (Figure 4-7C), and nitric acid (Figure 4-7F) are equivalent to the pure case. Figure 4-7D shows the effect of adsorption of 2-butanol. Clear evidence of organic adsorption is present with the pair of peaks at 2940 and 2837 cm^{-1}. Additionally the structural region below 1000 cm^{-1} shows more sharp adsorption modes.

The adsorption of ammonia is often considered to a be a determination of the number of acid centers on the surface of alumina (Kis75). Figure 4-7G gives the spectra of the ammonium hydroxide addition. Adsorption of NH_3 is expressed by the following equation.

$$NH_3 + O^{2-} \rightleftharpoons NH_2^- + OH^- \qquad (4\text{-}2)$$

This creates a surface with both hydroxyl and amide groups. Coordinative ammonia vibrates at 3400, 3355 and 1620 cm^{-1}, and the surface amide group is expected to vibrate at 1510 cm^{-1} (Kis75). Ammonia hydrogen bonded to surface oxygen ions has a broad adsorption band at 3100 cm^{-1}. Ammonia molecules are believed to be hydrogen bonded through the nitrogen atom with surface hydroxyl groups and also by the hydrogen atom with surface oxygen atoms. The spectra shown in Figure 4-7G does not indicate the

presence of bonded ammonia, as the vibrations due to surface adsorbed water at 3400 and 1650 cm^{-1} agree with all the other spectra. This suggests that the modification of the morphology is related to the presence of the basic pH rather than the specific adsorption of the ammonium ion.

The mechanism for morphological modification involves the effect of surface charging on the basal plane. Recent literature has demonstrated that the point of zero charge of the basal plane of α-alumina is between 3 and 5 (Lar97). The basal plane under basic conditions will have a lowered surface energy due to the surface charging effects (Gra47). Under conditions of near equilibrium growth where surface energy will influence the particle shape, a highly charged surface will have lower surface energy, and this plane will therefore assume a more dominant role in the surface. If no adsorption of the cation is evident on the surface, the pH must have played a role in the development of the particle morphology.

Purity of Solvent

The possibility of solvent-adsorbate reaction to form new components must also be addressed in order for an understanding of the effect of the adsorbate on particle morphology to be realized. Gas chromatography/mass spectroscopy was used to characterize the solvent samples after the synthesis reaction. Figure 4-8 presents the GC information. All samples show large 1,4-butanediol peaks at 15.8 to 18 minutes, the presence of THF at 4.8 to 5 minutes, and a small peak due to water at 1.77 minutes. Methanol is notable between 1.25 and 1.36 minutes into the scan. Many of the scans show a small amount of methanol present, indicating that either methanol has been produced or remained from the sample preparation. Minor peaks are also evident at 12.8

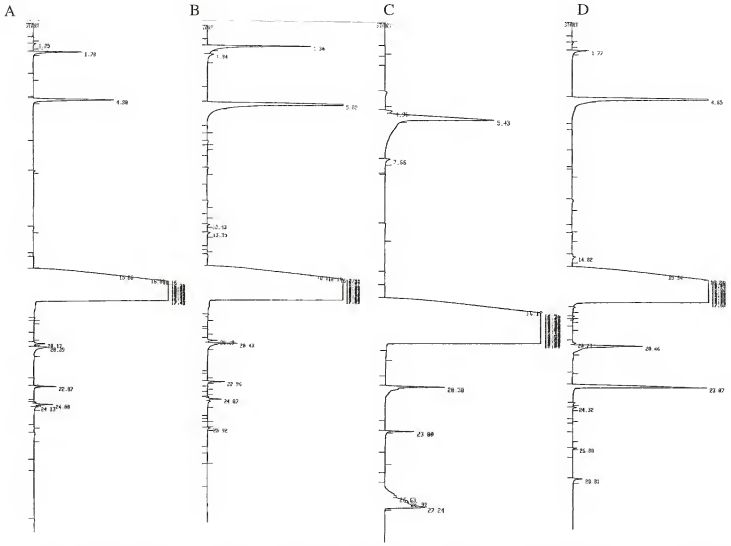

Figure 4-8. Gas Chromatography of solvent samples after the synthesis reaction. The gas chromatography heating schedule is 5 minutes at 30°C, heating at 10°C per minute to 250°C, and hold at temperature for 5 minutes. A. Tetrahydrofuran. B. Methanol. C. 2-Butanol. D. Acetic Acid. E. Nitric Acid. F. Ammonium Hydroxide. G. Pyridine. H. Tetraethylammonium Hydroxide.

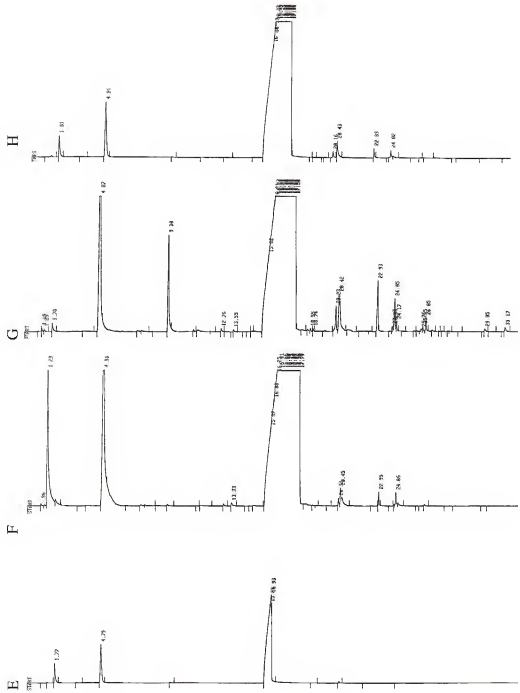

Figure 4-8. Gas Chromatography of solvent after reaction. (cont.)

and 13.3 minutes. These peaks are believed to result from low level of degradation products. Peaks greater than the twenty minute mark are due to the column and injection port. Figure 4-8G indicates that the pyridine addition experiences degradation. There are several minor peaks at 12.76 and 13.55 indicating solvent degradation. The color of the solvent in this synthesis reaction changed from clear to an orange color. The morphology produced from the use of pyridine may be the result of either the adsorption of pyridine, adsorption of degradation products, or the interaction of both the adsorbate and the pyridine with the particle surface. Pyridine may have catalyzed polymerization of the solvent. Other than pyridine, the adsorbates used in these experiments did not significantly degrade the solvent, and no color changes were observed.

Summary

The control of morphology through the use of specific adsorbates in non-aqueous solution synthesis involves consideration of solvent degradation, solution effects on particle surface charge as well as specific adsorption of the adsorbate to the particle surface. The composition of the liquid phase affects the surface energy of facets to stabilize specific habit planes. The solvent 1,4-butanediol stabilizes the basal plane (0001) and the $\{11\bar{2}0\}$ hexagonal prism planes. Methanol adsorption on the $\{11\bar{2}12\}$ habit planes was not reproduced, but 2-butanol was effective in creating these facets. Acetic acid was very effective in stabilization of the $\{11\bar{2}2\}$ decahedral habit planes, and did not affect nucleation kinetics. Nitric acid was not an effective adsorbate, but ammonium hydroxide and TEAOH both altered growth rates to promote a plate-like morphology. Pyridine was found to degrade the solvent and nucleation kinetics of

particle synthesis were influenced to broaden the particle size distribution. Pyridine additions promote a particle morphology composed of the basal, hexagonal prism, and decahedral planes.

Solvent degradation occurs by the dehydration of 1,4-butanediol to form tetrahydrofuran. Discoloration of the solvent is attributed to polymerization via a condensation mechanism. The dehydration of the solvent has been found to be independent of the presence of alumina. Acids and bases have been shown not to degrade the solvent under conditions of synthesis, and can be used for investigation of particle surface charging effects on morphological development.

CHAPTER 5

ZETA POTENTIAL PROPERTIES OF α-ALUMINA PARTICLES AS A FUNCTION OF HISTORY AND PARTICLE MORPHOLOGY

Introduction

α-Alumina is a key material manufactured and processed by the ceramic industry. Its material properties make it suitable for use as an insulator in electrical and semiconductor components, an effective abrasive, and a key refractory material (Git70). Processing of alumina components is usually performed using fine powders with appropriate solution pH and dispersant additives needed to provide desired rheological conditions. Due to the use of slurry processing, the colloidal characteristics of α-alumina have been of interest to the ceramic community for many years (Ces88a, Ces88b, Git70, Hid90, How90, Oka90, Sum91). Bulk production of α-alumina powder usually involves the calcination of hydrated phases of alumina such as gibbsite, bayerite, or diaspore to produce the thermodynamically stable alpha phase. Calcination is performed at 1200°C, and the resulting powder must be milled in order to reduce particle size to desired processing levels. The final powder morphology is approximately spherical, and the impacts from grinding can create structural defects in the surface. Typical alumina powders have been characterized for their zeta potential, and the isoelectric point is usually found at pH 8-9 (Git70, Kel88).

Glycothermal synthesis has recently shown the capability to form faceted particles of α-Al_2O_3 (Cho95). This solution phase precipitation technique produces particles without the structural defects resulting from grinding, although precipitation techniques do not eliminate the presence of dislocations or other structural defects (Soh92). By control of reaction conditions and the use of adsorbates, particles of controlled morphology can be synthesized. Interfacial properties of these powders will be the result of the habit planes which compose the surface. The colloidal characteristics that result relate to the effect of the synthesis environment and the history of the particles.

Background

In order to interpret colloidal behavior of fine particles in suspension, DLVO theory has been employed to relate such particle properties as the zeta potential to the stability of a suspension (Hun87). By considering the interparticle forces such as Van der Waals and electrostatic forces, the generation of energetic barriers to agglomeration of particles has been related to the concentration of indifferent ions, the adsorption of ions, and the development of layers of ions near the particle surface as a result of electric charge and dipole moment. The formation of electrical charge on the interface between a colloid and the suspending liquid is a primary component in the prevention of agglomeration of particles according to DLVO theory. Ceramic processing employs the use of pH and specific adsorbates to control surface charge in order to control process conditions such as rheology and solids loading (Rin95).

Colloids in suspension develop surface electrical charges by reaction with the surroundings to equalize the electrochemical potential of components in each phase. The

four mechanisms that cause the surface of a colloid to develop charge are the presence of defect structures in the lattice, surface ion imbalance, surface adsorption of ions or ionic exchange and, dissociation of surface acids (Hun87). The presence of defect structures cause charge imbalance in an ionic crystal, and lead to electrical fields. Such defects can occur by ion exchange between material ions and a solvated species, where the replacement is of lower charge. Space charge can also be generated by vacancies within the crystal, which manifest as surface charge (Kli65a, Kli65b). The crystal structure of a salt can favor the presence of one ion over the other on the surface to give a surface charge dependent on the concentration of the ions in solution. Alternatively, a colloid can be composed of surface molecules which dissociate like acids. Dissociation leaves a negative charge on the surface. Last, ions or ionic molecules can be adsorbed on the surface to such an extent that charge is generated.

Metal oxides are believed to form surfaces of hydroxide groups which can dissociate amphoterically by the following equations (Git70, Hun87).

$$AH_2^+ \rightleftharpoons AH + H^+ \qquad (5\text{-}1)$$

$$AH \rightleftharpoons A^- + H^+ \qquad (5\text{-}2)$$

The electric charge at the surface attracts ions of opposite charge and repels like charged ions. This creates the potential distribution in the solution known as the Gouy-Chapman layer. The metal oxide layer is made more complex because the activity of the potential determining ions on the surface is related to the potential of the surface. A Boltzmann expression is commonly used to relate surface activity to solution activity (Hea78). Oxides are known to generate much higher charge magnitudes as a function of pH than sparingly soluble salts (Hun87).

The modeling of the acid-base character of amphoteric oxides was developed by Healy and White (Hea78). The potential determining ions are H^+ ions, and the ratio of the concentration of surface species are controlled by the following surface dissociation constants.

$$K_+ = \frac{[AH][H^+]_s}{[AH_2^+]} \tag{5-3}$$

$$K_- = \frac{[A^-][H^+]_s}{[AH]} \tag{5-4}$$

The net surface charge density of the interface, σ, is related to the number of surface groups per unit area, N_s, and the electron charge, e, by the following relationship.

$$\sigma = eN_s \frac{[AH_2^+] - [A^-]}{[AH] + [AH_2^+] + [A^-]} \equiv eN_s\alpha \tag{5-5}$$

The fraction α has a range of plus to minus one, and the quantity relates the net number of charge sites to the total number of dissociation sites. The surface concentration of potential determining ions $[H^+]_s$ is related to the bulk concentration $[H^+]$ by the Boltzmann factor.

$$[H^+]_s = [H^+]\exp\left(-e\Psi_s/kT\right) \tag{5-6}$$

In a combined expression, the surface charge and the surface potential, Ψ_s, are related by the dissociation constants K_+ and K_-.

$$\sigma = eN_s \frac{(H^+/K_+)\exp(-e\Psi_s/kT) - (K_-/H^+)\exp(e\Psi_s/kT)}{1 + (H^+/K_+)\exp(-e\Psi_s/kT) + (K_-/H^+)\exp(e\Psi_s/kT)} \tag{5-7}$$

The use of the Healy-White model commonly determines the negative log values of K_- and K_+ through acid-base titration (Stu92). The larger the difference between the pK_+ and pK_-, called ΔpK, the greater the deviation from ideal behavior.

The interaction of metal oxide surfaces with the environment or specific adsorbates depends on the Lewis acid and base character of the surface ions (Hen94). On faces where metal ions are exposed, the Lewis acid strength is expected to be affected by ion charge, degree of coordinative saturation, and the availability of empty orbitals. Strong acid character is expected for high valence charge and/or small bandgap, in which empty orbitals are available. Lewis basicity on oxide surfaces is related to the 2p electron orbital of the oxygen anion. Coordination with cations and the magnitude of cation charge will affect the degree of basicity. Low cation charge and large cation radius lead to more basic character. As a result of the dependence of the Lewis properties on coordination, the arrangement of the ions on a habit plane will affect the colloidal properties of the surface.

As shown in Figure 5-1, the particles used in this study are characterized by the habit planes of their facets. These habit planes include the basal plane (0001), $(11\bar{2}0)$, $(11\bar{2}12)$, and the $(10\bar{1}2)$ habit planes. ATOMS© representations of each of these surfaces show the arrangement of anions and cations on the surface in Figure 5-2. Henrich and Cox review studies on the character of the habit planes, and provide an overview of the atomic structure present on each habit plane (Hen94). The basal plane of α-Al_2O_3 is composed of alternating layers of planar anions and non-planar cations. The layer of cations is not atomically uniform with respect to the planar hexagonal close

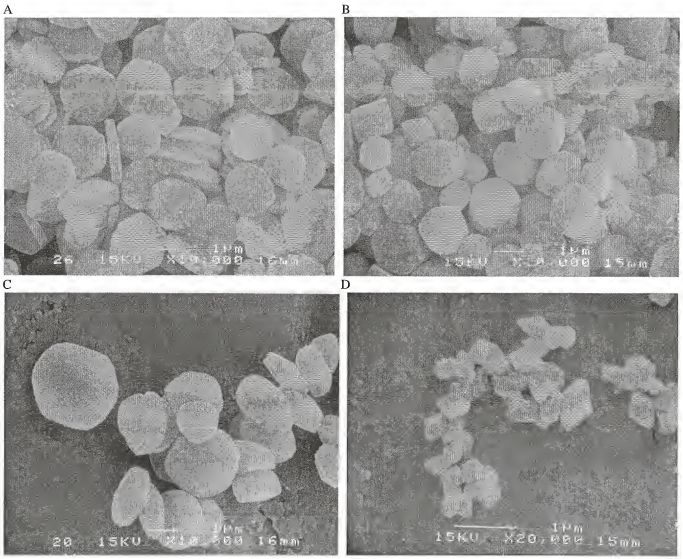

Figure 5-1. Scanning electron microscopy of particle morphologies. A. Platelet B. Prism C. Bipyramid D. Polyhedron.

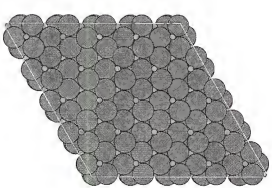

C

D

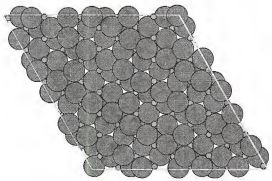

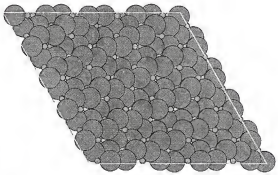

Figure 5-2. ATOMS© Structure of primary planes. A. Basal Plane (0001). B. Hexagonal prism $(11\bar{2}0)$. C. Bipyramid $(11\bar{2}12)$. D. Decahedral $(10\bar{1}2)$.

packed arrays of oxygen anions. If separated between the non-planar cation layer, each face will have half of the cations, and the Al^{3+} ions have only half the normal ligand bonds with the oxygen layer. These cations would react with the environment to form

surface species, or assume "relaxed" positions closer to the anion layer. Calculations suggest that the relaxation of surface cations is as much as 0.4 Å (Hen94).

No studies have been reported on the $(11\bar{2}0)$ and $(11\bar{2}12)$ habit planes. As seen in Figure 5-2B, the $(11\bar{2}0)$ habit is composed almost entirely of oxygen anions. This creates a polar surface. Aluminum cations have more than half their bulk ligand coordination. The $(11\bar{2}12)$ habit is a very open structure in which cations are highly exposed. The ligand coordination of Al^{3+} ions is reduced to approximately two oxygen anions. Such an uncoordinated surface will react with the environment or assume relaxed positions of the surface cations to further coordinate the cations with ligands.

The $(10\bar{1}2)$ habit plane is the locus for the vacancies of octahedral cation coordination sites in the corundum structure. The surface is non-polar and can be cleaved to form identical faces on either side of the cleavage plane. This facet only reduces the ligand concentration of cations by one, giving cations on defect free facets five coordinating anions. The incomplete O^{2-} octahedra are tilted with respect to the surface. LEED studies suggest that oxygen anions form ordered arrays on the surface, and calculational studies show that only modest perpendicular relaxation from bulk positions occurs on this plane (Hen94).

The generation of surface groups on each of the habit planes of interest involves the chemisorption of molecules to stabilize the surface. Chemisorption on metal oxides generally occurs via acid/base or donor/acceptor interactions (Stu92, Hen94). Cation sites are Lewis acids and oxide ions can act as basic sites and interact with acceptors such as H^+. A common dissociative reaction is the reaction of water with a surface to give hydroxyl groups. These are almost universally present on oxide surfaces (Hen94).

The investigations performed in this work are concerned with the chemisorption of alcohol groups with the surface, as both the solvent and the specific adsorbates used in particle synthesis will react via hydroxyl groups. Alcohols adsorb in a similar manner as water, with the reaction occurring through either a lone oxygen pair or dissociation by deprotonation (Hen94).

$$ROH + O^{2-} \rightleftharpoons RO^{-} + OH^{-} \tag{5-8}$$

This form of adsorption is more favored at defect sites, and produces both a methoxy and a hydroxyl group. A surface hydroxyl can also be replaced with an organic molecule through dissociative chemisorption.

$$ROH + CH_3OH \rightleftharpoons ROCH_3 + H_2O \tag{5-9}$$

The zeta potential of colloidal particles is related to the development of surface charge on the colloid, and the presence of a Stern layer. The surface charge is a function of the hydrolysis of the surface and thus the surface charge density will depend on the distribution of reactive sites. The presence of organic groups on the surface of the oxide will reduce the number of charge sites. This will lower the magnitude of charge development.

Generation of surface charge is often considered to relate to the dissociation of the surface hydroxyl groups on the surface of the metal oxide, but surface potential measurements include the effects of adsorption of ions. Oxygen anions at the surface will develop charge through the reaction of protons, but Al^{3+} ions can be present at the surface, and they will attract negatively charged ions. It is usually assumed that the attraction of hydroxyl ions OH^- to surface sites results in chemisorption, and the final

surface is assumed to consist only of surface -OH groups. In the case of trivalent species, cations can form surface hydroxo species (Stu92).

$$S\text{-}OH\ Al^{3+} + H_2O \rightleftharpoons S\text{-}O\text{-}AlOH^{+} + 2H^{+} \qquad (5\text{-}10)$$

The stable complexes of aluminum ions in solution relate to pH by stability constants (Bae86). As pH is made more basic, aluminum ions complex with additional OH^- ions to form different aqueous species, as shown in Figure 5-3. Speciation of the surface cations can be visualized as hydroxyl adsorption on surface hydroxo groups, and will change the surface charge and potential as a function of pH.

$$S\text{-}O\text{-}Al^{2+} + OH^- \rightleftharpoons S\text{-}O\text{-}AlOH^{+} + OH^- \rightleftharpoons$$
$$S\text{-}O\text{-}Al(OH_2)^0 + OH^- \rightleftharpoons S\text{-}O\text{-}Al(OH_3)^- \qquad (5\text{-}11)$$

The configuration of Al^{3+} on the surface of a facet will affect the zeta potential and isoelectric point of the surface. The total charge on the surface will relate to the number of positive and negative charges on the surface resulting from hydroxyl group charging and on the speciation behavior of surface aluminum sites.

Experimental

The procedure for glycothermal synthesis has been outlined previously (Cho95, Bel97). The reaction conditions in the 1000 ml hydrothermal vessel[1] were varied to produce each morphology. The platelet morphology was formed by reaction of 20 grams of gibbsite in 250 ml of 1,4 butanediol at 300°C for 36 hours at a shear rate of 240 rpm. The product was washed by five cycles of centrifugation and dispersion in methanol. The

[1] 1000 ml Hydrothermal Vessel, Model 236HC10, 316 Stainless Steel, Parr Instrument Co., Moline, IL.

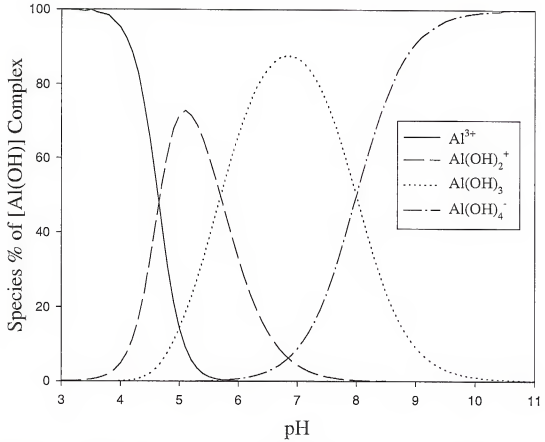

Figure 5-3. Aluminum-water speciation diagram generated using the OPAL© program.

prism morphology was synthesized in the 1000 ml hydrothermal vessel at 30 rpm. The solids loading was 15 grams of gibbsite in 350 ml of vacuum distilled 1,4-butanediol, and the reaction time was 30 hours.

The polyhedron shape was formed using 15 grams of gibbsite precursor in 250 ml of 1,4-butanediol in the 1000 ml hydrothermal vessel at a shear rate of 36 rpm. A seed concentration of 10^{10} α-alumina seeds/ml was used (Bel97). The reaction was performed at 300°C for 48 hours.

The bipyramid morphology was synthesized using the 1000 ml vessel. A volume of 250 ml of 1,4-butanediol which had been exposed to the air was used as the solvent. Exposure to the atmosphere allowed approximately 4% water to enter the solution. In place of gibbsite, 17 ml of Al-tri(sec)butoxide was added to the solvent, and the alcoxide reacted to form a gel immediately. The vessel was run at 240 rpm for 24 hours. The precipitate was cleaned by five cycles of centrifugation and dispersion in methanol.
A high surface area was desired for surface component analysis, so a fine powder was synthesized using α-alumina seeds to increase nucleation. The seeds used for increasing nucleation were a commercial α-alumina powder[2] with a 97 nm in effective diameter. The seeds were produced by suspending the powder in methanol, applying ultrasonication for 20 minutes, and collecting fine particles after two days. The powder was produced using 15 grams of gibbsite in 250 ml of solvent. A seed concentration of 9.5×10^{13} α-alumina seeds/ml was added, and the vessel was run at 300°C and 240 rpm for 24 hours. The resultant morphology was plate-like, as shown in Figure 5-4. Organic surface components were examined by washing this powder as synthesized in nitric acid at pH 4, and examining the supernatant with gas chromotography and mass spectroscopy. Diffuse reflectance spectroscopy was used to characterize the surface before and after the acid wash and after a three hour boiling treatment in deionized water.

Diffuse reflectance samples were prepared by using a 100:1 ratio of dry potassium bromide salt to α-alumina powder. The KBr and alumina were ground together in an

---

[2] α-Alumina, Sumitomo HIT-50, Sumitomo Chemical Co.

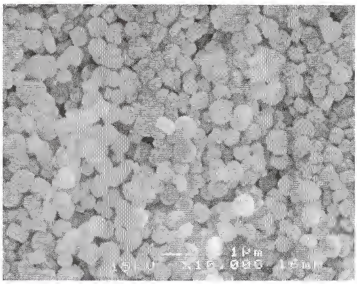

Figure 5-4. Scanning electron micrograph of the seeded platelet morphology used for surface structure analysis.

agate mortar and pestle until finely divided, and the mixture was then heated at 115°C for an hour to remove moisture.

Zeta potential was measured using the ZetaPlus, Zeta Potential Analyser[3] via diffuse light scattering technique. Samples were prepared by centrifuging the alumina powder in deionized water five times to transfer the powder from the washed methanol suspension. Stock solutions of KCl background electrolyte concentration were prepared and divided for pH modification. KOH and HCl were used to modify pH. Drops of concentrated solution were added to modify the pH of the background electrolyte, and midrange pH values were adjusted using the extreme concentrations of background electrolyte. Polyethylene vials were used to prepare 20 ml samples at each pH. Drops of

[3] Brookhaven Instruments Corporation, Brookhaven Corporate Park, Holtsville, New York 11742.

the alumina suspension in deionized water were added to give a dilute concentration of powder in pH adjusted KCl. Samples were allowed to equilibrate for one day. Afterwards, the suspension pH was measured and adjusted if necessary. Five minutes of ultrasonication was used on each sample before measurement to reduce agglomerates. The solution pH was measured before and after zeta potential measurement.

Results

Particle morphologies were synthesized by control of reaction conditions as described in the experimental section. The particles produced are shown in Figure 5-1. The platelet morphology is dominated by the basal plane (0001) and bound on edge habits by rough $\{11\bar{2}0\}$ facets. The particle surface is primarily composed of the basal plane, and characteristic properties related to the charging configuration of the basal plane should dominate measured zeta potential effects. The prism morphology is formed from identical habit planes as the platelet, but the proportion of particle surface area is dominated by the $\{11\bar{2}0\}$ facets rather than the basal plane. In the bipyramid morphology, the adsorption of 2-butanol has stabilized the high angle $\{11\bar{2}12\}$ facets over the plate-like axis, and the roughness of the sides may indicate that 2-butanol is also adsorbed on the $\{11\bar{2}0\}$ facets. The polyhedral morphology is characterized by $\{10\bar{1}2\}$ facets, and should provide information based on that habit plane.

The zeta potential for each morphology was measured initially after transferring to water from methanol, as well as after indicated times of static reaction with the aqueous environment. Figure 5-5A-C presents the shift in isoelectric point with time for each morphology. The surface of glycothermally synthesized alumina should be composed of

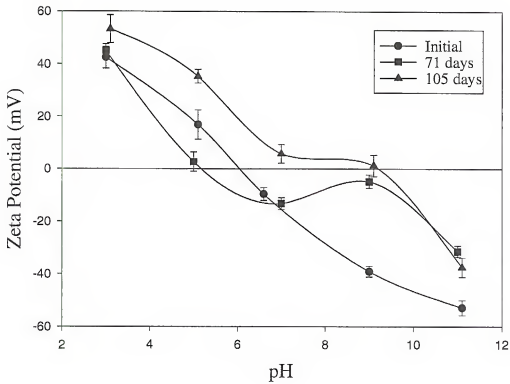

Figure 5-5A. Aging effects on zeta potential of the platelet morphology after aging in water for 71 and 105 days. Error bars are the 95% confidence interval.

chemisorbed organic solvent. Aging effects in zeta potential result from the exchange of organic ligands for hydroxyl groups on the particle surface.

In order to study equilibrium surfaces of the α-alumina powders, a solution of nitric acid at pH 4 was used to remove organic contaminants. The powders were immersed in static solution for two days. Following this treatment, the zeta potential was measured as a function of pH and ionic strength, using KCl as a background electrolyte, and HCl and KOH as acid and base. Figures 5-6A through 5-6D show the resulting zeta potentials. The final surface composition was measured by electron dispersive

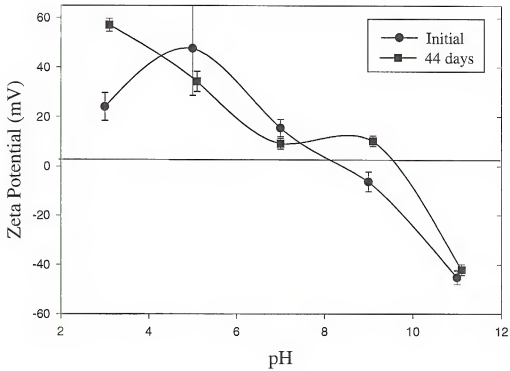

Figure 5-5B. Aging effects on zeta potential of the prism morphology after aging in water for 44 days. Error bars are the 95% confidence interval.

spectroscopy (EDS), and the results for the surface composition are presented in Table 5-1. Carbon levels representing organic contaminants are all approximately 8%.

Discussion

Structural Examination of Glycothermally Synthesized Alumina Surface

Figure 5-7 shows the infrared spectra of the fine platelet powder studied for the removal of surface organic groups. The synthesized powder and the powder after boiling in deionized water for three hours both show that physisorbed water is present on the

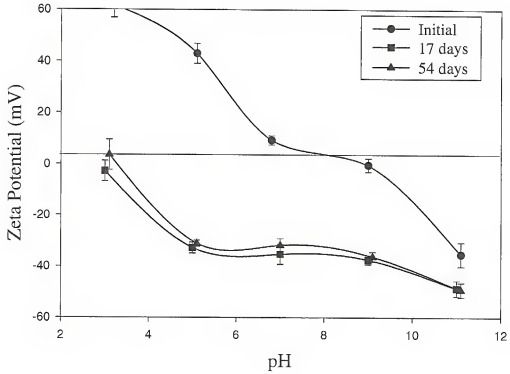

Figure 5-5C. Aging effects on zeta potential of the bipyramid morphology after aging in water for 17 and 54 days. Error bars are the 95% confidence interval.

surface from the broad peak at ~ 3300 cm^{-1}. Organic functional groups are not well defined, but there are small shoulders at 2979 and 2909 and 1344 cm^{-1}. These vibrations are typical of CH_2 and C-O-H vibrations, and suggest that 1,4-butanediol is present on the surface bonded by one hydroxyl group. After the acid wash and boiling treatment, the intensity of these peaks is diminished, but not removed. The bonding of alcohols is known to be very resilient, and can resist removal even in acid conditions (Gre62, Kag67).

The examination of the supernatant from the acid wash of the fine powder is presented in Figure 5-8. The graph shows the molecular weights of the minor

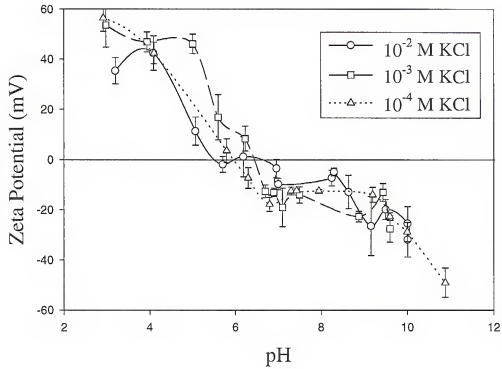

Figure 5-6A. Zeta potential of the platelet morphology after acid wash as a function of pH and ionic strength. Error bars are the 95% confidence interval.

components within the water. The series of peaks near 18 are components due to water, and the peaks clustered about 31 result from methanol. The small peaks at higher values like 45, 49, etc are indicative of higher molecular weight species dissolved from the particle surface. They could be fragments of larger molecules. The highest molecular weight molecules detected occurred at 115, 133 and 151 amu. Pure 1,4-butanediol has a molecular weight of 90, but the dissolved products may have oxidized or polymerized before release. Thus, the structure of organic adsorbates has not been established, but their presence is noticeable.

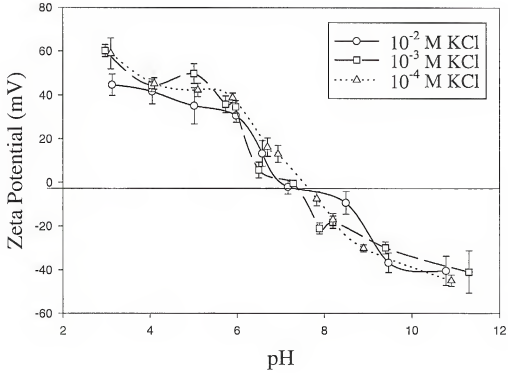

Figure 5-6B. Zeta potential of the prism morphology after acid wash as a function of pH and ionic strength. Error bars are the 95% confidence interval.

The surface groups present on the glycothermal platelets present a complex combination of possibilities. Synthesis in 1,4-butanediol will cause the chemisorption of 1,4-butanediol groups to the surface, and it is possible that both functional groups could be bonded. Bifunctional adsorption would create a hydrophobic surface by presenting -CH_2 groups to the surroundings. Monofunctional adsorption will exhibit amphoteric charging behavior that is independent of the charge character of the crystal surface. Polymerization of the solvent would create ether linkages which should not adsorb under

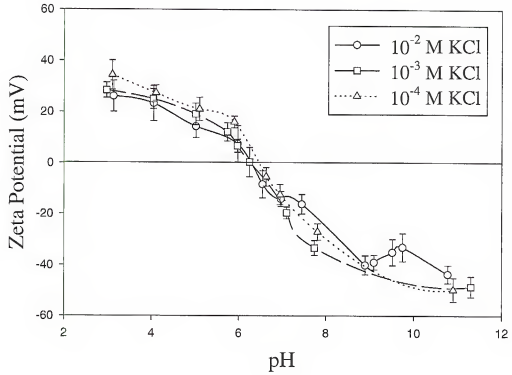

Figure 5-6C. Zeta potential of the bipyramid morphology after acid wash as a function of pH and ionic strength. Error bars are the 95% confidence interval.

synthesis conditions, but may form a steric barrier at room temperature. A dimer could adsorb at two sites to present an ether site to the solution. Such a surface would not exhibit hydrophobic character. The exchange of solvent groups for hydroxyl termination will be promoted by acidic conditions. The resulting surface will be amphoteric, but should exhibit charge properties that are dependent on the local ligand structure of the surface.

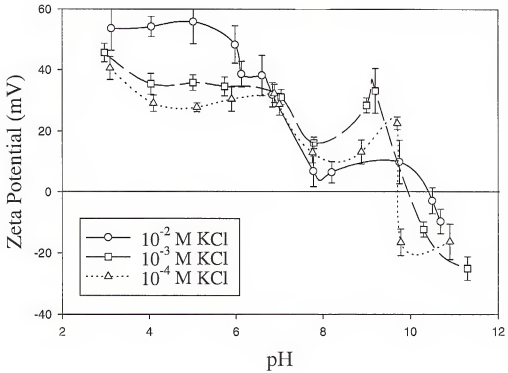

Figure 5-6D. Zeta potential of the polyhedron morphology after acid wash as a function of pH and ionic strength. Error bars are the 95% confidence interval.

Table 5-1. Electron dispersive backscattering results for the presence of adsorbed carbon groups on the surface of glycothermally synthesized platelets.

Morphology	Mass % Al	Mass % O	Mass % C
Platelet	46.72	45.76	7.52
Bipyramid	48.66	42.23	9.11
Prism	48.53	42.71	8.76
Polyhedra	48.57	42.36	9.07

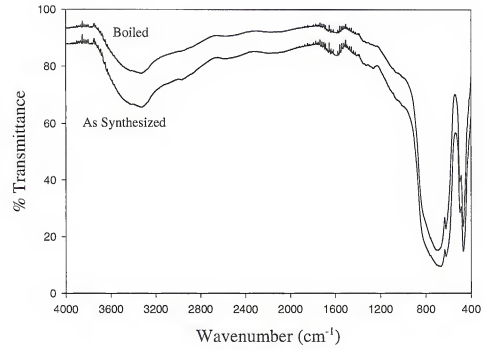

Figure 5-7. Diffuse reflectance infrared spectroscopy of as synthesized platelets and the platelets after boiling in deionized water for 3 hours. The average powder particle size is 0.5 microns.

Surface Charging Behavior of Morphological Forms

Upon transfer to aqueous suspension, it was obvious that the platelet and bipyramid morphologies were hydrophobic. Surface films and stable bubble structures covered the surface of the suspension, and the majority of powder of agglomerated at the bottom. Adhesion to the polyethylene containers was also apparent. The aging results show that each morphology initially has an isoelectric point near 9, but eventually experiences a different isoelectric point as shown in Figure 5-5A-C.

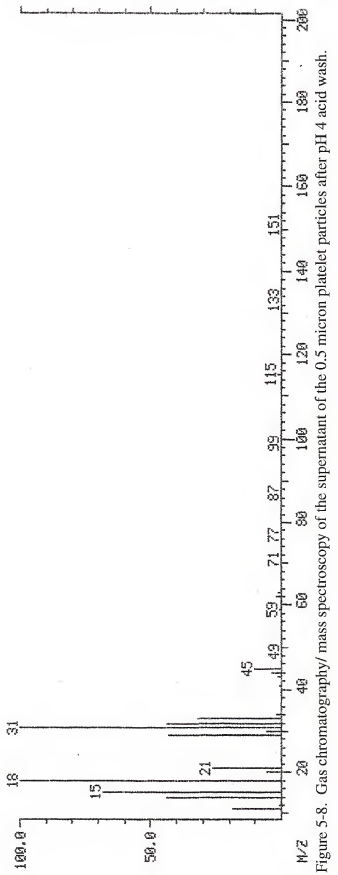

Figure 5-8. Gas chromatography/ mass spectroscopy of the supernatant of the 0.5 micron platelet particles after pH 4 acid wash.

Table 5-2. Concentration of Al^{3+} sites as a function of habit plane.

Habit Plane	Al^{3+} Sites/nm^2	Measured Isoelectric Point	
		Aged	Acid Washed
$(11\bar{2}12)$	2.2	3	6
(0001)	1.25	5	6
$(11\bar{2}0)$	1.1	8	7
$(10\bar{1}2)$	0.85		10

There are several differences in the number of surface aluminum ions, which are shown as the concentration of ions per unit area in Table 5-2. The isoelectric points become more acidic as the concentration of metal cation sites increases. This indicates that surface Al^{3+} do attract OH^- ions, and thus will promote negative surface charge. The arrangement of crystal anions will affect the number and strength of negative ion speciation. The platelet morphology has an isoelectric point that decreases from an initial value of ~9 to approximately pH 5, and may decrease further with continued aging. The basal plane has surface cations with only half of their available ligand bonding satisfied by the presence of the bulk material. There is little barrier to the adsorption of OH^- ions. As a result the isoelectric point is found to lie at approximately pH 5, and may decrease further with continued aging. This agrees well with results shown by Larson et al. (Lar97), which states that the isoelectric point of the basal plane lies between 3 and 5. Under acidic conditions, surface Al^{3+} ions should resemble the speciation of free Al^{3+} ions in solution.

The isoelectric point of the $\{11\bar{2}12\}$ plane was found to be approximately 3. The surface of this plane has low symmetry, and therefore should provide several sites for hydroxyl adsorption on Al^{3+} sites to generate a negative surface potential. The aging results of the bipyrimid morphology indicate that equilibrium of the reaction between the surface and the environment occurred under 17 days, as the results were reproduced after 54 days. This is due to the higher reactivity of secondary alcohols compared to primary alcohols. The platelet morphology was much less reactive to aging effects. Primary alcohols have the most stable hydroxyl groups, and the possibility for adsorption of both functional groups of the 1,4-butanediol would lend additional stability to the surface coverage of the basal plane. Such adsorption would explain the hydrophobicity observed when the powder was first transferred to aqueous suspension.

The $(11\bar{2}0)$ plane is primarily composed of O^{2-} ions, and exhibits an isoelectric point of 8. This value agrees well with values for commercial alumina published in the literature (Git70). Such a surface should be dominantly composed of hydroxyl groups. Metal cation sites are well coordinated by ligands, and surface speciation should not be a prevalent factor in charge development. Reaction with 1,4-butanediol would coat the surface with butoxyl termination instead of hydroxyl groups. The reaction of H^{+} ions with the surface oxygen ions to produce surface hydroxyl groups during aging would correlate with the Healy-White model of surface protonation /deprotonation (Hea78).

The use of the nitric acid wash to determine final, aged surfaces reduces the differences between the various morphologies. Both the platelet and the bipyramid morphologies have an isoelectric point near 6. The prism isoelectric point has decreased to pH 7. The use of an acid may have caused dissolution of the distinct crystallographic

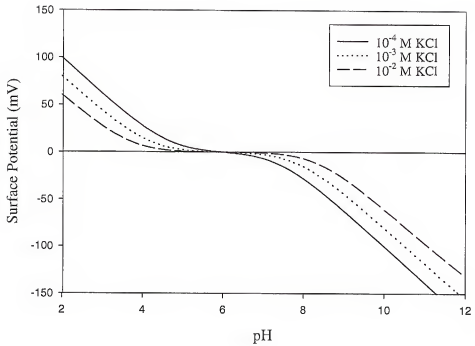

Figure 5-9. Comparison with the Healy-White model of surface charge generation. *ΔpK* = 8 and isoelectric point is 6.

character of the habit planes. As a result, the adsorption of hydroxyl groups to the Al^{3+} surface sites is no longer distinct as a function of each morphology. Additionally, the compression of zeta potential with background electrolyte concentration is not as effective as predicted by colloidal theory. Figure 5-9 shows the Healy-White model for surface potential for a surface with a ΔpK of 8 and an isoelectric point of 6. This indicates strong deviation from ideal, Nernstian behavior. The surface potential is twice as large as the experimentally determined values, but the model shows that the surface potential decreases by approximately half with a change from 10^{-4} M KCl to 10^{-2} M KCl.

Additionally, the development of potential requires the pH to be about one to two unitsaway from the isoelectric point. Figures 5-6A-C show the potential curves for the platelet, prism, and bipyramid morphologies. The platelet morphology has a maximum positive potential near 55 mV, and it seems to decrease sharply to the isoelectric point above pH 5. From pH 7 to 9, the zeta potential is negative and low at approximately -10 mV. At basic pH greater than 9, the magnitude of the zeta potential again begins to increase. These plateau regions of relatively constant potential could result from saturation of speciation of Al^{3+} sites.

The prism potential curves are more uniform, with a range of potential values from +55 mV to -40 mV. The various ionic strengths do not appreciably reduce the magnitude of the potential, in opposition to DLVO theory, but the high ionic strengths do exhibit lower potential magnitudes than low ionic strength. The material did not exhibit the plateau region of potential similar to the platelet. The expected surface structure of crystal anions forming hydroxyl groups on the surface agrees well with the resulting potential curves.

The bipyramid potential curves are the most uniform and reproducable. Zeta potential ranges from +40 to -60 mV. The higher magnitude of negative zeta potential suggests that there is more adsorption of OH^- ions as surface species. The low ligand coordination of the ideal habit plane suggests that there is little steric hindrance to coordination of surface Al^{3+} ions with solution hydroxyl ions. The expected decrease of zeta potential is found with increasing ionic strength, but the magnitude of reduction is only 10-15 mV. There is no distinct plateau region. This may be the result of surface

recrystallization or the formation of a basal plane step structure on the $\{11\bar{2}12\}$ habit planes.

The polyhedron morphology is dominated by the $\{10\bar{1}2\}$ habit planes, and an isoelectric point of ~10 was observed as shown in Figure 5-6D. The $\{10\bar{1}2\}$ face is the only face that has stable Al^{3+} vacancies, and therefore suggests that the surface is resistant to the speciation of hydroxyl groups. As such, the surface maintains positive charge until the concentration of OH^- is such that the surface must acquire adsorbed hydroxyl ions. This requires a high concentration of base in solution, and leads to the high isoelectric point. The drift of the isoelectric point with KCl concentration indicates that there is some adsorption of electrolyte on the surface.

The colloidal characteristics of these particles do not follow established trends of DLVO theory. The zeta potential measured at 10^{-2} M KCl displayed the highest zeta potential values at acidic conditions, which is counter to the effect of double layer compression due to background electrolyte. This indicates that the acid and background electrolyte must both interact with the surface to increase the magnitude of the surface charge. The zeta potential curves show that there is a minimum in positive potential at pH 8 before the isoelectric point of approximately 10 is reached. Multiple charge generating groups that exchange charge at various values of pH would reduce the total surface charge over a broad pH region. Once all groups were generating the same charge, zeta potential magnitudes would increase. This sort of behavior would occur if all surface groups were not removed by the acid treatment.

Summary

The particles used in this study have shown that the solvent used in their synthesis adsorbs to the surface to create a hydrophobic surface. Exposure to water causes the surface structure to age and change the isoelectric point, with the development of hydrophilic character. The zeta potential curves measured show that isoelectric point and charge magnitude are sensitive functions of morphology, and it is proposed that the development of charge depends on the coordination of negative ions with metal cation sites on the surface. The isoelectric point has been found to correlate with the ideal concentration of metal cation sites on the surface. The stability of the metal sites with respect to coordination will depend on the ionic packing arrangement of the surface, and the ligand coordination with aqueous species. Charge development is also related to the ligand coordination of the surface anions to surface cations.

CHAPTER 6

MORPHOLOGICAL CHANGES IN GLYCOTHERMALLY SYNTHESIZED ANISOTROPIC α-ALUMINA PARTICLES DURING SINTERING

Introduction

Glycothermal synthesis has been developed as a means of synthesizing α-Al_2O_3 of controlled morphology and size (Cho95, Cho96). Experiments by Cho et al. showed that 1,4-butanediol reacts with hydrous phases of aluminum hydroxide to form psuedo-boehmite with the resultant precipitation of α-alumina at temperatures as low as 270°C and in reactions times as low as twelve hours. Cho also demonstrated morphological control of the particles by varying the solids loading, reaction time, and stirring rate (Cho95). Particle sizes from 5 μm to 0.1 μm were obtained while maintaining morphological control. One of the forms of these particles is hexagonal platelets.

Powders formed via the solution synthesis technique characteristically have well defined crystal facets and potentially could result in the formation of equilibrium shapes. An equilibrium shape is derived from the Wulff plot, which describes the surface free energy of a particle (Gib64). An equilibrium morphology is characterized by the Wulff shape in accordance with the Gibbs-Curie theorem. This concept states that the sum of the product of the surface energy and the surface area of a particle is minimized (Wul01). The Wulff shape for an isotropic material is a sphere, but many ceramics are expected to

exhibit low energy cusps in the Wulff plot corresponding to stable crystallographic directions. These low surface energy directions create faceted morphologies, with anisotropic surface energy. The surface energy of the Wulff shape is related to the perpendicular distance of the facet from the center of mass by the following relationship (Def66, DeH93).

$$\frac{\gamma_{hkl}}{\lambda_{hkl}} = \text{constant} \tag{6-1}$$

where γ_{hkl} is the surface energy of the crystal face hkl and λ_{hkl} is the central distance of the crystal face from the center of mass. This relationship is valid for both faceted interfaces and for rounded interfaces (Her51). Equation 1 shows that surface energy and the central distance have a direct relationship at equilibrium. Lower energy facets have a smaller central distance, and the low energy facets will therefore dominate the surface area of the crystal particle.

The thermodynamic basis for the microstructural evolution of ceramic compacts has been well researched for materials of isotropic surface energy (Kel89, Lan89). The theory suggests that initial sintering occurs until equilibrium dihedral angles are achieved, driven by reduction of surface energy. Coarsening to remove grain boundary area involves the growth of one grain by mass transport from a neighbor, and is driven by differences in chemical potential. Grain growth generates non-equilibrium shapes which reinitiate sintering. Coarsening may or may not occur until the driving force for sintering is reduced by the assumption of stable particle morphology. Grain growth is necessary for the reduction of large pores, and has been related to the curvature between grains.

Curvature creates a chemical potential difference given by the Gibbs-Kelvin equation (DeH93).

$$\Delta\mu = \gamma_s \Omega \left(\frac{1}{R_2} - \frac{1}{R_1} \right) \tag{6-2}$$

where $\Delta\mu$ is the chemical potential difference, γ_s is isotropic surface energy, Ω is molar volume, and R_1 and R_2 are the principle radii of curvature at the surface. For a pore within the compact, pore closure is a function of pore coordination number and dihedral angle, rather than a kinetic process. A high bulk density compact is expected to have smaller pores, and therefore densify under optimal sintering conditions without high degrees of grain growth. This equation has been used to explain sintering phenomena, but it is derived for the isotropic case which does not describe most ceramics.

Morphological changes in particles of anisotropic surface energy involve mass transport both to form low energy facets and to reduce facet edge lengths (Sea85). The thermodynamic requirements for the formation of intermediate shapes as a non-equilibrium shape approaches equilibrium is expressed by the following relationship (Sea94).

$$\delta G = \sum_{i=1}^{m} (\sigma_i \delta A_i + \mu^* \delta n_i) + \sum_{j=1}^{k} \varepsilon_j \delta l_j \tag{6-3}$$

where δG is the change in Gibbs free energy, σ_i is the surface energy of facet *i* with area A_i, and ε_j is the unit energy of an edge of length l_j. μ° is the chemical potential of the condensed phase in its standard state and n_i is the number of moles that can be assigned to the *i*th surface by construction of a pyramid with the apex at the center of mass and base formed by the crystal facet. A crystal will be unstable to changes in morphology which

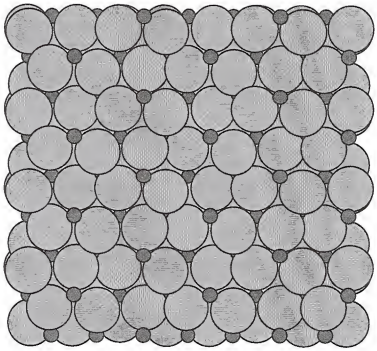

Figure 6-1. ATOMS© plane representation of the basal plane (0001) of α-alumina. (Input: space group Rb3c, a = 4.758 Å, c = 12.991 Å. Al^{3+} ionic radius = 0.39 Å, O^{2-} ionic radius = 0.90 Å.)

reduce the value of this equation. The α-Al_2O_3 particles used in this study have a basal plane dominant morphology, and the high planar packing density, as shown in Figure 6-1, is expected to provide a low surface energy to the platelet morphology. Additionally, the lack of curvature does not support the commonly offered mechanism for the development of the driving force for sintering. Lastly, the anisotropic shape of these particles provides

an opportunity for improved characterization of sintering as a function of particle packing as well as lending insight into surface energy effects during sintering.

Several aspects of powder processing must be considered in the interpretation of the results of the sintered ceramic pieces (Pas87). Foremost, particle packing is a critical variable. Higher green densities lead to higher final densities due to the reduction in the formation of large pores and reduction in diffusion distances. Glycothermally produced platelets have shown typical packing characteristics in tap density tests, achieving values of 30% theoretical density.

Porosity is as critical as packing, since both the mean pore size and the pore size distribution affect the final shrinkage and the final density achievable in the powder (Lan88). Pores in a ceramic microstructure can be classified as stable or unstable by evaluation of the pore size to grain size ratio. It was shown by Kingery and Francois (Kin76) that a critical ratio for densification exists in which pores exceeding the critical ratio will be stable, and those below this ratio will be eliminated. Ordered regions or domains sinter before less densely packed regions, and these ordered domains may undergo final sintering or discontinuous grain growth. Zheng and Reed (Zhe89) found the critical pore size to grain size ratio for α-alumina to be 0.5, indicating that pores larger than half the mean grain size were stable and those below would be eliminated on sintering. Previous work on alumina has shown that sintering of submicron alumina (Yeh88a) can occur as low as 1150°C and a broad particle size distribution improves packing characteristics which result in higher final densities (Yeh88b).

Glycothermally synthesized powders pose properties unique to existing powder processing technology, such as unknown surface energy and particle packing

characteristics. An evaluation of sintering phenomena provides insight into the benefits and challenges of low surface energy yet highly anisotropic particles.

Experimental

α-Al_2O_3 platelets were synthesized by glycothermal treatment at 300°C for 12 hours with an α-Al_2O_3 seed concentration of 4×10^8 [1] and a stirring speed of 240 rpm. Hydral™[2] was used as the reaction precursor. Following synthesis, the particles were washed by five cycles of centrifugation, decantation, and redispersion in methanol followed by five cycles of centrifugation, decantation, and redispersion in ethanol. Phase identification was performed using X-ray diffraction and indicated phase-pure α-Al_2O_3. [3]

Glycothermally synthesized powders were slip cast to prepare compacts for evaluation of morphology and density. Slips of powder in deionized water were prepared with a solids loading of 50 weight %. Darvan C was added at 1.9 wt% with respect to the α-Al_2O_3 powder to promote dispersion. Slip casting was performed using a teflon tube 0.5 inches in diameter as a mold placed over 0.22 μm filter paper on top of an absorbant plaster of paris substrate. After forming, the pellet was sectioned with a razor blade to provide samples for sintering evaluation. Samples were stored at ambient humidity (approximately 70%).

---

[1] Parr Instrument Company, Moline, IL
[2] Alcoa Chemicals, Pittsburg, PA
[3] Phillips APD 3720, Mount Vernon, NY

Sintering was performed in air for a three hour duration at the test temperature (1100, 1300, 1400, 1500 and 1600°C) in a box furnace.[4] The furnace was ramped at 10°C/min until 100°C below the sintering temperature, ramped at 8°C/min to the sintering temperature, held for three hours at the sintering temperature, and then cooled to ambient temperature at approximately 10°C/min. Samples were sputtered with Au-Pd prior to analysis of morphological changes by scanning electron microscopy[5]. Density measurements were taken using the Archimedes method in ethanol.

Results and Discussion

Morphological Evolution

An understanding of the sinterability of α-Al_2O_3 platelets requires insight into the effects of particle dispersion and particle packing. Figure 6-2 shows the morphology of the glycothermally produced platelets and particle packing prior to sintering. The typical shape is a platelet or flake approximately 0.3 - 0.8 μm in diameter which have an approximate height of one tenth of the basal plane diameter. The edges are not planar or uniform in these particles. Some twinning is also evident in which a portion of a basal plane extends from the surface of a platelet at a high angle. The particle surfaces aligned into domain structures due to their anisotropic morphology. Misalignment between domain structures due to packing behavior or twins also created void structures on the order of one micron in size. The particle arrangement into domains may be due to capillary forces created as the particles were cast, or perhaps a result of particle

---

[4] Lindberg/Blue M, Asheville, NC

[5] JSM 6400, JEOL Ltd., Tokyo, Japan

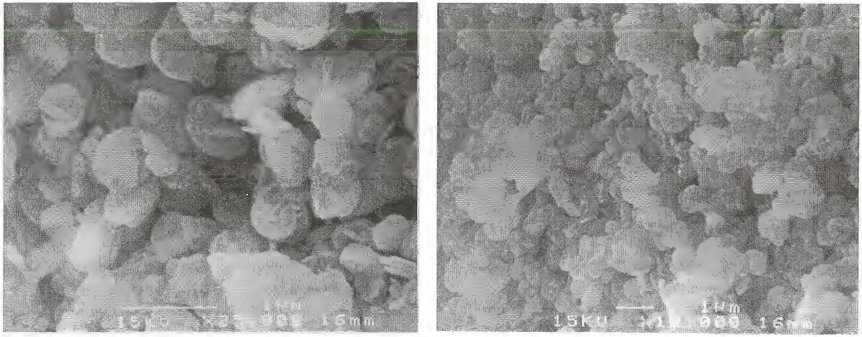

Figure 6-2. SEM photomicrographs of the fracture surface of the slipcast α-Al_2O_3 pellet before sintering.

aggregation from van der Waals attraction in the suspending medium.

Figure 6-3 shows the fracture surface of the α-Al_2O_3 compact held at 1100°C for three hours in air. The effect of particle packing arrangements are evident here, as Figure 6-3A presents an agglomerated particle arrangement, in which the particles have developed necks at points of contact. Particle morphology has changed as well, with the development of smoother surfaces. Figure 6-3B shows a local particle domain, in which the basal planes are oriented in a parallel arrangement. This domain has formed an aggregate grain with several levels indicating their initial particle shape. Due to the random nature of particle alignment, it is likely that this type of grain contains internal voids.

In the powder compact, local domains of platelets are formed by alignment of basal plane faces. Between these domains are randomly oriented platelets as well as significant pore regions and channels. Some of these pores between domains are on the order of the initial particle face size of 0.5 μm, whereas aligned platelets have virtually no interparticle porosity. Lange reported that particle domains densify at 800°C for a Reynolds A-16 SG powder in agreement with pore coordination number effects on the pore stability (Lan88). The glycothermally produced α-Al_2O_3 platelets corroborate Lange's statements that "...small, multiple particle packing units densify and support grain growth prior to bulk shrinkage. Grain growth and rearrangement processes decrease the coordination number of remaining pores to allow them to disappear during latter stages of sintering."

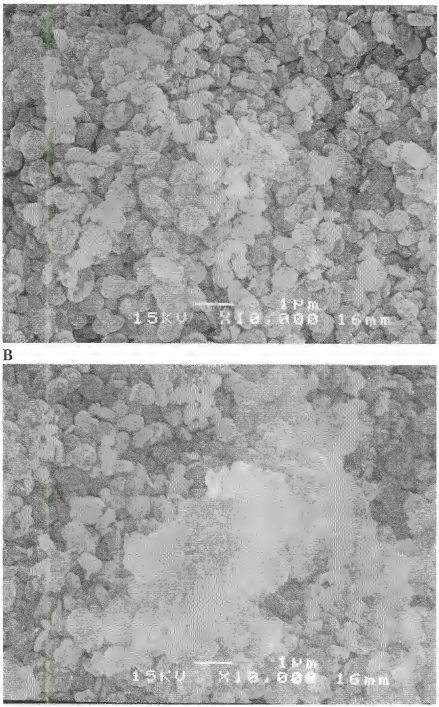

Figure 6-3. SEM photomicrographs of the fracture surface of the slipcast α-Al_2O_3 pellet after sintering at 1100 °C for three hours. (A) Randomly oriented particles. (B) Domain structure.

As shown in Figure 6-4A, the particle morphology has changed from 0.3 μm - 0.8 μm platelets to more equiaxed particles of the same scale. The increase in volume indicates that grain growth occurred only in the particle domains. If the particles had changed morphology without sintering, the achievement of a rounded polyhedral shape would require a reduction in diameter in order to conserve mass. The particles have obviously gained mass, indicating that the particles within local domains have sintered. The new, larger grains have formed necks to their nearest neighbors, and the morphology is mixed between some faceted and rounded surfaces. Highly interconnected porosity with void areas on the same order as the particles is present. Consideration of morphological changes by Searcy and Bullard indicates that the kinetics of morphological change favor the development of small terraces or steps of stable morphological habits before the development of a macroscopic equilibrium shape (Sea94). This can cause the illusion of rounding if the resolution of the examination is limited. The limiting scale of these terraces and steps of stable habit is balanced by the formation of edge and corner energies in the micro-faceted shape. The elimination of these edge and corner energies becomes the driving force for sintering after the development of limiting facets. Mullins (Mul63) and Brailsford and Gjosein (Bra75) predicted that if self-diffusion acts as a rate limiting mechanism, rounding can persist during shape changes for faceted particles. Computer modeling of this phenomena supports these observations (Bul94).

Considering Figure 6-4A, the particles or grains have developed a fine rough texture on the particle surface. The limiting scale of the roughness is very small, and is perhaps beyond the resolution of the scanning electron microscope. The surface texture

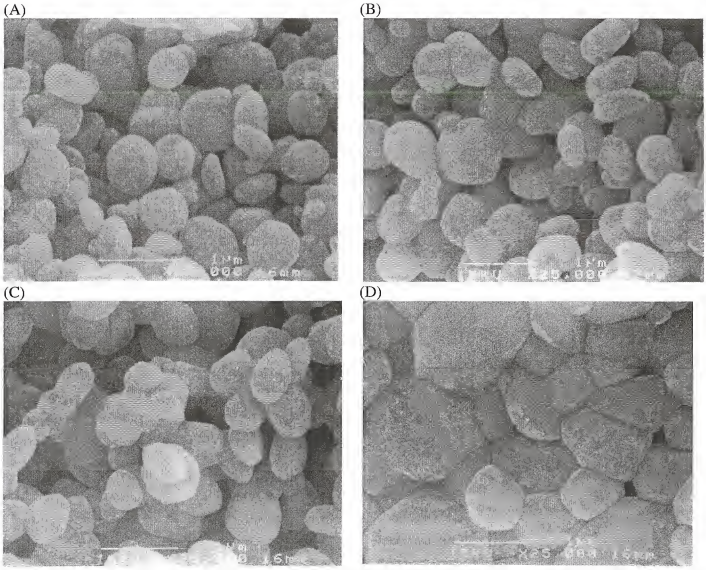

Figure 6-4. SEM photomicrographs of the fracture surface of the slipcast α-Al_2O_3 pellet after sintering for three hours in air at (A) 1300 °C, (B) 1400 °C, (C) 1500 °C, and (D) 1600 °C.

may result from the thermodynamic requirement that facets must be maintained down to a limiting facet size. The resolution of the photomicrograph is insufficient to resolve the character of the surface roughness, and the limiting size of a facet of alumina cannot be estimated from this data.

The sintering of local domains is unusual with respect to Lange's arguments, as virtually no porosity exists between the grains, and no curvature is present to enhance sintering (Lan88). The domains may have undergone initial sintering at 800°C or even lower temperatures. In any case, barriers to sintering would include grain to grain mismatch or impurities. Consideration of the hexagonal lattice structure reveals that the angular mismatch of lattice structures between two grains can be no more than 15°. The atomic arrangement of the basal plane, shown in Figure 6-1, is very dense as well as stoichiometric, and it is possible that a diffusing ion could quickly assume a lattice position in the adjacent grain. In such close proximity, boundary diffusion between the grains could allow for a single grain to dominate a neighbor and form a single particle. Curvature effects may be involved in the grain growth process in the form of Rayleigh instabilities (Ray79).

Figure 6-4B shows the particle morphology after three hours of sintering at 1400°C. The particle size has not noticeably grown from the 1300°C sample, and porosity is not appreciably decreased. Grain boundaries are more developed and exhibit curvature. Figure 6-4C shows that at 1500°C, the particle body remains highly porous, but faceting of the particles is obvious. Planar interfaces appear to be developing between particles. Particle surfaces exposed to the vapor phase develop facets to

minimize surface free energy. The high pore coordination number of the pores prevents the development of a fully dense ceramic microstructure.

Figure 6-4D shows the morphology at 1600°C after three hours of sintering. Grain growth is clearly evident in the crystals, and has reached a size exceeding the critical ratio of 0.5 derived by Zheng and Reed (Zhe89). Visible porosity has decreased greatly. The crystal facets appear planar, with macroscopic steps in some cases. Some concavity is noticeable in the interfaces.

Clearly, the sintering results for the glycothermally produced particles show that particle packing must be greatly improved in order to achieve near theoretical densities. Density results are presented in Table 6-1 for the powders as a function of sintering conditions. The bulk density of the compacts generally increases with sintering temperature, with a corresponding increase in the percent of theoretical density achieved. The wide scatter in the results may have resulted from the initial particle packing due to the inhomogeneity of the original powder compact. However, the closed density of the samples decreases with temperature. This indicates that the progress of grain growth occurs with either the entrapment of porosity within the grains, or with capture of stable shaped pores within grain structures. Additionally, the percent open porosity decreases to a value of 2.4% at 1600°C for a bulk density of 3.32 g/cm^3. Large pores are likely present within the microstructure. Removal of this type of pore requires grain growth or transport mechanisms such as lattice diffusion to remove the porosity as vacancies. The high temperatures required for this diffusion mechanism also promote exaggerated grain growth.

Table 6-1. Immersion density values for samples sintered at varying temperatures.

Sintering Temperature (°C)	Bulk Density (g/cm^3)	Closed Density (g/cm^3)	Percent Open Porosity	Percent Theoretical Density
1100	2.02	3.80	46.7	50.8
1300	2.42	3.67	25.6	60.8
1400	2.15	3.79	28.4	53.9
1500	2.82	3.39	28.3	71.0
1600	3.32	3.45	2.4	83.3

In addition to Zheng and Reed (Zhe89), Yeh and Sacks (Yeh88a, Yeh88b) considered the effects of particle packing and size distribution on the consolidation of alumina compacts, and stated that the green density can indicate the effectiveness of the dispersion and the particle packing, and green density affects sintering rate. Increased green densities and improved microstructure homogeneity significantly improves sinterability. Yeh and Sacks showed that a narrow particle size distribution does not provide intrinsic benefits during sintering of spherical powders. A broad size distribution gives tighter packing of spheres, and results in higher densities. A broad distribution of anisotropic powders may not have the same packing characteristics however, but this study does not investigate the effect of the particle size distribution of anisotropically shaped particles. It may be that the amount of dispersant used (1.9 wt% to powder) was insufficient to coat the surface area of the particles effectively. This could lead to bridging flocculation which could explain the high porosity seen in the samples. Mechanical compression rather than slipcasting may improve particle arrangement to create a more uniform green microstructure.

Surface Energy Calculations

Curvature effects were first derived as the predominant driving force in sintering processes, but many studies now attribute surface energy as a major factor (Bra75, Mul63, Sea85, Sea94). This work, involving particles of controlled, faceted shape, negates the general considerations of curvature as a contributing factor in sintering. It has been rationalized that the appearance of curved surfaces from these faceted particles is a scaling effect (Bra75, Mul63, Sea94), with microfacets present locally on the surface of the alumina particles. Determination of the activation energy for transformation from one morphological form to another would provide insight into the sintering behavior of glycothermally produced powders.

Calculations of surface energy changes require knowledge of the equilibrium shape of alumina, as well as a determination of the surface energy value as a function of crystal habit plane. DeHoff presented an average surface energy value of 905 mJ/m^2 for Al_2O_3 at 1850°C in his text (DeH93). Choi et al. presented an equilibrium shape for α-alumina based on TEM observations of cavities (Cho97). Figure 6-5 shows this Wulff shape with the determined ratio of surface energy to the basal plane. As DeHoff's value of the surface energy is an average equilibrium value, the central distance and area of each facet can be used to estimate the surface energy proportional to each habit plane. Derived surface energy values for α-Al_2O_3 based on the observations of Choi et al. are given in Table 6-2 and Table 6-3 gives the surface area per habit plane for the platelet and equilibrium morphologies. The basal plane has the lowest surface energy value.

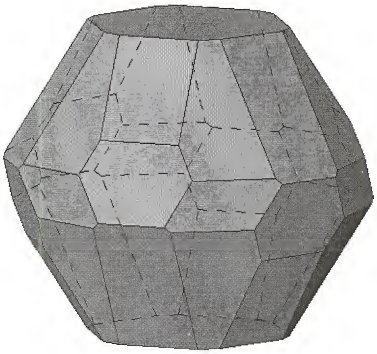

Figure 6-5. Theoretical equilibrium shape for α-Al_2O_3 (from Cho97). With respect to the basal plane (0001), surface energy ratios follow: $\gamma(\bar{1}012) = 1.05$, $\gamma(1\bar{2}10) = 1.12$, $\gamma(11\bar{2}3) = 1.06$, and $\gamma(10\bar{1}1) = 1.07$.

Table 6-2. Calculation of α-alumina surface energy as a function of crystallographic habit from data at 1850°C (DeH93).

Indices	Central Distance*	Surface Energy(mJ/m^2)
0001	1.00	859
$\bar{1}012$	1.05	902
$1\bar{2}10$	1.12	962
$11\bar{2}3$	1.06	911
$10\bar{1}1$	1.07	919

*from reference 22.

Table 6-3. Surface area values of the facets as a function of morphology.

Platelet Morphology		
Indices	Individual Surface	Total Area for Particle (%)
$1\bar{2}10$	3.33	20.0
0001	40.0	80.0
Equilibrium Morphology*		
Indices	Individual Surface	Total Area for Particle (%)
0001	10.04	20.1
$\bar{1}012$	3.08	18.5
$1\bar{2}10$	1.56	9.35
$11\bar{2}3$	3.01	36.1
1011	2.65	15.9

*from reference 22.

Face areas were estimated from SHAPE©[23] figures and normalized to equivalent particle volumes. Geometrical considerations yield the following calculations for the surface energy of a platelet and an equilibrium shape of ~4.44 μm^3 volume.

$$\Sigma\gamma_{platelet} = 2 \times (859\ mJ/m^2) \times A_{001} + 6 \times (962\ mJ/m^2) \times A_{110} = 2.28 \times 10^{-8}\ mJ \qquad (6\text{-}4)$$

The equilibrium shape has a surface energy of 1.14×10^{-8} mJ per particle at this volume. The morphological change from platelet to the equilibrium shape gives a $\Delta G = -1.14 \times 10^{-8}$ mJ. The platelet morphology has a strong driving force for sintering, as it can reduce its surface energy by 50%. These calculations suggest that the platelet morphology will begin sintering at lower temperatures in order to reduce surface energy. The observations of platelet sintering agree with these results in that the domain structures undergo sintering quickly, and particle rounding occurs at low temperatures.

Conclusions

Basal plane sintering in ordered domains occurred readily in glycothermal platelets, but particle packing effects created pores that inhibited the achievement of full theoretical densities. Improved particle packing is needed to achieve theoretical densities. The development of rounded morphologies during sintering has been explained as a scaling effect. Calculations of the reduction in surface energy as platelets achieve equilibrium shape indicate that the platelet morphology has a strong driving force for sintering, which would provide for the development of dense microstructures at lower temperatures. Sintering has also been observed at temperatures as low as 1100°C and may occur at lower temperatures. When two particles align such that the basal planes are adjacent, the observed sintering between planes with high atomic density indicates that the absence of curvature between these basal planes does not inhibit sintering.

CHAPTER 7

CONCLUSIONS AND FUTURE WORK

This investigation has evaluated the theoretical and experimental aspects of particle morphology involved in the glycothermal synthesis of α-alumina. Thermodynamic theory has been applied to elucidate the conditions for equilibrium of a particle in liquid phase solution. Solution conditions have been varied, and the effect on morphology has been illustrated to relate to the surface charge of each habit plane. Experimental investigations have explored the suitability of additives during synthesis for morphological modification. Additive investigations into non-aqueous synthesis require considerations of solvent stability, and 1,4-butanediol was found to exhibit stability to the moderate addition of acids and bases. The surface charge of defined habit planes was explored through investigations of colloidal behavior of various morphological forms, and aging effects were noted from the adsorption of the solvent during precipitation. Finally, morphological variations during sintering were performed with platelet shaped particles. Morphological changes were related to the equilibrium shape, and estimates of the driving force for sintering were calculated. The effects of crystallographically defined habit planes were noted in each study.

The thermodynamic derivation of the equilibrium shape of a particle in a solvent has shown that the surface maintains an equilibrium electrochemical balance with the

surroundings. The surface energy of each habit plane thus can be related to the solution composition. The variation of pH will affect surface charge and therefore cause a reduction in surface energy away from the point of zero charge. The effect on morphology was illustrated by assuming surface charge and surface energy constants for three habit planes. Future examination of the validity of these derivations can be performed by determining the surface energy and charge characteristics of individual habit planes by work of adhesion and acid-base titration of crystallographically characterized alumina samples.

The use of adsorbates to control morphology requires that a two dimensional "phase" is formed between the crystal and the solvent by the additive. Additionally, adsorption must not interfere with nucleation kinetics and thermodynamic stability of the desired phase. Additives such as nitric acid and tetrahydrofuran were not found to affect the growth rates of the various habit planes, whereas acetic acid promotes the stability of the $\{11\bar{2}2\}$ habit planes, and 2-butanol stabilized the $\{11\bar{2}12\}$ habit planes. Pyridine acted to modify the particle morphology, but deleteriously affected the nucleation rate and solvent stability. The addition of base altered morphology through modification of surface charge, as predicted by the theoretical derivation of surface charge effects on morphology. Additional studies using other adsorbates remains a topic for investigation. The reaction mechanism for precipitate formation can be investigated from kinetic studies. This would assist in the development of faster production rates. Variables involving the development of supersaturation via alternative precursors (such as diaspore) could also affect morphology, reaction kinetics and particle size.

The colloidal characteristics of glycothermally produced α-alumina were found to vary with both particle morphology and environmental history. The isoelectric point of each particle shows a relationship with the character of the habit planes, and increasing the number of surface cation sites via dominant particle faces relates to more acidic isoelectric points. Infra-red examinations of the surface structure were unsuccessful in revealing the exact nature of the surface groups present on each habit plane. Future examination using LEEDS or AFM will improve insight into the nature of surface structure.

Finally. sintering studies show that faceted particles develop microstructure via similar mechanisms to established theory, but the particle packing characteristics dictate the development of particle morphology. When facets are aligned so that there is no porosity between grains, sintering can occur at lower temperatures. This creates a porous microstructure if a uniform green body is not produced. This will lead to difficulty in achieving a theoretically dense body for anisotropically shaped particles. Calculations were made on the driving force for sintering through the achievement of the equilibrium shape. Using literature values for the surface energy and equilibrium shape, the surface energy as a function of habit plane was derived and used to estimate the driving force for morphological change. Future work involving sintering studies can be used to determine the activation energy for sintering as a function of dominant habit planes. Additional work in sintering glycothermally produced alumina will relate to particle packing characteristics and to the character of faceted surfaces. Promotion of dense bodies (or porous bodies) requires a study of the packing characteristics of various morphological forms.

APPENDIX A

STANDARD OPERATING PROCEDURE FOR VACUUM DISTILLATION OF 1,4 BUTANEDIOL.

Required Equipment

The following equipment is required for the procedure.
1000 ml bulb with 24/40 fittings
24/40 glass plug
distillation elbow piece with thermocouple fitting
distillation thermocouple
cooling column
vacuum joint
100 ml initial collection bulb
500 ml product collection bulb
Cold finger
Coolant dewar
vacuum pump
circulating coolant source
heating mantle
temperature controller
thermal insulation (foam or glass fiber)

Procedure

Vacuum distillation involves using vacuum and heat to separate contaminants of differing vapor pressures from a desired solvent (usually organic). The high vapor pressure components will be preferentially collected in the initial 10%. Low vapor pressure components will remain in the final 10%. The collection procedure will provide

80% of the initial volume of distilled material in the product fraction. The volumes given for the equipment are arbitrary, in that the initial contaminant volume will determine the collected volume of the initial and product fractions. The volume of the material to be distilled in one run should equal one third of the volume of the bulb used for the contaminated solvent. The initial fraction and product fraction bulbs must then accommodate 10% and 80% of the distillate volume.

The steps of the distillation are as follows. Equipment references are appropriate to Dr. Adair's laboratory at the University of Florida.

Assemble the glassware according to Figure A, using vacuum grease or other sealant on all joints. Use the 100 ml initial fraction bulb. Fit cooling hose between the cooling column and the coolant source.

Place thermal insulation about the 1000 ml bulb and distillation elbow. The insulation should include the entire apparatus down over the fitting of the cooling column.

Turn on the recirculating coolant. The temperature setting should be no lower than 18 °C. 1,4 butanediol freezes at 16 °C. Room temperature tap water or a cold antifreeze mixture can be used.

Load the contaminate bulb with 350 ml of contaminated 1,4 butanediol. Place the glass plug in the open port of the 1000 ml bulb.

Turn on the vacuum. Allow 15 minutes to remove entrapped air, or until bubbles are no longer formed in the solvent. Entrapped air can lead to violent bubbling.

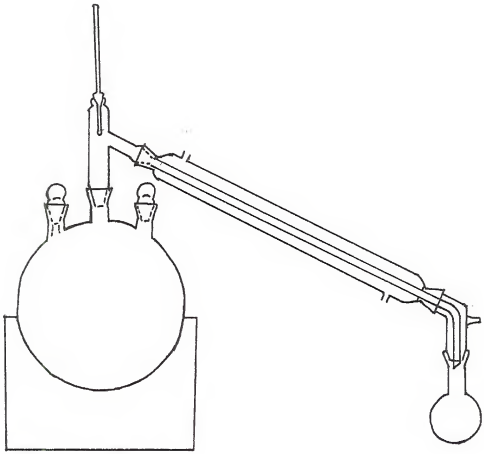

Figure A. Assembly of vacuum distillation equipment.

Set the temperature controller to setting 6. After about 20 minutes, distillation should occur. The thermometer will increase rapidly from room temperature to >100 °C at the beginning of distillation.

Collect the initial fraction (35 ml) in the 100 ml bulb.

Turn off vacuum, and remove the initial bulb. Fit the product bulb to the vacuum joint and turn the vacuum on. Perform this operation as expeditiously as possible.

Collect the product (280 ml).

Turn off the vacuum and turn off the heat.

Remove the product bulb. Transfer the product to a closed container.

Remove the insulation from the 1000 ml bulb and turn off the recirculating coolant.

Allow the 1000 ml bulb to cool, and place the remaining 10% fraction in a chemical waste container.

Clean all glassware.

Operational Notes

The temperature required for the distillation is a function of the level of vacuum applied. A strong vacuum such as is applied by the grey vacuum pump will cause distillation at ~103 °C. A weaker pump will require higher temperature. If a strong vacuum does not cause distillation near this temperature, the system may not be sealed. Also, distillation may initially occur at a lower temperature due to the more volatile components. The temperature should approach the target value by the end of the collection of the initial fraction.

Violent bubbling in the 1000 ml bulb can reduce the efficiency of the distillation. Boiling chips can be used to initiate bubbling at low rates. In general, the presence of entrapped air causes violent bubbling in 1,4 butanediol.

Limitations

Water is a component that is not removed by vacuum distillation. Sodium sulfate (anhydrous) is recommended to remove water from the product. $NaSO_4$ should be placed

in the 1000 ml bulb prior to vacuum being applied. Bubbling can cause $NaSO_4$ crystals to be thrown up the distillation elbow and possibly contaminate the product. The equipment can be tilted to reduce the likelihood of material entering the elbow, and vacuum should be held for 30 minutes to ensure that entrapped gasses are removed.

APPENDIX B

This program is written for MATHCAD Version7. It is designed to calculate the surface charge and surface potential for an amphoteric surface using the relationships developed by T. W. Healy and L. R. White (Hea78, Hea80). These sources contain some errors in unit conversions which have been corrected for this treatment. Constants and input factors used in these relationships are as follows.

$k := 1.3805 \times 10^{-23}$	Boltzmann's Constant (J/K)
$e := 0.1602 \times 10^{-18}$	Charge on an electron (C)
$\varepsilon 0 := 8.854 \times 10^{-12}$	Permittivity of free space (C^2/m J)
$R := 8.314$	Gas Constant (J)
$NA := 6.023 \times 1023$	Avogadro's Number (1/mol)
$Faraday := 96940$	Faraday's Constant (C/mol)
$T := 298$	Temperature (K)
$\varepsilon := 78.5$	Dielectric constant of water

pH is used as a range variable for the determination of potential.

$$pH := 2, 2.1 .. 12$$

Input factors for the Healy-White model are the dissociation constants for the charge development of negative and positive surface groups. Input is given as the negative log or pK values.

$$pKpos := 6$$

$$pKneg := 14$$

$$\Delta pK := pKneg - pKpos \qquad \Delta pH := \Delta pK - pH$$

$$\Delta pK = 8$$

$$\delta = 2\left(10^{-\Delta pK/2}\right) \qquad pHzero = \frac{(pKpos + pKneg)}{2}$$

$\delta = 2 \times 10^{-4}$ $pHzero = 10$

Input the number of surface sites, Ns, in the number of sites per m^2.

$Ns := 0.85 \times 10^{18}$

Input the concentration of background electrolyte, in molar units, M.

$c := 10^{-4}$ $Z := 1$ Ionic charge on the electrolyte

The Debye-Huckel parameter is calculated below (1/m).

$$\kappa = \left(\frac{2 Faraday^2 c Z^2 10^3}{\varepsilon 0 \varepsilon R T} \right)^{1/2}$$

$\kappa = 3.304 \times 10^7$

Gamma is a parameter used in the determination of charge. It assumes the bulk electrolyte concentration is given in mol/L.

$$\gamma = \frac{10^{-3} Ns \kappa}{4 NAc}$$

$\gamma = 116.559$

The Nernst Potential is given by the following relationship.

$$\Psi N(pH) = \frac{kT 2.303 (pHzero - pH)}{e}$$

$$yN(pH) := e^{\frac{\Psi N(pH)}{kT}}$$

The determination of surface potential, yzero, requires the solution of the following equality. This solution utilizes a given-find sequence which is nested in a dummy equation. This must be done because such sequences cannot perform iterative calculations.

Guess value for yzero. Solution := 5

Given

$$\frac{\sinh\left(\frac{solution}{2}\right)}{\gamma} = \delta \frac{\sinh\left(yN(pH) - solution\right)}{1 + \delta\cosh(yN(pH) - solution)}$$

$yzero(pH) := find(solution)$

The surface potential is determined from the solution to the above equality (V).

$$\Psi zero(pH) := (yzero(pH))kT/e$$

The net fraction of ionized surface groups is given by alpha, determined from the Nernst and zero potentials.

$$\alpha(pH) := \frac{\left(\delta\sinh(yN(pH) - yzero(pH))\right)}{1 + \delta\cosh\left(yN(pH) - yzero(pH)\right)}$$

The surface potential is given from the fraction of ionized groups.

$$\sigma(pH) := e \times Ns \times \alpha(pH)$$

The data files are exported by the following commands.

WRITE("alpha") := $\alpha(pH)$

WRITE("charge") := $\sigma(pH)$

WRITE("psizero") := $\Psi zero(pH)$

A spreadsheet program such as Microsoft Excel can be used to download the results and prepare graphs.

LIST OF REFERENCES

Ada97 J. H. Adair, R. V. Linhart, and H. Karaup, "OPAL, A Computer Program for the Determination of Speciation and Solubility, " http://zirconia.mse.ufl.edu.

Ada90 A. W. Adamson, Physical Chemistry of Surfaces, Interscience Publishers, a division of John Wiley and Sons, New York, N. Y., 1990.

All80 D. L. Allara, "Organic Monolayer Studies Using Fourier Transform Infrared Reflection Spectroscopy," in Vibrational Spectroscopies for Adsorbed Species, ACS Symposium Series 137, Edited by A. T. Bell and M. L. Hair, American Chemical Society, pp. 37-49, 1980.

Alu96 Alumina, syn (corundum), JCPDS - Powder Diffraction File, #46-1212, International Centre for Diffraction Data, Newton Square, PA, 1996.

Atk90 R. C. Atkins and F. A. Carey, Organic Chemistry; A Brief Course, McGraw-Hill Publishing Co., New York, NY, 1990.

Bae86 C. F. Baes, Jr., and R. E. Mesmer, The Hydrolysis of Cations, Kreiger Publishing Company, Malabar, Florida, 1986.

Bel97 N. S. Bell, S. B. Cho, and J. H. Adair, "Size Control of α-Alumina Particles Synthesized in 1,4-Butanediol Solution by α-Alumina and α-Hematite Seeding," *J. Am. Ceram. Soc.*, in press.

Bib85 D. M. Bibby and M. P. Dale, "Synthesis of Silica-Sodalite from Non-aqueous Systems," *Nature*, 317, 12 September, 1985.

Big95 S. Biggs and P. Mulvaney, "Surfactant and Polymer Adsorption: Atomic Force Microscopy Measurements," pp. 255-266 in Surfactant Adsorption and Surface Stabilization, ACS Symposium Series 615, Editor R. Sharma, American Chemical Society, 1995.

Boi88 R. Boistelle and J. P. Astier, "Crystallization Mechanisms in Solution," *J. Crystal Growth*, **90**, 14-30 (1988).

Bra75 A. D. Brailsford and N. A. Gjostein, "Influence of Surface Energy Anisotropy on Morphological Changes Occuring by Surface Diffusion," *J. Appl. Phys.*, **46** [6] 2390-2397 (1975).

Buc51 H. E. Buckley, Crystal Growth, John Wiley and Sons, Inc., New York, NY, 1951.

Bul94 J. W. Bullard, A. M. Glaeser, and A. W. Searcy, "Shape Changes by {100} Lithium Fluoride Ridge-Channel Arrays and of Lithium Fluoride Particles at Sintering Temperatures," *J. Am. Ceram. Soc.*, **77** [9] 2319-26 (1994).

Bur51 W. K. Burton, N. Cabrera and F. C. Frank, "The Growth of Crystals and the Equilibrium Structure of their Interfaces," *Phil. Trans. Roy. Soc. London*, **A243** 299-358 (1951).

Cah74 J. W. Cahn and D. W. Hoffman, "A Vector Thermodynamics for Anisotropic Surfaces II. Curved and Faceted Surfaces," *Acta Mat.*, **22** 1205-1214 (1974).

Ces88a J. Cesarano III and I. A. Aksay, "Stability of Aqueous α-Al_2O_3 Suspensions with Poly(methacrylic acid) Polyeletrolyte," *J. Am. Ceram. Soc.*, **71** [4] 250-55 (1988).

Ces88b J. Cesarano III and I. A. Aksay, "Processing of Highly Concentrated Aqueous α-Alumina Suspensions Stabilized with Polyelectrolytes," *J. Am. Ceram. Soc.*, **71** [12] 1062-67 (1988).

Chi88a P.-P. Chiang, M. D. Donohue, and J. L. Katz, "A Kinetic Approach to Crystallization from Ionic Solution: II Crystal Nucleation," *J. Colloid Interface Science*, **122** 251-265 (1988).

Chi88b P.-P. Chiang and M. D. Donohue, "A Kinetic Approach to Crystallization from Ionic Solution: I Crystal Growth," *J. Colloid Interface Science*, **122** 230-250 (1988).

Chi88c P.-P. Chaing and M. D. Donohue, "The Effect of Complex Ions on Crystal Nucleation and Growth," *J. Colloid Interface Science*, **126** 579-591 (1988).

Cho95 S. B. Cho, S. Venigalla, and J.H. Adair, "Morphological Control of α–Al_2O_3 Particles in 1,4-Butanediol Solution," pp. 139-150 in *Ceramic Transactions*, Vol. 54, Science, Technology, and Application of Colloidal Suspensions, edited by J.H. Adair, J.A. Casey, C.A. Randall, and S. Venigalla, American Ceramic Society, Westerville, OH, 1995.

Cho96 S. B. Cho, S. Venigalla, and J. H. Adair, "Morphological Forms of α-Alumina Particles Synthesized in 1,4-Butanediol Solution," *J. Am. Ceram. Soc.*, **79** [1] 88-96 (1996).

Cho97 J. H. Choi, D. Y. Kim, B. J. Hockey, S. M. Wiederhorn, C. A. Handwerker, J. E. Blendell, W. C. Carter, and A. R. Roosen, "The Equilibrium Shape of Internal Cavities in Sapphire," *J. Am. Ceram. Soc.*, **80** [1] 62-68 (1997).

Cur85 P. Curie, *Bull. Soc. Miner. France*, **8** 195 (1885).

Cur52 G. O. Curme and F. Johnson, Eds., Glycols, Reinhold Publishing Corporation, New York, NY, 1952.

Def66 R. Defay, I. Prigogine, A. Bellemans, and D. H. Everett, Surface Tension and Adsorption, John Wiley and Sons, Inc., New York, N.Y., 1966.

Daw89 W. J. Dawson, "Hydrothermal Synthesis of Advanced Ceramic Powders," *Am. Ceram. Soc. Bull.*, **67** [10] 1673-1678 (1989).

DeH93 R. T. DeHoff, Thermodynamics in Materials Science, McGraw-Hill, Inc., New York, N.Y., 1993.

Dem73 L. M. Dem'yanets and A. N. Lobachev, "Some Problems of Hydrothermal Crystallization," pp. 1-26 in Studies in Soviet Science, Crystallization Processes under Hydrothermal Conditions, Edited by A. N. Lobachev, Consultants Bureau, New York, NY, 1973.

Don37 J. D. H. Donnay and D. Harker, "A New Law of Crystal Morphology Extending the Law of Bravais," *Amer. Min.*, **22** 446-467 (1937).

Dor84 E. Dorre and H. Hubner, Alumina, Processing, Properties and Applications, Springer-Verlag, Berlin, 1984.

Duc94 W. A. Ducker, Z. Xu, D. R. Clarke, and J. N. Israelachvili, "Forces between Alumina Surfaces in Salt Solutions: Non-DLVO Forces and the Implications for Colloidal Processing," *J. Am. Ceram. Soc.*, **77** [2] 437-443 (1994).

Erv51 G. Ervin, Jr. and E.F. Osborn, "The System Al_2O_3-H_2O," Journal of Geology, **59** 381-394 (1951).

Est93 J. Estrin, "Precipitation Process," pp. 131-149 in Handbook of Industrial Crystallization, Edited by A. S. Myerson, Butterworth-Weinemann, Boston, MA, 1993.

Esu95 K. Esumi, "Adsorption of Polymer and Surfactant from their Binary Mixtures on Alumina," pp. 138-152 in Surfactant Adsorption and Surface Stabilization, ACS Symposium Series 615, Editor R. Sharma, American Chemical Society, 1995.

Fan86 A. J. Fanelli and J. V. Burlew, "Preparation of Fine Alumina Powder in Alcohol," *J. Am. Ceram. Soc.*, **69** [8] C-174-C-175 (1986).

Fow93 F. M. Fowkes, "Additivity of Intermolecular Forces at Interfaces. I. Determination of the Contribution to Surface and Interfacial Tensions of Dispersion Forces in Various Liquids," *J. Phys. Chem.* **67** 2538-2541 (1963).

Gad75 J. A. Gadsden, Infrared Spectra of Minerals and Related Inorganic Compounds, Butterworths, London, 1975.

Gib64 J. W. Gibbs, The Scientific Papers of J. Willard Gibbs, Thermodynamics, Vol. I, Dover Publications, Inc., New York, N.Y., 1964.

Git70 W. H. Gitzen, "Alumina as a Ceramic Material," Special Publication No. 4, The American Ceramic Society, Westerville, Ohio, 1970.

Gra47 D. C. Grahame, "The Electrical Double Layer and the Theory of Electrocapillarity," pp. 441-501 in Chemical Reviews, Vol. 41, Edited by W. A. Noyes, Jr., The American Chemical Society, Baltimore, MD, 1947.

Gra42 D. C. Grahame and R. B. Whitney, "The Thermodynamic Theory of Electrocapillarity," *J. Am. Chem. Soc.*, **64** 1548-1552 (1942).

Gre62 R. G. Greenler, "Infrared Study of the Adsorption of Methanol and Ethanol on Aluminum Oxide," *J. Chem. Phys.*, **37** [9] 2094-2100 (1962).

Haa69 R. Haase, Thermodynamics of Irreversible Processes, Addison-Wesley Publishing Co., Reading, MA, 1969.

Har73 P. Hartman, "Structure and Morphology," pp. 367-402 in Crystal Growth: An Introduction, Edited by P. Hartman, North-Holland, Amsterdam, 1973.

Har80 P. Hartman and P. Bennema, "The Attachment Energy as a Habit Controlling Factor. I. Theoretical considerations, " *J. Cryst. Growth*, **49** 145-156 (1980).

Har55 P. Hartman and W. G. Perdok, "On the Relations Between Structure and Morphology of Crystals I," *Acta Cryst.*, **8** 49-52 (1955).

Hea80 T. W. Healy, "Colloidal Behavior of Materials with Ionizable Group Surfaces," *Pure and Appl. Chem.*, **52** 1207-1219 (1980).

Hea78 T. W. Healy and L. R. White, "Ionizable Surface Group Models of Aqueous Interfaces," *Adv. Colloid Interface Sci.*, **9** 303-345 (1978).

Hen94 V. E. Henrich and P. A. Cox, The Surface Science of Metal Oxides, Cambridge University Press, New York, 1994.

Her51 C. Herring, "Some Theorems on the Free Energies of Crystal Surfaces," *Phys. Rev.*, **82** [1] 87-93 (1951).

Her50 C. Herring, "Effect of Change of Scale on Sintering Phenomena," *J. Appl. Phys.*, **21** [4] 301-303 (1950).

Hid95 P. Hidber, T. Graule, and L. Gauckler, "Interactions of Dispersants and Binders with α-Alumina in Aqueous Suspensions," pp. 23-30 in Science, Technology, and Applications of Colloidal Suspensions, Ceramic Transactions, Vol. 54, Edited by J. H. Adair, J. A. Casey, C. A. Randall, and S. Venigalla, The American Ceramic Society, Westerville, OH, 1995.

Hir87 S. Hirano, "Hydrothermal Processing of Ceramics," *Am. Ceram. Soc. Bull.*, **66** [9] 1342-1344 (1987).

Hir97 J. Hirschler and J. C. Fontecilla-Camps, "Protein Crystal Growth Rates are Face-specifically Modified by Structurally Related Contaminants," *J. Crystal Growth*, **171** 559-565 (1997).

Hof72 D. W. Hoffman and J. W. Cahn, "A Vector Thermodynamics for Anisotropic Surfaces, I. Fundamentals and Application to Plane Surface Junctions," *Surf. Sci.*, **31** 368-388 (1972).

Hor90 R. G. Horn, "Surface Forces and Their Action in Ceramic Materials," *J. Am. Ceram. Soc.*, **73** [5] 1117-1135 (1990).

Hor88 R. G. Horn, D. R. Clarke, and M. T. Clarkson, "Direct Measurement of Surface Forces between Sapphire Crystals in Aqueous Solutions," *J. Mater. Res.*,**3** [3] 413-416 (1988).

How90 K. E. Howard, C.D.E. Lakeman, and D. A. Payne, "Surface Chemistry of Various Poly(vinyl butyral) Polymers Adsorbed onto Alumina," *J. Am. Ceram. Soc.*, **73** [8] 2543-46 (1990).

Hua95 L. Huang, C. Maltesh, and P. Somasundaran, "Interactions Between Pentadecylethoxylated Nonylphenol and Tertacyltrimethylammonium Chloride Mixtures at the Alumina-Water Interface," pp. 241-254 in

Surfactant Adsorption and Surface Stabilization, ACS Symposium Series 615, Editor R. Sharma, American Chemical Society, 1995.

Hun87 R. J. Hunter, Foundations of Colloid Science, Vol. 1, Clarendon Press, Oxford, 1987.

Hun93 R. J. Hunter, Introduction to Modern Colloid Science, Oxford Science Publications, Oxford, 1993.

Ino97 M. Inoue, T. Nishikawa, T. Nakamura, and T. Inui, "Glycothermal Reaction of Rare-Earth Acetate and Iron Acetylaacetonate: Formation of Hexagonal $ReFeO_3$," *J. Am. Ceram. Soc.*, **80** 2157-2160 (1997).

Ino91 M. Inoue, H. Otsu, H. Kominami, and T. Inui, "Synthesis of Yttrium Aluminum Garnet by the Glycothermal Method," *J. Am. Ceram. Soc.* **74** [6] 1452-1454 (1991).

Ino95 M. Inoue, H. Otsu, H. Kominami, T. Inui, "Synthesis of Submicron Spherical Crystals of Gadolinium Gallium Garnets by the Glycothermal Method," *J. Mat. Sci. Lett.*, **14** (1995) 1303-1305.

Ino89 M. Inoue, H. Tanino, Y. Kondo, and T Inui, "Formation of Microcrystalline α-Alumina by Glycothermal Treatment of Gibbsite," *J. Am. Ceram. Soc.*, **72** [2] 352-353 (1989).

Isr92 J. N. Israelachvili, Intermolecular and Surface Forces, Academic Press, London, 1992.

Kag67 R. O. Kagel, "Infrared Investigation of the Adsorption and Surface Reactions of the C_1 through C_4 Normal Alcohols on γ-Alumina," *J. Phys. Chem.*, **71** [4] 844-850 (1967).

Kai95 A. Kaiser, A. Berger, D. Sporn, and H. Bertagnolli, "Lyothermal Synthesis of Nanocrystalline $BaTiO_3$ and TiO_2 Powders," pp. 51-55 in Ceramic Processing Science and Technology, Eds., H. Hausner., G. L. Messing, and S. Hirano, Ceramic Transactions, Vol. 51, The American Ceramic Society, Westerville, OH, 1995.

Kai94 A. Kaiser, D. Sporn, and H. Bertagnolli, "Phase Transformation and Control of Habit in Lyothermal Synthesis of α-Al_2O_3," *J. Euro. Ceram. Soc.*, **14** 77-83 (1994).

Kat87 A. Kato, "Recent Production Methods of Ultrafine Ceramics Powders," pp. 459-469 in Materials Science Monographs, Vol. 38, High Tech Ceramics,

Part A, Edited by P. Vincenzini, Elsevier Science Publishers B. V., Amsterdam, 1987.

Kel89 B. J. Kellett and F. F. Lange, "Thermodynamics of Densification: I, Sintering of Simple Particle Arrays, Equilibrium Configurations, Pore Stability, and Shrinkage," *J. Am. Ceram. Soc.*, **72** [5] 725-34 (1989).

Kel88 J. F. Kelso and T. A. Ferrazzoli, "Surface Chemistry Effects in Concentrated Aqueous Dispersions of Bayer Process Calcined Aluminas," pp. 433-439 in Ceramic Transactions, Vol. 1, G. L. Messing, E. R. Fuller, Jr. And H. Hausner, Eds., The American Ceramic Society Inc., Westerville, Ohio, 1988,.

Ken59 G. C. Kennedy, "Phase Relations in the System Al_2O_3-H_2O at High Temperature and Pressures," *Am. J. Sci.*, **257** [10] 563-573 (1959).

Kin76 W. D. Kingery and B. Francois, "The Sintering of Crystalline Oxides, I. Interaction Between Grain Boundaries and Pores"; pp. 471-496 in Sintering and Related Phenomena. Edited by G.C. Kuczynski, N. A. Hooton, and C.F. Gibbon, Gordon and Breach Science Publishers, New York, 1976.

Kis75 A. V. Kiselev and V. I. Lygin, Infrared Spectra of Surface Compounds, John Wiley and Sons, New York, NY, pp. 237-262, 1975.

Kli65a K. L. Kliewer and J. S. Koehler, "Space Charge in Ionic Crystals. I. General Approach with Application to NaCl," *Phys. Rev.* **140** [4A] A1226-A1240 (1965).

Kli65b K. L. Kliewer, "Space Charge in Ionic Crystals. II. The Electron Affinity and Impurity Accumulation," *Phys. Rev.* **140** [4A] A1241-A1246 (1965).

Klu93 D. L. Klug, "The Influence of Impurities in Solvents on Crystallization," pp. 65-87 in Handbook of Industrial Crystallization, Edited by A. S. Myerson, Butterworth-Heinemann, Boston, MA. 1993.

Koo95 L. K. Koopal and T. Goloub, "Self-Assembly of Ionic Surfactants Adsorbed on Mineral Oxides: Surface Charge and Salt Effects," pp. 78-103 in Surfactant Adsorption and Surface Stabilization, ACS Symposium Series 615, Editor R. Sharma, American Chemical Society, 1995.

Kuz64 V. A. Kuznetsov, "Growth Rate of Corundum Faces in Hydrothermal Conditions," *Kristallografiya,* **9** 123-124 (1964).

Kuz65 V. A. Kuznetsov, "Hydrothermal Crystallization Kinetics of Corundum," *Kristallografiya,* **10**, 663-667 (1965).

Kuz71 V. A. Kuznetsov, "Kinetics of the Crystallization of Corundum, Quartz, and Zincite," pp. 52-61 in Hydrothermal Synthesis of Crystals Edited by A. N. Lobachev, Consultants Bureau, New York, NY, 1971.

Lan88 F. F. Lange, "The Sinterability of Agglomerated Powders," *J. Am. Ceram. Soc.,* **67** [2] 83-88 (1988).

Lan89 F. F. Lange and B. J. Kellett, "Thermodynamics of Densification: II, Grain Growth in Porous Compacts and Relation to Densification," *J. Am. Ceram. Soc.*, **72** [5] 735-41 (1989).

Lar97 I. Larson, C. J. Drummond, D. Y. C. Chan, and F. Grieser, "Direct Force Measurements between Silica and Alumina," *Langmuir*, **13** 2109-2112 (1997).

Lau43 A. W. Laubengayer and R. S. Weisz, "A Hydrothermal Study of Equilibria in the System Alumina-Water," *J. Am.Ceram. Soc.*, **65** 247-250 (1943).

Lau73 R. A. Laudise, "Hydrothermal Growth," pp. 162-209 in Crystal Growth, Edited by P. Hartman, North-Holland Publ. Co., New York, NY, 1973.

Lau58 R. A. Laudise and A. A. Ballman, "Hydrothermal Synthesis of Sapphire," *J. Am. Chem. Soc.*, **65** 2655-2657 (1958).

Lee88 D. H. Lee, R. A. Condrate, Sr., and J. S. Reed, "FTIR Spectral Study of Polyacrylate Adsorption on Alumina," pp. 67-80 in Science, Technology, and Applications of Colloidal Suspensions, 1988.

Liu97 X. Y. Liu, "Interfacial Structure Analysis for the Prediction of Morphology of Crystals and Implications for the Design of Tailor-made Additives," *J. Crystal Growth*, **174** 380-385 (1997).

Lup83 C. H. P. Lupis, Chemical Thermodynamics of Materials, North-Holland, New York, New York, 1983.

Mad97 M. Madono, R. P. Racher, and M. K. Kunka, "Alumina," *Am. Ceram. Soc. Bull.*, **76** [6] 65-69 (1997).

Man96 T. Manth, D. Mignon, H. Offermann, "The Role of Hydrodynamics in Precipitation," *J. Crystal Growth*, **166** 998-1003 (1996).

Mat97 Mathcad 7, Mathsoft International, 101 Main Street, Cambridge, MA 02142, http://www.mathsoft.com.

Mat87 E. Matijevic, "Colloid Science in Ceramic Powder Preparation," pp.441-458 in Materials Science Monographs Vol. 38A, High Tech Ceramics Part A, Edited by P. Vincenzini, Elsevier Science Publishers B. V., New York, NY, 1987.

Mat92 E. Matijevic, "Control of Powder Morphology," pp. 513-527 in Chemical Processing of Advanced Materials, Edited by L. L. Hench and J. K. West, John Wiley and Sons, Inc., 1992.

Mat67 S. Matsushima, G. C. Kennedy, J. Akella, and J. Haygarth, "A Study of Equilibrium Relations in the System Al_2O_3-SiO_2-H_2O and Al_2O_3-H_2O," *A.m J. Sci.*, **265** [1] 28-44 (1967).

Mor80 B. A. Morrow, "Raman Spectroscopic Studies of Surface Species," pp. 119-140 in Vibrational Spectroscopies for Adsorbed Species, ACS Symposium Series 137, Edited by A. T. Bell and M. L. Hair, American Chemical Society, , 1980.

Mul63 W. W. Mullins, "Solid Surface Morphologies Goverened by Capillarity," pp.17-65 in Metal Surfaces: Structure, Energetics, and Kinetics. ASM, Metals Park, OH, 1963.

Mun97 R. G. Munro, "Evaluated Material Properties for a Sintered α-Alumina," *J. Am. Ceram. Soc.*, **80** [8] 1919-1928 (1997).

Mye93 A. S. Myerson and R. Ginde, "Crystals, Crystal Growth, and Nucleation," pp. 33-63 in Handbook of Industrial Crystallization, Edited by A. S. Myerson, Butterworth-Heinemann, Boston, MA, 1993.

Mye97 A. S. Myerson and A. F. Izmailov, "Relationsip between Diffusivity and Viscosity for Supersaturated Electrolyte Solutions," *J. Crystal Growth*, **174** 369-379 (1997).

Nan87 G. H. Nancollas, "The Mechanism of Growth and Dissolution of Sparingly Soluble Salts," Ceramic Transactions, Vol 1, pp. 8-22. Ceramic Powder Science II, Ed. by G. L. Messing, and E.R. Fuller, Jr., Proceedings of the 1st International Conference on Ceramic Powder Processing Science, Orlando, FL, No. 1-4, 1987.

Nie83 A. E. Nielsen, "Precipitates: Formation, Coprecipitation, and Aging," pp. 304-306 in Treatise on Analytical Chemistry, Part I, Theory and Practice, 2nd Ed., Vol. 3, Edited by I. M. Lokthoff and P. J. Elving, John Wiley and Sons, Inc., 1983.

Nyv85 J. Nyvlt, O. Sohnel, M. Matuchova, and M. Broul, The Kinetics of Industrial Crystallization, Chemical Engineering Monographs Vol. 19, Elsevier, New York, NY, 1985.

Oka90 H. Okamoto, M. Hashiba, Y. Nurishi, and K. Hiramatsu, "Fluidity and Dispersion of Alumina Suspension at the Limit of Thickening by Ammonium Polyacrylates," Chapman and Hall, Ltd., (1990) 383-387.

Par83 G. D. Parfitt and C.H. Rochester, Adsorption from Solution at the Liquid/Solid Interface, Academic Press, London, 1983.

Pas87 J. A. Pask and A. G. Evans, Eds., "Ceramic Microstructures '86," Plenum Press, New York, 1987.

Pin87 S. H. Pine, Organic Chemistry, McGraw-Hill Book Co., New York, NY, 1987.

Ray79 Lord Rayleigh, "On the Instability of Jets," *Proc. London Math. Soc.*, **10**, 4-13 (1879).

Rin96 T. A. Ring, Fundamentals of Ceramic Powder Processing and Synthesis, Academic Press, New York, 1996.

Ros88 S. Ross and I. D. Morrison, Colloidal Systems and Interfaces, John Wiley and Sons, New York, NY, 1988.

Ruc90 E. Ruckenstein and B. Nowakowski, "A Kinetic Theory of Nucleation of Liquid," *J. Colloid Interface Sci.*, **137** 583-592 (1990).

San97 C. Sane, T. Kashiwagi, N. Nagashima, and T. Kawakita, "Effects of Additives on the Growth of L-glutamic Acid Crystals (β-Form)," *J. Crystal Growth*, **178** 568-574 (1997).

Sea85 A. W. Searcy, "Driving Force for Sintering of Particles with Anisotropic Surface Energies," *J. Am. Ceram. Soc.*, **68** [10] C-267-C-268 (1985).

Sea94 A. W. Searcy and J. W. Bullard, "Thermodynamics and Kinetics of Surface Area Changes of Faceted Particles," *J. Am. Ceram. Soc.*, **77** [9] 2314-2318 (1994).

Soh92 O. Sohnel and J. Garside, Precipitation Basic Principles and Industrial Applications, Butterworth, Oxford, 1992.

Som89 S. Somiya, Hydrothermal Reaction for Materials Science and Engineering; An Overview of Research in Japan, Elsevier Science Publishers, Ltd., New York, NY, 1989.

Som87 S. Somiya and M. Yoshimura, "Hydrothermal Processing of Ultrafine Single-Crystal Zirconia and Hafnia Powders with Homogeneous Dopants," pp. 43-55 in Advances in Ceramics, Vol. 21, Ceramic Powder Science. Edited by G. L. Messing, K. S. Mazdiyasni, J. W. McCauley, and R. A. Haber, The American Ceramic Society, Inc., Columbus, Ohio, 1987.

Sto92 J. S. Stolken and A. M. Glaeser, "The Morphological Evolution of Cylindrical Rods with Anisotropic Surface Free Energy via Surface Diffusion," *Scripta Metallurgica et Materialia* **27** 449-454 (1992).

Stu92 W. Stumm, Chemistry of the Solid-Water Interface, Processes at the Mineral-Water and Particle Water Interface in Natural Systems, John Wiley and Sons, Inc., New York, 1992.

Sum91 S. Sumita, W. E. Rhine and H. K. Bowden, "Effects of Organic Dispersants on the Dispersion, Packing, and Sintering of Alumina," *J. Am. Ceram. Soc.*, **74** [9] 2189-96 (1991).

Suy91 Y. Suyama and T. Yamaguchi, "Powders for Advanced Ceramics: Characterization and Synthesis," pp. 121-151 in Fundamentals of Ceramic Engineering, Edited by P. Vincenzini, Elsevier Science Publishers, London, UK, 1991.

Sut95 A. P. Sutton and R. W. Balluffi, Interfaces in Crystalline Materials, Monographs on the Physics and Chemistry of Materials, Vol. 51, Oxford University Press, Inc., New York, 1995.

Wal79 A.G. Walton, The Formation and Properties of Precipitates, Robert E. Krieger Publishing Co., Huntington, New York, 1979.

Wer94 J. H. Wernet and M. P. Wernet, "Stabilized Alumina/Ethanol Colloidal Dispersion for Seeding High Temperature Air Flows," *NASA Technical Memorandum 106591*, National Aeronautics and Space Administration, Lewis Research Center, 1994.

Wul01 G. Wulff, "Zur Frage der Geshwindigheit des Wachstums und der Auflosung der Kristallflachen," *Z. Krist.*, **34** 449-530 (1901).

Yeh88 T. Yeh and M. D. Sacks, "Low-Temperature Sintering of Aluminum Oxide," *J. Am. Cer. Soc.*, **71** [10] 841-844 (1988).

Yeh88 T. Yeh and M. D. Sacks, "Effect of Particle Size Distribution on the Sintering of Alumina," *J. Am. Ceram. Soc.*, **71** [12] C-484-C-487 (1988).

Zhe89 J. Zheng and J. S. Reed, "Effects of Particle Packing Characteristics on Solid-State Sintering," *J. Am. Cer. Soc.*, **72** [5] 810-817 (1989).

BIOGRAPHICAL SKETCH

Nelson S. Bell is the second son of Joseph and Eunice Bell, born on January 8th, 1970 and was raised as a native of Augusta, Georgia. He attended the Georgia Institute of Technology from 1988 to 1993 as a student on the Co-operative plan. During his undergraduate studies, he was employed as a Co-op student by the Oak Ridge National Laboratory in the Metals and Ceramics Division. He was awarded a Georgia Merit Scholarship and was the first recipient of the A. T. Chapman Memorial Scholarship before graduating with Highest Honors. He then joined the Materials Chemistry Group under Dr. James H. Adair at the University of Florida in pursuit of a doctoral degree. In 1993 he was awarded a Graduate Fellowship by the Department of Materials Science and Engineering. He is currently a member of the American Ceramic Society, and has secured a one year term of post-doctoral study at the Max Planck Institute in Stuttgart, Germany.

I certify that I have read this study and that in my opinion it conforms to acceptable standards of scholarly presentation and is fully adequate, in scope and quality, as a thesis for the degree of Doctor of Philosophy.

James H. Adair, Chairman
Associate Professor of Materials Science and Engineering

I certify that I have read this study and that in my opinion it conforms to acceptable standards of scholarly presentation and is fully adequate, in scope and quality, as a thesis for the degree of Doctor of Philosophy.

Robert T. DeHoff
Professor of Materials Science and Engineering

I certify that I have read this study and that in my opinion it conforms to acceptable standards of scholarly presentation and is fully adequate, in scope and quality, as a thesis for the degree of Doctor of Philosophy.

Michael D. Sacks
Professor of Materials Science and Engineering

I certify that I have read this study and that in my opinion it conforms to acceptable standards of scholarly presentation and is fully adequate, in scope and quality, as a thesis for the degree of Doctor of Philosophy.

David E. Clark
Professor of Materials Science and Engineering

I certify that I have read this study and that in my opinion it conforms to acceptable standards of scholarly presentation and is fully adequate, in scope and quality, as a thesis for the degree of Doctor of Philosophy.

Daniel R. Talham
Associate Professor of Chemistry

This dissertation was submitted to the Graduate Faculty of the College of Engineering and to the Graduate School and was accepted as partial fulfillment of the requirements for the degree of Doctor of Philosophy.

December, 1997

Winfred M. Phillips
Dean, College of Engineering

Karen A. Holbrook
Dean, Graduate School